POLY(LACTIC ACID)/CELLULOSE NANOCRYSTAL COMPOSITE BLOWN FILMS FOR FOOD PACKAGING APPLICATIONS

By

Sonal Sanjay Karkhanis

A DISSERTATION

Submitted to
Michigan State University
in partial fulfillment of the requirements
for the degree of

Packaging-Doctor of Philosophy

2020

ABSTRACT

POLY(LACTIC ACID)/CELLULOSE NANOCRYSTAL COMPOSITE BLOWN FILMS FOR FOOD PACKAGING APPLICATIONS

By

Sonal Sanjay Karkhanis

Poly(lactic acid) (PLA), a bio-based polymer, has several attractive properties such as excellent stiffness, reasonable strength, excellent flavor and aroma barrier, as well as good grease and oil resistance. Despite these attributes, PLA's applicability as a flexible food packaging material is limited due to several drawbacks such as brittleness, poor water vapor and moderate oxygen barrier properties as well as film processing difficulties due to its insufficient melt strength. This study was aimed at overcoming these drawbacks to widen PLA's applicability in the food packaging industry.

Firstly, the effectiveness and efficiency of two newly developed food grade multifunctional epoxies with low and high epoxy equivalent weights in chain extending/branching PLA were studied in a torque rheometer, in order to overcome the issue of PLA's insufficient melt strength. Both chain extender (CE) grades not only chain-extended PLA effectively as indicated by a significant increase in the mixing torque as well as PLA's melt viscosity and molecular weight, but also branched it leading to its reduced crystallinity. Infrared results indicated that chain extension occurred through the ring opening reaction of epoxy groups in the CE with PLA's hydroxyl and/or carboxyl groups. This chain extension/branching was beneficial in overcoming PLA film's brittleness since its impact strength increased almost linearly with the CE content.

Secondly, cellulose nanocrystals (CNCs) were added to a PLA matrix to increase its crystallinity and act as impermeable regions in order to improve its barrier properties. However, CNCs were difficult to disperse in non-polar polymers due to their high polarity and strong

hydrogen bonding forces. Therefore, two different solvent-free approaches of incorporating and dispersing CNCs into the PLA matrix were examined. The first approach consisted of melt-blending PLA and CNCs in an internal mixer whereas the second method involved direct dry-mixing of PLA and CNCs in a high intensity mixer, before film manufacture through the blown film extrusion process. Good distribution and barrier performance improvement were achieved by both methods. However, the direct dry-blending technique appeared to be the better approach for adding CNCs into the PLA matrix because it exposed the samples to less heat; thus, minimizing thermal degradation as demonstrated by the quantified number of chain scissions, molecular weight and melting temperature results.

Thereafter, the influence of CNC addition level and environmental testing conditions on the water vapor (WVP) and oxygen (OP) permeability of direct dry-blended PLA/CNC films were studied. Both WVP and OP of PLA and PLA/CNC nanocomposite films varied exponentially with temperature as expected from the Arrhenius equation, whereas the WVP remained constant with relative humidity (RH) as expected from Fick's law. Additionally, the values of WVP and OP negatively correlated with the degree of crystallinity. Depending on testing temperature or humidity, optimum improvements in WVP (30-40%) and OP (65-75%) of PLA films occurred at 1% CNCs, a CNC content that correlated very well with the maximum increase in crystallinity.

Finally, the potential of the developed PLA/1% CNC films with enhanced barrier performance in extending the shelf-life of a moisture-sensitive food product (crackers) was assessed and mathematically modeled. Interestingly, the crackers packaged in the CNC-based films had approximately 40% longer shelf-life compared to the ones packaged in neat PLA, irrespective of the RH. The overall results of this research indicate that the PLA/CNC films developed in this study have tremendous potential for food packaging applications.

Dedicated to my parents
Sanjay and Mohana Karkhanis

ACKNOWLEDGEMENTS

I am extremely thankful to my advisor Dr. Laurent Matuana (School of Packaging, Michigan State University) for his time, support and guidance. He has been an excellent teacher and mentor to me and always pushed me to be a better researcher. He has constantly helped me improve myself in all aspects of my career including scientific writing, and communication as well as presentation skills. Moreover, I am extremely thankful to my committee members, Dr. Eva Almenar (School of Packaging, Michigan State University), Dr. Donatien-Pascal Kamdem, and Dr. Yan Liu (Biosystems and Agricultural Engineering, Michigan State University) for their insightful suggestions, invaluable time commitment and expertise.

I would also like to acknowledge Mr. Aaron Walworth (School of Packaging, Michigan State University) for helping me learn and set up equipment used as a part of this study. Additionally, I am grateful to my research group for their help and critique of this research.

We gratefully acknowledge the USDA Forest Service and The U.S. Endowment for Forestry and Communities-P^{3}Nano (Grant No. P3-8b) for financial support of this research work. Also, I extend my heartfelt gratitude to the School of Packaging, its faculty and staff.

Finally, I must express my very profound gratitude to my parents for providing me with unfailing support and continuous encouragement. They have always been there for me whenever I needed them. I am also very grateful to my friends, who were my family away from home, and who were always around to listen to my countless practice presentations for conferences, committee meetings, and my comprehensive exam. Thank you.

TABLE OF CONTENTS

LIST OF TABLES xi

LIST OF FIGURES xiii

Chapter 1 1
INTRODUCTION 1
1.1 Introduction 1
1.2 Objectives 9
1.3 Hypothesis 10
1.4 Structure of Dissertation 10
REFERENCES 11

Chapter 2 16
BACKGROUND AND LITERATURE REVIEW 16
2.1 Introduction 16
2.2 Poly(lactic acid) 16
2.2.1 Synthesis of PLA 16
2.2.2 Properties of PLA 18
2.2.2.1 Thermal properties 19
2.2.2.2 Mechanical properties 19
2.2.2.3 Barrier properties 19
2.2.2.4 Rheological properties 21
2.3 Improvement of PLA's properties 23
2.4 Chain extenders (CEs) 24
2.4.1 Commonly used CEs 24
2.4.2 Properties of CEs 25
2.4.3 Use of CEs in PLA matrix 26
2.4.4 Addition of CEs into PLA matrix 27
2.4.5 Techniques for verifying chain extension of PLA 29
2.4.5.1 Gel permeation chromatography (GPC) 29
2.4.5.2 Viscosity measurements 31
2.4.5.2.1 Melt flow index (MFI) 31
2.4.5.2.2 Torque rheometry 33
2.4.5.3 Fourier transform infrared spectroscopy (FTIR) 35
2.4.5.4 Differential scanning calorimetry (DSC) 39
2.4.5.5 Falling dart impact strength 40
2.5 Cellulose nanocrystals (CNCs) 41
2.5.1 Production of CNCs 42
2.5.2 Properties of CNCs 42
2.5.3 Use of CNCs in bio-based polymer matrices 43
2.6 Dispersion of cellulose nanomaterials in polymer matrices 44
2.6.1 Solvent-casting 44
2.6.2 Solvent dispersion prior to melt compounding 46

2.6.3 Melt-processing....47
2.6.4 Techniques for studying dispersion of CNCs into polymer matrices....48
2.6.4.1 Light microscopy....48
2.6.4.2 Ultraviolet-Visible (UV-Vis) Spectroscopy....49
2.7 Barrier performance of PLA/CNC films....51
2.7.1 Barrier measurement....51
2.7.1.1 Isostatic method....52
2.7.1.2 Quasi-isostatic method....53
2.8 Shelf-life of moisture-sensitive food....56
2.8.1 Sorption isotherm of a moisture-sensitive food product....57
2.8.1.1 Background....57
2.8.1.2 Mathematical models....59
2.8.1.2.1 Linear, quadratic and cubic models....59
2.8.1.2.2 Guggenheim Anderson de Boer (GAB) model....60
2.8.1.2.3 Goodness of fit using root mean square (RMS) value....63
2.8.2 Shelf-life of food packaged in films....64
2.8.2.1 Experimental shelf-life determination of product-package system....64
2.8.2.2 Shelf-life modeling....65
REFERENCES....70

Chapter 3....78
EXPERIMENTAL....78
3.1 Materials....78
3.2 Sample manufacturing....79
3.2.1 Preparation of PLA/CE composites....79
3.2.2 Preparation of PLA/CNC composites....80
3.2.2.1 Direct dry-blending (DB)....80
3.2.2.2 Melt blending process (MB)....80
3.2.2.3 PLA/CNC film manufacturing....81
3.3 Property evaluation....82
3.3.1 Fourier transform infrared spectroscopy (FTIR)....82
3.3.1.1 FTIR of PLA/CE blends....82
3.3.1.2 FTIR of PLA and PLA/1% CNC composite films prepared by both DB and MB processes....82
3.3.2 Gel permeation chromatography....83
3.3.3 Melt flow index (MFI)....84
3.3.4 Differential scanning calorimetry (DSC)....85
3.3.5 Thermogravimetric analysis (TGA)....86
3.3.6 Light microscopy....86
3.3.7 Ultraviolet-visible (UV-Vis) spectroscopy....86
3.3.8 Residence time of PLA/CE blends in the extruder....87
3.3.9 Falling dart impact strength....87
3.3.10 Water vapor permeability (WVP)....88
3.3.11 Oxygen permeability (OP)....89
3.4 Shelf-life of crackers packaged in direct dry-blended PLA/1% CNC films....90
3.4.1 Moisture sorption isotherm of crackers....90

3.4.1.1 Initial moisture content (IMC) 90
3.4.1.2 Equilibrium moisture content (EMC) 91
3.4.2 Shelf-life of crackers packaged in PLA and PLA/CNC films 92
3.5 Statistics 93
REFERENCES 94

Chapter 4 98
RESULTS AND DISCUSSION 98
4.1 Extrusion blown films of poly(lactic acid) chain-extended with food grade multifunctional epoxies 98
4.1.1 Effectiveness and efficiency of multifunctional epoxy grades in chain extending PLA 98
4.1.2 Extrusion-blown chain-extended PLA films 112
4.1.3 Effect of chain extender content on the dart impact strength of PLA films 116
4.2 Performance of poly(lactic acid)/cellulose nanocrystal composite blown films processed by two different compounding approaches 118
4.2.1 Effect of blending process on CNC dispersion and PLA's optical properties 118
4.2.2 Effects of CNC addition and blending process on PLA's thermal properties 121
4.2.3 Effects of CNC addition and blending process on the degradation of PLA 126
4.2.4 Effects of CNC addition and blending process on the WVTR and OTR of PLA 135
4.3 Water vapor and oxygen barrier properties of extrusion-blown poly(lactic acid)/cellulose nanocrystals nanocomposite films 136
4.3.1 Effect of CNC content on water vapor permeability (WVP) and oxygen permeability (OP) of films 137
4.3.2 Effect of CNC content on water vapor permeability (WVP) and oxygen permeability (OP) of films 144
4.4 Potential of extrusion-blown poly(lactic acid)/cellulose nanocrystals nanocomposite films for improving the shelf-life of a dry food product 152
4.4.1 Moisture sorption of food 152
4.4.2 Experimental shelf-life of crackers packaged in PLA and PLA/CNC composite films 156
4.4.3 Shelf-life modelling of crackers packaged in PLA and PLA/CNC in films 158
APPENDICES 161
APPENDIX A: Extrusion blown films of poly(lactic acid) chain-extended with food grade multifunctional epoxies 162
APPENDIX B: Performance of poly(lactic acid)/cellulose nanocrystal composite blown films processed by two different compounding approaches. 172
APPENDIX C: Water vapor and oxygen barrier properties of extrusion-blown poly(lactic acid)/cellulose nanocrystals nanocomposite films. 176

APPENDIX D: Potential of extrusion-blown poly(lactic acid)/cellulose nanocrystals nanocomposite films for improving the shelf-life of a dry food product. 179
REFERENCES 182

Chapter 5 189
CONCLUSIONS 189
5.1 Conclusions 189
5.2 Future work 195

LIST OF TABLES

Table 2.1 Comparison of PLA properties with other petroleum-based polymers [19-22]. 20

Table 2.2 Properties of chain extenders [28,31,32]. 25

Table 2.3 Models to predict moisture sorption isotherms [88,90]. 60

Table 2.4 Models to predict shelf-life of moisture sensitive foods [88-91]. 66

Table 3.1 Properties of chain extenders. 78

Table 3.2 Theoretical and measured relative humidity (RH) conditions generated in desiccators with saturated salt solutions. 92

Table 4.1 Mixing time of PLA with both grades of multifunctional epoxies in torque rheometer. 101

Table 4.2 Band assignments for the wavenumbers of peaks used in FTIR analysis and corresponding functional groups. 105

Table 4.3 Molecular weights, dispersity indices and melt flow index values of PLA chain-extended with CE 4468. 109

Table 4.4 Processing parameters recorded during extrusion-blown film and residence times as a function of CE 4468 content in PLA. 113

Table 4.5 Molecular weights and dispersity indices of PLA films chain-extended with CE 4468. 114

Table 4.6 DSC analysis for PLA as well as direct dry-blended (DB) and melt-blended (MB) PLA/1% CNC films. 125

Table 4.7 Molecular weights of PLA, direct dry-blended PLA/CNC (DB) and melt-blended PLA/CNC (MB) films as well as unprocessed PLA pellets, and PLA pellets subjected to DB and MB processes. 128

Table 4.8 Band assignments for the wavenumbers of peaks used in FTIR analysis and corresponding functional groups [6,36,50-55]. 132

Table 4.9 WVTR and OTR of PLA as well as direct dry-blended (DB) and melt-blended (MB) PLA/1% CNC films. 135

Table 4.10 Effect of CNC content on the water vapor and oxygen activation energy (E_p) and pre-exponential factor (A_0) of PLA films. 148

Table 4.11 Time for crackers packaged in PLA and PLA/CNC films to reach critical moisture. content of 8% at different relative humidity conditions and a constant temperature of 25°C. 157

Table 4.12 Water vapor permeability values of PLA and PLA/CNC films at different relative humidity conditions and a constant temperature of 23°C. 158

Table 4.13 Predicted and experimental shelf-life of crackers packaged in PLA and PLA/CNC films stored at various relative humidity conditions. 160

Table A.1 Stock temperature and mixing torque of PLA and its blends with CE 4400 as a function of time generated by a torque rheometer. 163

Table A.2 Stock temperature and mixing torque of PLA and its blends with CE 4468 as a function of time generated by a torque rheometer. 167

Table A.3 Molecular weights, zero-shear viscosity and crystallinity values of PLA chain-extended with CE 4468 in an internal mixer. 171

Table A.4 Effect of CE content on the crystallinity and failure mass of PLA films. 171

Table B.1 Effects of CNC addition and blending process on the transparency of PLA and PLA/CNC composite films. 173

Table B.2 Carboxyl indices using the intensities of reference peaks at 2994 cm^{-1} and 2945 cm^{-1} of PLA, PLA/1% CNC (DB) and PLA/1% CNC (MB) films. 175

Table C.1 Water vapor permeability (23°C and 85% RH), oxygen permeability (23°C and 0% RH) as well as crystallinity of PLA/CNC films. 177

Table C.2 Effects of CNC content and testing temperature on the WVP of PLA films at 85% RH. 177

Table C.3 Effects of CNC content and relative humidity (RH) on the WVP of PLA films at 23°C. 178

Table C.4 Effects of CNC addition and testing temperature on the OP of PLA films at 0% RH. 178

Table D.1 Moisture contents of crackers as a function of time recorded at 25°C and various storage relative humidity conditions. 180

Table D.2 Equilibrium moisture content values of crackers obtained experimentally and predicted by GAB equation at 25°C. 181

LIST OF FIGURES

Figure 2.1 Chemical structure of L-Lactic acid and D-Lactic acid. 17

Figure 2.2 Stereochemistry of lactide. 18

Figure 2.3 Typical viscosity vs shear rate curve. 22

Figure 2.4 Schematic diagram of separation of small and large molecules in GPC [48]. 30

Figure 2.5 Typical plot of zero-shear viscosities determined from the MFI data as a function of weight-average molecular weight of chain extended PLA. 32

Figure 2.6 Typical curve of torque of neat PLA as a function of time generated by a torque rheometer. 34

Figure 2.7 Schematic representation of a FTIR instrument. 36

Figure 2.8 Typical FTIR spectrum of PLA. 37

Figure 2.9 Generalized reaction mechanism of a multifunctional epoxy chain extender with the hydroxyl and carboxyl end groups in PLA. 38

Figure 2.10 Schematic representation of a differential scanning calorimeter [57]. 40

Figure 2.11 Falling dart impact tester [59]. 41

Figure 2.12 Chemical structure of CNC [60]. 42

Figure 2.13 Cellulose nanocrystal agglomerations. 44

Figure 2.14 Solvent-casting process [77]. 45

Figure 2.15 Liquid-feeding process [72]. 47

Figure 2.16 Light microscope [80]. 49

Figure 2.17 Typical spectra of PLA's light transmission as a function of its wavelength generated by a UV-Vis spectrophotometer. 50

Figure 2.18 Isostatic method of permeability measurement. 52

Figure 2.19 Plot of flow rate as a function of time generated by the isostatic method. 53

Figure 2.20 Quasi-isostatic method of water vapor permeability measurement. 54

Figure 2.21 Plot of flow rate as a function of time generated by the quasi-isostatic method.....55

Figure 2.22 Overview of the shelf-life determination process. 56

Figure 2.23 Typical moisture sorption isotherm.....58

Figure 2.24 A typical plot of the experimental values for a_w/EMC as a function of a_w. 61

Figure 2.25 Plot of moisture content as a function of time for shelf-life determination. 65

Figure 4.1 Typical curves of torque and stock temperature of neat PLA as a function of time generated by a torque rheometer. 99

Figure 4.2 Typical curves of stock temperature and mixing torque of PLA blends with CE 4468 [(a) and (c)] as well as CE 4400 [(b) and (d)] as a function of time generated by a torque rheometer. 100

Figure 4.3 Generalized reaction mechanism of a multifunctional epoxy chain extender with the hydroxyl and carboxyl end groups in PLA.....103

Figure 4.4 Infrared spectra of PLA, CE 4468, and PLA blended with different CE contents in an internal mixer. Absorbance in the y-axis is in arbitrary units.....104

Figure 4.5 Generalized reaction mechanism of a multifunctional epoxy chain extender with the hydroxyl and carboxyl end groups in PLA.....106

Figure 4.6 End torque of PLA chain-extended with low (CE 4468) and high (CE 4400) epoxy equivalent weight multifunctional epoxies as a function of their contents.....107

Figure 4.7 Zero-shear viscosities as a function of weight-average molecular weights of PLA/CE blends processed in an internal mixer. Insert shows the viscosity vs. molecular weight trend of these blends at low zero-shear viscosity values. 111

Figure 4.8 Effect of CE content on the crystallinity of PLA processed in an internal mixer. 112

Figure 4.9 Effect of CE content on the crystallinity of PLA films. 114

Figure 4.10 Typical residence time distribution curves of PLA with (a) 0.25% CE and (b) 0.5% CE. 115

Figure 4.11 Effect of CE content on the failure mass of PLA films.....117

Figure 4.12 Light microscope of (a) PLA, (b) PLA/1% CNC (DB) and (c) PLA/1% CNC (MB) films. 119

Figure 4.13 Effects of CNC addition and blending process on the transparency of PLA and PLA/CNC composite films.....119

Figure 4.14 (a) Non-isothermal thermograms, (b) Non-isothermal DTG and (c) Isothermal thermograms of PLA and PLA/CNC composite films. 122

Figure 4.15 Proposed β-C-H transfer mechanism for degradation of PLA. 130

Figure 4.16 Infrared spectra of PLA and PLA/CNC composite films prepared by direct dry (DB)- and melt-blending (MB) processes. 131

Figure 4.17 Carboxyl indices using the intensities of reference peaks at 2994 cm^{-1} and 2945 cm^{-1} of PLA, PLA/1% CNC (DB) and PLA/1% CNC (MB) films. 134

Figure 4.18 Effect of CNC content on the WVP (23°C and 85% RH) and OP (23°C and 0% RH) of PLA films. 137

Figure 4.19 WVP and OP of PLA and PLA/CNC nanocomposite films as a function of crystallinity obtained from (a) 1st heat and (b) 2nd heat. In the 1st heat the crystallinities were 4.5 ± 0.1; 5.1 ± 1.0; 5.4 ± 0.8; and 6.2 ± 0.2 whereas in the 2nd heat they were 1.5 ± 0.4; 2.8 ± 0.4; 4.5 ± 0.4; and 4.7 ± 0.4 for PLA with 0; 0.5; 1; and 2% CNC, respectively. 138

Figure 4.20 Digital microscope images of PLA films with various CNC contents of (a) 0.5%; (b) 1%; and (c) 2% as well as (d) CNC agglomeration frequency as a function of their diameters in the nanocomposite films.....141

Figure 4.21 Effect of CNC content on the transparency of PLA films.....143

Figure 4.22 Visual clarity of PLA and PLA/CNC nanocomposite films. 143

Figure 4.23 Effects of (a) CNC content and testing temperature on the WVP of PLA films at 85% RH and (b) CNC addition and testing temperature on the OP of PLA films at 0% RH.....145

Figure 4.24 WVP and OP of PLA and nanocomposite films at various temperatures as a function of percent crystallinity obtained from 1st heat [(a) and (b)] and 2nd heat [(c) and (d)]. 146

Figure 4.25 Effects of CNC content and RH on the (a) WVTR and (b) WVP of PLA films at 23°C. 150

Figure 4.26 WVP of PLA and PLA/CNC nanocomposite films tested at various relative humidity conditions as a function of films' crystallinity obtained from (a) 1st heat and (b) 2nd heat. 151

Figure 4.27 Moisture contents of crackers as a function of time recorded at 25°C and various storage relative humidity conditions. 153

Figure 4.28 Moisture sorption isotherm of crackers at 25°C. 154

Chapter 1

INTRODUCTION

1.1 Introduction

Over the past few years, environmental issues such as pollution, depletion of natural resources and solid waste disposal have become major global concerns [1]. A specific concern is the field of packaging, which produces great amounts of non-degradable plastic waste that is accumulated in landfills and oceans, causing climate change and harm to terrestrial as well as aquatic life [2]. In fact, 63% of the current plastic waste comes from packaging applications of which less than 14% is recyclable [2]. To circumvent this growing environmental problem caused by non-degradable petroleum-based plastics, research efforts have focused on the development of alternative packaging materials that are compostable and biodegradable [1].

Poly(lactic acid) (PLA) is one of the most extensively researched compostable and biodegradable aliphatic polyester because of its potential to replace conventional petroleum-based polymers for medical and other industrial applications [1]. It has several desirable properties such as high stiffness, reasonable strength, excellent flavor and aroma barrier, as well as good grease and oil resistance compared to conventional petroleum-based polymers [3-8]. Despite these attributes, PLA has several drawbacks such as brittleness, poor water vapor and moderate oxygen barrier properties as well as and processing difficulties due to its insufficient melt strength and low thermal stability, leading to a narrow processing window [3-8]. PLA's inadequate melt strength poses challenges for its manufacture into flexible film through processes that require stretching or orientation, such as blown and cast film extrusion, as well as foaming whereas its brittleness leads to film rupture and failure in many packaging performance tests. Moreover, the barrier properties

of a film to water vapor and gas are critical properties for food packaging materials due to their role in food's deteriorative reactions and microbial growth. Therefore, it is of paramount importance to improve PLA's melt strength, brittleness as well as water and gas barrier properties in order for it to be used as a flexible packaging material.

Firstly, chain extenders (CE) or melt strength enhancers such as multifunctional epoxies, 1,4-butane di-isocyanate, and hexamethylene di-isocyanate among others are often blended with PLA matrix to increase its melt strength [9-16]. These additives increase PLA's molecular weight by introducing chain branching, thereby increasing its shear and elongational viscosities. This leads to improved melt strength which facilitates the blown film extrusion process and other processes such as casting and foaming [9-16].

In our previous work, PLA films were successfully manufactured without any CE by controlling the melt rheology through processing temperature and other extrusion-blown processing conditions such as the processing speed ratios and internal air pressures [3]. However, these blown films teared easily due to their brittleness and did not survive several packaging performances tests such as oxygen permeation. Consequently, chain extenders are needed in the formulations to increase PLA's ductility [15].

Although blending PLA with the afore-mentioned additives increases the ductility of films used in several packaging applications, they also have various drawbacks. For example, multifunctional epoxies have not been approved for food-grade applications by the United States Food and Drug Administration (FDA) [3,17]. On the other hand, di-isocyanates are under scrutiny due to their toxicity, risk of occupational hazards, and their impact on the inherent biodegradability of PLA [3,18].

Recently, new FDA approved food-grade multifunctional epoxies with varying reactivities (low and high epoxy equivalent weight) have been developed. Unfortunately, limited studies have been reported on their use to melt strengthen PLA and reduce its brittleness. Therefore, *this study investigated the effectiveness and efficiency of these multifunctional additives in chain extending and branching PLA, improving its processability through the blown film extrusion process and reducing the brittleness of PLA films*.

Secondly, crystallization is one of the ways to improve PLA's barrier properties because of the tortuosity effect created by impermeable crystallites [4,5,19,20]. Orientation of the film through drawing and annealing during processing can increase PLA's crystallinity. For instance, in one study the crystallinity of PLA was increased through annealing at 130^{o}C for 10 minutes resulting in 50% reduction in water permeability compared to its amorphous counterpart [20]. Additionally, PLA's crystallinity can also be increased through incorporation of organic and inorganic nucleating agents. However, natural and bio-based additives are preferred in order to preserve the inherent biodegradability of PLA.

Cellulose nanomaterials (CNs) such as cellulose nanocrystals (CNCs) and cellulose nanofibers (CNFs) are recently gaining interest amongst researchers as natural and bio-based nucleating agents [21-27]. Although, well-dispersed CNs can increase PLA's crystallinity, their dispersion into PLA matrix is a challenge. CN particles tend to agglomerate due to their high surface area to volume ratio when the aqueous medium that they are produced in is eliminated by freeze or spray drying. Moreover, CN particles are difficult to disperse in non-polar polymers due to their high polarity and strong hydrogen bonding forces [28]. Various approaches such as solvent-casting and melt-compounding have been investigated to disperse cellulose nanomaterials into a polymer matrix [21-33].

Recently, Pei and co-workers investigated the dispersion of chemically modified CNCs into a PLA matrix [27]. In this work, a predetermined amount of silylated CNC (SCNC) was dispersed in an organic solvent and mixed with a previously prepared solution of PLA. The mixture was stirred, cast on a glass petri dish and dried to form PLA/SCNC nanocomposite films. High degree of SCNCs' dispersion was achieved into the PLA matrix due to fiber treatment that reduced agglomeration. The PLA/1% SCNC films had higher crystallinity compared to the PLA films, leading to a 27% increase in tensile modulus. However, the elongation at break of the PLA/1% SCNC films was significantly lower than that of PLA films due to the poor interfacial adhesion between the PLA and nanoparticles resulting in insufficient stress transfer [27]. In another study, Fortunati and co-workers reported a reduction of 34% in water vapor permeability of PLA when 1% CNC modified with an acid phosphate ester of ethoxylated nonylphenol was added to the PLA matrix using the solvent casting technique [21].

PLA/cellulose nanofiber (CNF) composites have also been prepared using a two-step process [28]. The solvent casting technique was used to prepare a master batch, which was then crushed, diluted and dry-mixed with PLA, melt-compounded in an extruder, pelletized and finally injection molded. The PLA/5% CNF samples prepared by the described technique had 24% and 21% increase in tensile modulus and tensile strength, respectively. Nonetheless, large standard deviation in the values of tensile modulus reported indicated a non-homogenous dispersion of CNFs in the PLA matrix [28].

Another approach to disperse CNFs into a PLA matrix has been examined by other investigators who prepared aqueous suspensions of CNF in a slurry of plasticizer, acetone and water [29]. The prepared suspension was melt-compounded with PLA pellets in a twin-screw extruder equipped with a liquid feeder and vents for removal of acetone and water. The obtained

extrudate was then compression molded into films for testing of mechanical properties. The results indicated that addition of only 1% CNF increased the elongation at break of the plasticized PLA by 27% due to the slippery effect of CNFs coated with plasticizer and the crazing phenomenon attributed to the presence of CNFs [29].

In a more recent study, PLA and 1% cellulose nanocrystal as well as chitin nanocrystal (ChNC) nanocomposite films were obtained using liquid feeding in a vented twin-screw extruder prior to compression molding [30]. A plasticizer [20% triethyl citrate (TEC)] was used to liquid feed the two types of nanocrystals while acting as a processing aid to enhance their dispersion into the PLA matrix. This liquid feeding technique resulted in moderate dispersion of CNCs as well as ChNCs in the PLA matrix, with some amount of agglomerations still present for both types of nanocrystals. However, significant increase in the yield strength (316% for CNCs and 478% for ChNCs) as well as Young's modulus (267% for CNCs and 300% for ChNCs) were obtained for the nanocomposite films compared to their counterpart PLA/TEC films without any nanocrystals [30].

The above-described liquid feeding approach has also been successfully used to produce plasticized PLA/polybutylene adipate-co-terephthalate (PBAT) blown films with talc and ChNC [31]. In this study, a masterbatch of PLA, 5% ChNCs and 20% glycerol triacetate plasticizer (GTA) was prepared using the previously described liquid feeding technique in a vented twin-screw extruder. This masterbatch was diluted with PLA and PBAT and mixed with talc to produce films with 1% ChNCs, 6% talc, 9% GTA, 25% PBAT and 59% PLA. The final composites were then blown into films and evaluated for optical, thermal, mechanical and barrier properties amongst others. The researchers found that addition of ChNCs increased the viscosity and melt strength of PLA, thus aiding in the blown film processing of the films. Moreover, the addition of 1% ChNCs

increased the tensile modulus, tensile strength, tear resistance and puncture resistance of the film by 74%, 64%, 80% and 300%, respectively. In contrast, the nanocomposite films did not have improved thermal stability or barrier performance compared to their reference films [31].

Processing aids such as polyvinyl alcohol (PVOH) have also been used to improve the dispersion of CNCs into the PLA matrix [32]. Enhanced dispersion of CNCs into PLA can be achieved by reacting the hydroxyl groups in PVOH with the hydrophilic CNCs and the vinyl acetate groups with the hydrophobic PLA. In one study, PLA/CNC nanocomposites were manufactured using PVOH by two different feeding methods: dry feeding PVOH/CNC pellets with PLA and liquid feeding PVOH/CNC suspension into molten PLA during extrusion in a vented twin-screw extruder. The composite materials were then compression-molded into films prior to testing for dispersion and mechanical performance. The results showed that poor interfacial adhesion between PLA and PVOH resulted in phase separation with a continuous PLA phase and discontinuous PVOH phase, irrespective of the feeding method. Furthermore, the CNCs were dominantly present in the PVOH phase due to their higher affinity to PVOH than PLA. Consequently, the nanocomposite films had poor mechanical properties due to the immiscibility of PLA and PVOH resulting in phase separation [32].

Although good nanoparticle dispersion into PLA matrix was reported by different solvent casting and liquid feeding techniques, these have various drawbacks [21,27-29,33]. Solvent blending and casting techniques require drying of films, which add more energy consumption in film manufacture, and solvent disposal could also be an issue for this process because some solvents may be harmful to workers and the environment. Additionally, trace amounts of solvents can remain in the produced films, which could pose regulatory compliance issues. The residual

solvent can also act as a plasticizer, thereby reducing the strength, stiffness and barrier properties of the produced films [34].

Due to the drawbacks of solvent-based mixing techniques, alternative approaches to manufacture PLA/CNC composite films with improved barrier properties should be considered. Melt-processing is one of the important solvent-free processing methods for introducing nanocomposite materials in the market where high-volume production is required [35]. However, limited studies have been reported on improving the barrier performance of PLA using melt-processing [25,26]. In one such study employing melt-processing, improvements of 20% and 60% in water vapor and oxygen barrier of extrusion-cast PLA films were reported when 1% cellulose nanocrystals derived from coffee silverskin were melt-mixed with PLA in a twin-screw extruder [25]. Similar results have been reported for PLA/CNC-based cast films produced by a single-step reactive extrusion process [26].

Due to the limited research on improving the barrier performance of PLA using solvent-free approaches, alternative solvent-free approaches to manufacture PLA/CNC composite films should be considered. In this work, two solvent-free approaches of adding CNCs into the PLA matrix were examined. The first approach was to melt-blend CNCs with PLA in a three-piece internal batch mixer to maximize homogenous dispersion of CNCs into the matrix while minimizing the loss of CNCs that may occur in high volume mixers [36]. Although this technique eliminates the use of solvents, it is a time-consuming batch process that subjects heat-sensitive PLA to additional thermal history. Therefore, a second approach employing conventional direct dry-blending was also examined. In this method, CNCs were directly added to the PLA matrix during conventional dry-compounding. Compared with melt-blending, this less time-consuming approach minimizes exposure of PLA to high temperature.

To the best of our knowledge, these investigated solvent-free blending approaches have not been previously used to manufacture PLA/CNC composite blown films. Consequently, *the performance of PLA/CNC blown films prepared by the melt-blending and direct dry-blending techniques in terms of particle dispersion, optical, thermal, molecular weight and barrier properties were compared in this study to identify the most effective blending approach*.

The barrier properties of a film to moisture and gas are critical properties for food packaging materials due to their role in food's deteriorative reactions and microbial growth [37-39]. Moisture gain or loss in food products can cause defects such as freezer burn, non-enzymatic browning, starch retrogradation, mold and microbial growth, as well as flavor, color and textural changes, amongst others [37,38]. For instance, dry foods (e.g., crackers) and moist products (e.g., cake) are often susceptible to textural changes such as sogginess and brittleness due to moisture gain and loss, respectively, so they require a package that can provide some moisture barrier. Oxygen-sensitive food products are susceptible to oxidative reactions resulting in loss of nutrients and other undesirable changes in flavor, appearance as well as texture [37,38]. These products need packages that provide some oxygen barrier. Additionally, it is well-documented that different conditions of temperature and relative humidity (RH) strongly influence both the barrier properties of films and the food quality during distribution and storage [37]. Therefore, once a new plastic film for food packaging applications is developed, it is of utmost importance to characterize its barrier properties in different environment conditions in order to assess its potential in extending food shelf-life throughout the supply chain.

Despite known effects of testing environmental conditions on the barrier performance of materials, no research has been carried out to examine the influence of temperature and RH on the barrier properties of nanocellulose-based PLA blown-films with various CNC contents. Therefore,

the influence of CNC addition level and environmental testing conditions on the barrier properties of PLA/CNC blown films as well as their thermal and optical properties were studied in this work. Moreover, *the potential of the manufactured nanocomposite films in extending the shelf-life of moisture-sensitive food products were assessed*.

1.2 Objectives

The main goal of this research project is to gain fundamental understanding of nanoscale dispersion and distribution of CNCs into a PLA matrix in order to develop a nanocomposite film with improved barrier performance through solvent-free processing methods for food packaging applications. To achieve this objective, the following specific objectives were proposed:

1. Investigate the effectiveness and efficiency of two food-grade multifunctional epoxies with varying reactivities in chain extending and branching PLA, improving its processability through the blown film extrusion process and improving the ductility of PLA films.

2. Compare the performance of PLA/CNC blown films prepared by the melt-blending and direct dry-blending techniques in terms of particle dispersion, optical, thermal, molecular weight and barrier properties to identify the most effective blending approach.

3. Evaluate the effects of CNC addition level and environmental testing conditions on the barrier properties of PLA/CNC films as well as their thermal and optical properties. The ultimate goal of this study is to gain an in-depth understanding of the mechanisms governing improvement in barrier properties, to model and to establish relationships

between environmental testing conditions and barrier properties as well as to optimize the CNC content.

4. Assess the effectiveness of manufactured nanocomposite films in extending the shelf-life of moisture-sensitive food products.

1.3 Hypothesis

This research is intended to test the hypothesis that the addition of highly crystalline CNC nucleating agents into a PLA matrix will lead to nanocomposite films with improved barrier properties and extended shelf-life of packaged food.

1.4 Structure of Dissertation

The first chapter of the thesis introduces the rationale of this research. A background on poly(lactic acid) (PLA), cellulose nanocrystals (CNC), and current approaches used to incorporate CNC into a PLA are reviewed in Chapter 2. The experimental methods, including material specifications, equipment, sample manufacturing and property evaluation are described in Chapter 3. The results of the effects of blending techniques, CNC and two food-grade multifunctional epoxy addition levels and environmental testing conditions on the performance of PLA/CNC blown films, as well as the manufactured films' effectiveness in extending the shelf-life of moisture-sensitive food products are discussed in Chapter 4. Chapter 5 gives the summary of the findings inferred from the experimental data and proposed future work.

REFERENCES

REFERENCES

1. Muller, J., Gonzalez-Martinez, C., and Chiralt, A., Combination of poly(lactic) acid and starch for biodegradable food packaging, Materials, 10(8): 952 (2017).

2. Parker, L., Fast facts about plastic pollution, Retrieved from National Geographic: https://news.nationalgeographic.com. Accessed in October, 2019.

3. Karkhanis, S.S., Stark, N.M., Sabo, R.C., and Matuana, L.M., Blown film extrusion of poly(lactic acid) without melt strength enhancers, Journal of Applied Polymer Science, 134(34): 45212 (2017).

4. Karkhanis, S.S., Stark, N.M., Sabo, R.C., and Matuana, L.M., Performance of poly(lactic acid)/cellulose nanocrystal composite blown films processed by two different compounding approaches, Polymer Engineering and Science, 58(11): 1965-1974 (2017).

5. Karkhanis, S.S., Stark, N.M., Sabo, R.C., and Matuana, L.M., Water vapor and oxygen barrier properties of extrusion-blown poly(lactic acid)/cellulose nanocrystals nanocomposite films, Composites Part A: Applied Science and Manufacturing, 114: 204-211 (2018).

6. Vijayarajan, S., Selke, S.E.M., and Matuana, L.M., Continuous blending approach in the manufacture of epoxidized soybean-plasticized poly(lactic acid) sheets and films, Macromolecular Materials and Engineering, 299(5): 622-630 (2014).

7. Xing, C. and Matuana, L.M., Epoxidized soybean oil-plasticized poly (lactic acid) films performance as impacted by storage, Journal of Applied Polymer Science, 133(12): 43201 (2016).

8. Matuana, L.M., Karkhanis, S.S., Stark, N.M., and Sabo, R.C., Cellulose Nanocrystals as barrier performance enhancer of extrusion-blown PLA films for food applications, Biotech, Biomaterials and Biomedical - TechConnect Briefs, 3: 1-4 (2016).

9. Mallet, B., Lamnawar, K., and Maazouz, A., Improvement of blown film extrusion of poly(lactic acid): structure-processing-properties relationships, Polymer Engineering and Science, 54(4): 840-857 (2014).

10. Mallet, B., Lamnawar, K., and Maazouz, A., Compounding and melt strengthening of poly(lactic acid): shear and elongational investigations for forming process, Key Engineering Materials, 554-557: 1751-1756 (2013).

11. Mihai, M., Huneault, M.A., and Favis, B.D., Rheology and extrusion foaming of chain-branched poly(lactic acid), Polymer Engineering and Science, 50(3): 629-642 (2010).

12. Pilla, S., Kim, S.G., Auer, G.K., Gong, S., and Park, C.B., Microcellular extrusion-foaming of polylactide with chain-extender, Polymer Engineering and Science, 49(8): 1653-1660 (2009).

13. Di, Y., Iannace, S., Di Maio, E., and Nicolais, L., Reactively modified poly (lactic acid): properties and foam processing, Macromolecular Materials and Engineering, 290(11): 1083-1090 (2005).

14. Tuominen, J., Kylmä, J., and Seppälä, J., Chain extending of lactic acid oligomers. 2. increase of molecular weight with 1,6-hexamethylene diisocyanate and 2,2′-bis(2-oxazoline), Polymer 43(1): 3-10 (2002).

15. Dong, W., Zou, B., Yan, Y., Ma, P., & Chen, M., Effect of chain-extenders on the properties and hydrolytic degradation behavior of the poly(lactide)/poly(butylene adipate-co-terephthalate) blends, International Journal of Molecular Sciences, 14(10): 20189-20203 (2013).

16. Jaszkiewicz, A., Bledzki, A. K., & Meljon, A., Online observations and process analysis of chain extended polylactides during injection moulding, Polymer Degradation and Stability, 101(1): 65-70 (2014).

17. United States Department of Agriculture, Retrieved from USDA economic research service: https://www.ers.usda.gov. Accessed in October, 2016.

18. Brun, E., Expert Forecast on Emerging Chemical Risks Related to Occupational Safety and Health, Office for Official Publications of the European Communities, Luxemburg, pp. 33 (2009).

19. Liu, Y. and Matuana, L.M., Surface texture and barrier performance of poly(lactic acid)-cellulose nanocrystal extruded-cast films, Journal of Applied Polymer Science, 136(22): 47594 (2019).

20. Duan, Z. and Thomas, N.L., Water vapour permeability of poly(lactic acid): crystallinity and the tortuous path model, Journal of Applied Physics, 115: 064903 (2014).

21. Fortunati, E., Peltzer, M., Armentano, I., Torre, L., Jimenez, A., and Kenny, J. M., Effects of modified cellulose nanocrystals on the barrier and migration properties of PLA nano-biocomposites, Carbohydrate Polymers, 90(2): 948-956 (2012).

22. Espino-Pérez, E., Bras, J., Ducruet, V., Guinault, A., Dufresne, A., and Domenek, S., Influence of chemical surface modification of cellulose nanowhiskers on thermal, mechanical, and barrier properties of poly(lactide) based bionanocomposites, European Polymer Journal, 49: 3144-3154 (2013).

23. Sanchez-Garcia, M.D. and Lagaron, J.M., On the use of plant cellulose nanowhiskers to enhance the barrier properties of polylactic acid, Cellulose, 17: 987-1004 (2010).

24. Yu, H.Y., Zhang, H., Song, M.L., Zhou, Y., Yao, J., and Ni, Q.Q., From cellulose nanosperes, nanorods to nanofibers: various aspect ratio induced nucleation/reinforcing effects on polylactic acid for robust-barrier food packaging, ACS Applied Materials and Interfaces, 9(50): 43920-43938 (2017).

25. Sung, S.H., Chang, Y., and Han, J., Development of polylactic acid nanocomposite films reinforced with cellulose nanocrystals derived from coffee silverskin, Carbohydrate Polymers, 169: 495-503 (2017).

26. Dhar, P., Gaur, S.S., Soundararajan, N., Gupta, A., Bhasney, S.M., Milli, M., Kumar, A., and Katiyar, V., Reactive extrusion of polylactic acid/cellulose nanocrystal films for food packaging applications: influence of filler type on thermomechanical, rheological, and barrier properties, Industrial and Engineering Chemistry Research, 56(16): 4718-4735 (2017).

27. Pei, A., Zhou, Q., and Berglund, L.A., Functionalized cellulose nanocrystals as biobased nucleation agents in poly(l-lactide) (PLLA) - crystallization and mechanical property effects, Composites Science and Technology, 70(5): 815-821 (2010).

28. Jonoobi, M., Harun, J., Mathew, A.P., and Oksman, K., Mechanical properties of cellulose nanofiber (CNF) reinforced polylactic acid (PLA) prepared by twin screw extrusion, Composites Science and Technology, 70(12): 1742-1747.

29. Herrera, N., Mathew, A.P., and Oksman, K., Plasticized polylactic acid/cellulose nanocomposites prepared using melt-extrusion and liquid feeding: mechanical, thermal and optical properties, Composites Science and Technology, 106: 149-155 (2015).

30. Herrera, N., Salaberria, A.M., Mathew, A.P., and Oksman, K., Plasticized polylactic acid nanocomposite films with cellulose and chitin nanocrystals prepared using extrusion and compression molding with two cooling rates: Effects on mechanical, thermal and optical properties, Composites Part A: Applied Science and Manufacturing, 83: 89-97 (2016).

31. Herrera, N., Roch, H., Salaberria, A.M., Pino-Orellana, M.A., Labidi, J., Fernandes, S.C., Radic, D., Leiva,A., and Oksman, K., Functionalized blown films of plasticized polylactic acid/chitin nanocomposite: Preparation and characterization, Materials and Design, 92: 846-852 (2016).

32. Bondeson, D. and Oksman, K., Polylactic acid/cellulose whisker nanocomposites modified by polyvinyl alcohol, Composites Part A: Applied Science and Manufacturing, 38: 2486-2492 (2007).

33. Shi, Q., Zhou, C., Yue, Y., Guo, W., Wu, Y., and Wu, Q., Mechanical properties and in vitro degradation of electrospun bio-nanocomposite mats from PLA and cellulose nanocrystals, Carbohydrate Polymers, 90(1): 301-308 (2012).

34. Rhim, J.W., Mohanty, A.K., Singh, S.P., and Ng, P.K., Effect of the processing methods on the performance of polylactide films: thermocompression versus solvent casting, Journal of Applied Polymer Science, 101(6): 3736-3742 (2006).

35. Oksman, K., Aitomaki, Y., Mathew, A.P., Siqueira, G., Zhou, Q., Butylina S., Tanpichai, S., Zhou, X., Hooshmand, S., Review of the recent developments in cellulose nanocomposite processing, Composites Part A: Applied Science and Manufacturing, 83: 2-18 (2016).

36. Faruk, O. and Matuana, L.M., Nanoclay reinforced HDPE as a matrix for wood-plastic composites, Composites Science and Technology, 68(9): 2073-2077 (2008).

37. Siracusa V., Food packaging permeability behaviour: a report, International Journal of Polymer Science, 2012: 1-11 (2012).

38. Roudaut, G. and Debeaufort, F., Chemical deterioration and physical instability of food and beverages, Woodhead Publishing, Oxford, pp. 143-185 (2010).

39. Almenar, E., Weathering the technological changes of modified atmosphere packaging, Retrieved from Packaging Digest: https://www.packagingdigest.com/food-packaging/weathering-technological-changes-modified-atmosphere-packaging. Accessed in September, 2020.

Chapter 2

BACKGROUND AND LITERATURE REVIEW

2.1 Introduction

Consistent with the scope of this study, a background and literature review on the current approaches used to manufacture composite films of poly(lactic acid) (PLA) with chain extenders (CE) and/or cellulose nanomaterials (CNCs) are presented in this chapter. The review focuses on the techniques used to incorporate and disperse these additives (CEs and CNCs) into the PLA matrix and their effect on PLA's properties. Additionally, the potential use of composite films to extend the shelf-life of moisture-sensitive food products is also discussed.

2.2 Poly(lactic acid)

Poly(lactic acid) is a biobased, biodegradable and compostable thermoplastic derived from renewable resources such as corn, sugar beets and rice [1]. It exhibits reasonable strength, high stiffness, good heat sealability, excellent flavor and aroma barrier, as well as good grease and oil resistance [2-4].

2.2.1 Synthesis of PLA

Lactic acid, the basic building block of PLA, is a simple chiral molecule which exists as two optically active enantiomers, L and D-lactic acid (Figure 2.1). It can be converted into three types of cyclic dimmers: L-lactide, D-lactide and meso-lactide (Figure 2.2).

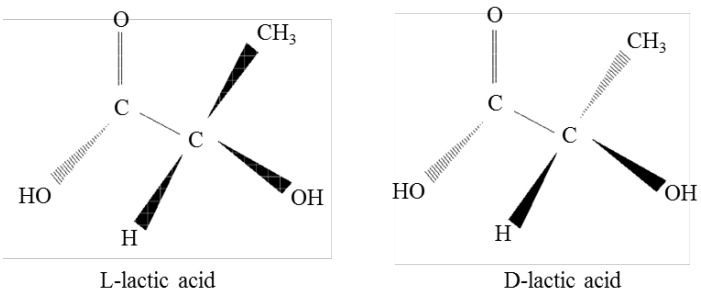

Figure 2.1 Chemical structure of L-Lactic acid and D-Lactic acid.

Lactic acid is produced by fermentative or chemical synthesis [5]. The most popular route for producing lactic acid is by bacterial fermentation using genetically modified Lactobacillus to convert sugar and starches into lactic acid [6,7]. Other routes for chemical synthesis of lactic acid include base-catalyzed degradation of sugars, oxidation of propylene glycol, reaction of acetaldehyde, carbon monoxide, and water at high temperature and pressure, hydrolysis of chloropropionic acid, and nitric acid oxidation of propylene, among others [8].

PLA is usually produced from lactic acid by two methods: (1) direct polycondensation of lactic acid or (2) ring opening polymerization (ROP) of lactide. The direct polycondensation method requires higher reaction times and entails the use of solvent to produce low to intermediate molecular weight PLA. Conversely the ROP method uses catalyst and produces PLA with controlled molecular weight [6,9]. Cargill Dow LLC is one of the manufacturers of PLA which has exploited the ROP of lactide to produce about 300 million pounds of NatureWorks PLA per year [10].

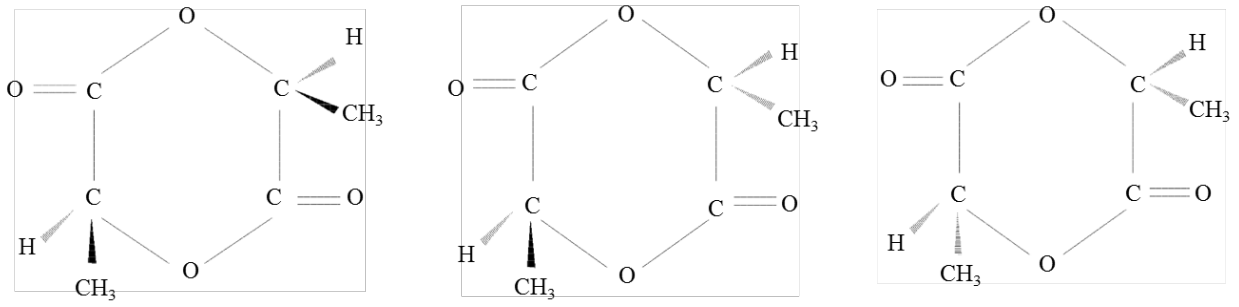

Figure 2.2 Stereochemistry of lactide.

The ROP of lactide can be carried out using anionic, cationic or co-ordination mechanisms [11,12]. Anionic mechanisms often result in back-biting reactions and other side reactions due to the highly active anionic reactants. Moreover, cationic mechanisms result in undesirable side chain reactions due to nucleophilic attacks on the activated monomers or propagating species. These mechanisms result in polymer chains with low molecular weight and low crystallinity. Conversely, coordination polymerization with metal catalysts such as tin (II) octoate, result in high molecular weight polymer chains with a high degree of crystallinity. Consequently, coordination polymerization is the preferred method for the industrial production of PLA [13].

2.2.2 Properties of PLA

The thermal, rheological, mechanical and barrier properties of PLA vary with the degree of crystallinity. The degree of crystallinity of PLA can be controlled by adjusting the relative amounts of L and D-lactide stereoisomers in the polymer. Generally, PLA made from more than 93% L-lactic acid is semi-crystalline while PLA made from 50-93% L-lactic acid is amorphous [14]. Semi-crystalline PLA has higher glass transition and melting temperatures than amorphous PLA. It also tends to have better mechanical, barrier and rheological properties.

2.2.2.1 Thermal properties

PLA has a glass transition temperature between 40 and 70^{o}C and a melt temperature between 130 and 180^{o}C [15]. Thermal properties of PLA vary with the L-lactide content; higher L-lactide content increases T_m and T_g [16].

2.2.2.2 Mechanical properties

PLA has mechanical properties comparable to those of conventional polymers. It has an elastic modulus between 3000-4000 MPa and a tensile strength between 50-70 MPa (Table 2.1) [17]. However, PLA has low impact strength compared to other petroleum-based plastics (Table 2.1). PLA's impact strength increases with increasing molecular weight and crystallinity [18]. It is also highly sensitive to notching and material processing. The notched Izod impact resistance of semi-crystalline PLA ranges from 3-7 kJ/m^2 while the unnotched Izod impact resistance ranges from 18-35 kJ/m^2 [17].

2.2.2.3 Barrier properties

Barrier properties of packaging materials determine the ability of the material to obstruct the flow of permeants such as water vapor, oxygen (O_2) and carbon dioxide (CO_2). These properties are particularly useful in determining the applications of polymers in food packaging. For instance, a dry food product is more likely to be packaged in a plastic that is a good barrier to water vapor to prevent water absorption and consequently sogginess of the product.

Barrier properties of materials are generally characterized by parameters such as permeability, diffusivity and solubility. Higher permeability of a material decreases its barrier properties. Auras and co-workers reported that PLA has O_2 and CO_2 permeability coefficients

comparable to those of polyethylene terephthalate (PET), but lower than polystyrene (PS) [19]. A comparison of PLA's barrier properties with those of other petroleum-based polymers is listed in Table 2.1.

Table 2.1 Comparison of PLA properties with other petroleum-based polymers [19-22].

Properties	PLA	PET	PS	PP
T_g (^{0}C)	55	75	105	-10
Density (g/cc)	1.24	1.33	1.05	0.9
Tensile Strength at Break (MPa)	53.09	54.47	44.82	31.03
Tensile Modulus (MPa)	3447	2758	2896	896
% Elongation	6	130	7	120
Gardner impact (kg-cm)	0.58	3.23	5.18	8.06
Water vapor permeability at 23^{o}C (10^{-13} kg-m/m^2-s-Pa)	80-360	110	670	225
Oxygen permeability at 25^{o}C, 70% RH (10^{-17} kg-m/m^2-s-Pa)	0.121	0.0188	27	498
Carbon dioxide permeability at 25^{o}C, 0% RH (10^{-17} kg-m/m^2-s-Pa)	2.77	0.173	15.5	1080

2.2.2.4 Rheological properties

Rheology is the study of flow and deformation of matter. It is extremely important to understand the flow behavior (or rheology) of a plastic because plastics are usually shaped into articles in their molten state. Generally, flow properties of a plastic are measured by measuring their shear viscosity. Shear viscosity of a fluid is defined as its resistance to flow when subjected to shear. The shear viscosity of plastics is molecular weight and temperature dependent; higher molecular weight increases the shear viscosity while higher temperature decreases it [23].

Figure 2.3 shows a typical curve for logarithmic shear viscosity vs logarithmic shear rate. At very low shear rates, the viscosity is independent of shear rate. This region of the graph is known as the Newtonian region. In contrast, the region where the viscosity varies with shear rate is known as the power-law region or the non-Newtonian region. The viscosity in the Newtonian region, at very low shear rates is known as the zero-shear viscosity (η_0) whereas the viscosity in the non-Newtonian region is known as the shear viscosity.

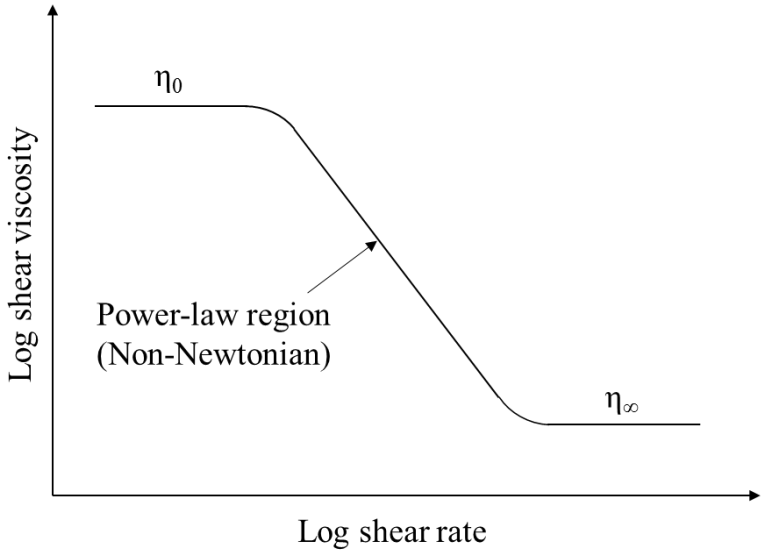

Figure 2.3 Typical viscosity vs shear rate curve.

Another important rheological parameter is the melt strength. Melt strength is the maximum force required to break an extruded strand and is related to shear and elongational viscosities of plastics. Elongational viscosity can be defined as the resistance of a fluid in extension. Generally, the elongational viscosity varies directly with the shear viscosity, i.e., as the shear viscosity increases, the elongational viscosity increases and vice versa (Equation 2.1). Moreover, higher shear and elongational viscosities result in higher melt strength.

$$\eta_e = \frac{9 \cdot (n+1)^2 \cdot (\Delta P_e)^2}{32 \cdot \eta_a \cdot \gamma_a^2} = \frac{9 \cdot (n+1)^2 \cdot (\Delta P_e)^2 \cdot \eta_a}{32 \cdot \tau_a^2} \qquad \text{(Equation 2.1)}$$

where η_e is the elongational viscosity, n is the flow behavior index, ΔP_e is the pressure drop at the capillary entrance, η_a is the apparent shear viscosity, τ_a is the apparent shear stress and γ_a is the apparent shear rate.

Melt strength is especially important in blown and cast film extrusion, as well as foaming. Low shear and elongational viscosities of PLA resulting in low melt strength limit its processing into films by blown and cast film extrusion [24]. In blown film extrusion, PLA's lack of melt strength hinders the formation of an inflatable polymer tube and leads to accumulation of the polymer near the die exit, known as melt sag. Researchers have blended PLA with additives [25-30] in order to increase its molecular weight and consequently melt strength, as described in section 2.4 of the literature review.

It is important to note that PLA is susceptible to hydrolytic and thermal degradations, which affect viscosity measurements and processing of PLA. It is hence crucial to dry the material before processing. Additional stabilizers may be added to prevent polymer degradation [23].

2.3 Improvement of PLA's properties

As mentioned previously, PLA has low impact strength, insufficient melt strength, poor water vapor and moderate oxygen barrier properties. These drawbacks limit PLA's in the flexible packaging industry. Firstly, PLA's low impact strength and insufficient melt strength can be overcome by altering its processing conditions, blending it with additives such as chain extenders, and/or by electron beam irradiation, amongst others. Secondly, PLA's barrier properties can often be improved by increased crystallinity through adjusting the processing conditions (stretching and cooling rates) or modifying the material formulations (use of organic and/or inorganic additives). In this study, food grade chain extenders and cellulose nanocrystals were selected to improve the melt strength and barrier properties of PLA, respectively [24-28].

2.4 Chain extenders (CEs)

Chain extenders are generally low molecular weight compounds that are used to increase the molecular weight of a polymer by introducing chain extension and/or branching. Increasing the molecular weight of a polymer leads to its increased viscosity and melt strength.

2.4.1 Commonly used CEs

Chain extenders are commonly used to increase the molecular weight of polycondensation polymers such as polyesters and polyamides with functional end groups. The chain extension occurs by reacting the end groups of polycondensation polymers with a bi- or multi-functional reactive compound [29,30]. Bi-functional chain extenders couple with two end groups per chain resulting in a linear, chain-extended polymer. High amounts of such bi-functional CEs are needed to get a significant increase in molecular weight of polycondensation polymers. On the other hand, multifunctional CEs lead to non-linear chain extension (branching), crosslinking and sometimes gelation depending on the functionality and additive concentration [29,30].

Polyester chains have -COOH and -OH end groups whereas polyamides have -NH_2 and -COOH end groups. Since CEs react with the end groups of polymers, some proposed chemistries for CEs used in polycondensation polymers include diepoxides, bis-oxazolines, diisocyanates, dianhydrides, diesters and carbodiimide [29,30].

Chain extension of polymerization polymers such as polyolefins and polystyrene are limited because of a lack of functional end groups. For polymers containing double bonds (example: polyethylene), some amount of branching and crosslinking is introduced during processing in the presence of radical generators such as peroxides and hydroxylamine esters.

Limited chain extension of polypropylene can be achieved by combining radical generators and multifunctional acrylates [29].

Since the focus of this dissertation is chain extension of PLA in particular, only CEs used in PLA are discussed in the following sub-sections.

2.4.2 Properties of CEs

The functional side group, molecular weight and weight equivalent of some commonly used CEs are listed in Table 2.2 [28,31,32].

Table 2.2 Properties of chain extenders [28,31,32].

Chain Extender	Functional side group	Molecular weight (Da)	Weight equivalent (g/mol)
Joncryl® 4368	Epoxy	6800	285
Joncryl® 4468	Epoxy	7250	310
Joncryl® 4400	Epoxy	7100	485
Joncryl® 3229	Maleic acid anhydride	8300	450
Pyromellitic dianhydride	Acid anhydride	218	
Hexamethylene diisocyanate	Isocyanate	168	

2.4.3 Use of CEs in PLA matrix

PLA has several desirable properties such as high stiffness, reasonable strength, excellent flavor and aroma barrier, as well as good grease and oil resistance compared to conventional petroleum-based polymers [24-28,33,34]. However, its applicability in flexible packaging is limited due to several drawbacks such as brittleness, poor water barrier properties, and processing difficulties due to its insufficient melt strength and low thermal stability, leading to a narrow processing window [35-38]. The low melt strength of PLA is attributed to the chain scission reactions that occur when it is subjected to shear and high temperature in an extruder [39]. These reactions lower its molecular weight and negatively impact molecular weight dependent properties such as shear and elongational viscosities, resulting in insufficient melt strength [39]. PLA's inadequate melt strength poses challenges for its manufacture into flexible film through processes that require stretching or orientation, such as blown and cast film extrusion, as well as foaming [40].

Chain extenders (CE) such as multifunctional epoxies, diisocyanates, and dianhydrides (as mentioned in section 2.4.1) are often blended with PLA matrix to increase its melt strength and reduce its brittleness [31,32,35-37,41-44]. These additives introduce chain branching and/or chain extension in PLA, thereby resulting in increased molecular weight, shear and elongational viscosities, melt strength and reduced brittleness. PLA's improved melt strength facilitates its processing through the blown film extrusion process and other processes such as casting and foaming [31,32,35-37,41-44].

2.4.4 Addition of CEs into PLA matrix

Several researchers have investigated the effect of CE addition into PLA matrix. Some such efforts are discussed in this section.

Attempts have recently been made to increase the melt strength of PLA using multi-functional epoxies for foaming applications. For example, Mihai and co-workers investigated the shear and elongational viscosities of extrusion foamed amorphous and semicrystalline PLA with the addition of up to 2% multi-functional styrene-acrylic-epoxy copolymer using carbon dioxide (CO_2) as a blowing agent [37]. They reported an increase in these viscosities and strain hardening of PLA with increasing chain extender content, irrespective of PLA's crystallinity. The chain extension reduced foam density of crystalline PLA from 65 to 36 kg/m^3 owing to better cell wall stabilization induced by chain branching at low blowing agent concentration (5% CO_2). Nevertheless, amorphous PLA foams were unaffected by chain extenders.

Multi-functional epoxies have also been used to melt strengthen PLA for blown film applications. Recently, Mallet and coworkers investigated various formulations of PLA with multi-functional epoxy, nucleating agents and plasticizers to melt strengthen and blow PLA film [35,36] They reported an increase in shear and elongational viscosities of PLA with increasing multi-functionalized epoxy content. Additionally, they produced extrusion-blown neat PLA films with a blow-up ratio (BUR) of about 3.5 but resorted to melt blending PLA with 0.5% multi-functional epoxy to enlarge its processing window. This PLA/multi-functional epoxy formulation blended with 10% polyethylene glycol (PEG), 1% N,N'-ethylenebis (stearamide) (EBSA) and 1% talc enlarged the processing window even more. However, the obtained film was translucent due to enhanced kinetics of crystallization of PLA enabled by the addition of these additives [35,36].

Moreover, two-step reactive modification of PLA with chain extenders such as 1,4-butane di-isocyanate in combination with 1,4-butanediol has been successfully used to increase PLA's viscosity by increasing its molecular weight. Di and coworkers added 1,4-butanediol in the first step to react with PLA's carboxyl group and then added 1,4-butane di-isocyanate in the second step to react with PLA's hydroxyl group to chain-extend PLA [42] They varied the amounts of these chain extenders to study their effect on the viscosities of PLA and their implications for foaming applications. They reported that excessive 1,4-butanediol degrades PLA while more 1,4-butane di-isocyanate produces highly cross-linked, high molecular weight PLA. The favorably viscous, cross-linked PLA allowed for the production of low-density foams with smaller cell-size and higher cell density compared to neat PLA [42].

Other chain extenders functionalized with maleic acid anhydride reactive groups have also been used to chain extend injection molded PLA. In one such study, the influence of chain extension achieved using two different chain extenders (epoxidized and maleated) on injection molding parameters such as injection pressure, melt temperature and flowability was studied and compared. The addition of the maleated chain extender to the PLA matrix did not affect any of the injection molding parameters due to a lack of interaction between the additive and the terminal end groups of PLA. On the other hand, the epoxidized CEs reacted with PLA very rapidly leading to an increase in injection pressure and melt temperature as well as reduced flowability [32]. Other researchers have also reported successful chain extension of PLA with epoxidized CEs [45].

Although blending PLA with the afore-mentioned additives increases the melt strength and ductility of PLA, they also have various drawbacks. For example, multifunctional epoxies have not been approved for food-grade applications by the United States Food and Drug Administration

(FDA) [24,46]. On the other hand, di-isocyanates are under scrutiny due to their toxicity, risk of occupational hazards, and their impact on the inherent biodegradability of PLA [24,47].

2.4.5 Techniques for verifying chain extension of PLA

2.4.5.1 Gel permeation chromatography (GPC)

Gel permeation chromatography (GPC) or size exclusion chromatography (SEC) is a separation technique used to separate macromolecules (or polymers) of different sizes from each other. The primary purpose of the GPC technique is to determine the various types of molecular weights of polymers and provide information about its molecular weight distribution [48,49]. Number-average (M_n), weight-average (M_w), z-average (M_z), viscosity-average (M_v) molecular weights and dispersity index are commonly determined through this versatile technique [48,49].

GPC uses a porous material as the stationary phase and a liquid as a mobile phase. The diameters of the pores of the porous material can range from 5 to 100,000 nm and are used to detect molecular weights of 500 to 1 million Da [48,49]. Polymers comprise of chains with different sizes which penetrate the pores according to their size. Smaller molecules freely diffuse and penetrate into all portions of the pores and are retained for a longer time, resulting in longer elution times. On the other hand, larger molecules elute faster due to their limited ability to penetrate the smaller pores. This results in a difference in the rates at which the molecules pass down the column (the larger molecules travel faster than the smaller molecules) [48,49]. Detectors (generally ultraviolet or refractive index) monitor the amount of polymer eluted during each time interval, thereby generating a plot of the detector response as a function elution time. Comparison of the elution time of the samples with those of monodisperse samples of known molecular weight

allow the entire molecular weight distribution (MWD) to be determined. Molecular weights (M_n, M_w, M_v and M_z) can then be calculated from the MWD [48,49].

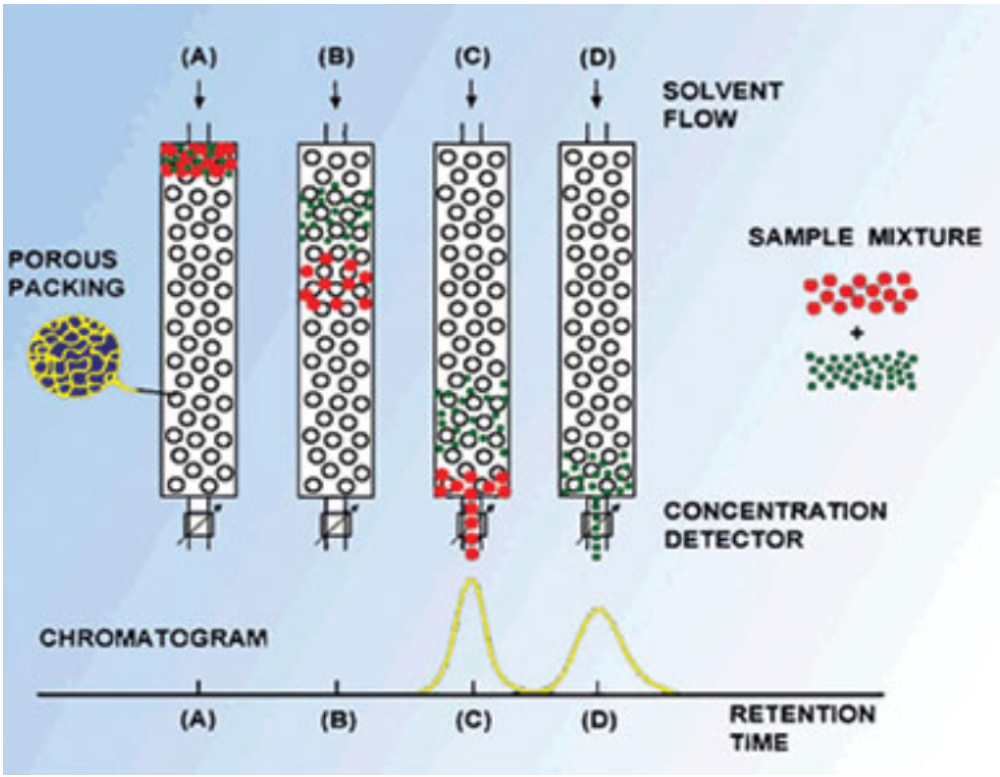

Figure 2.4 Schematic diagram of separation of small and large molecules in GPC [48].

GPC can be used to detect the chain extension reaction of PLA since chain extension an increase in molecular weight is associated with chain extension. Several researchers have reported increased molecular of weight of PLA due to the addition of chain extenders [31,32,42-45].

2.4.5.2 Viscosity measurements

Chain extension and/or branching can also be monitored by the viscosity of a polymer melt since an increase in viscosity is associated with chain extension [31,32]. Melt flow index and torque rheometry were used in this study to monitor the viscosity of PLA [28]. However, it should be noted that several other techniques such as capillary rheometry, shear oscillatory measurements using dynamic mechanical analysis, and rotational as well as extensional rheometers can be used to estimate the viscosity of a polymer.

2.4.5.2.1 Melt flow index (MFI)

The melt flow index (MFI) is a measure of the ease of flow of melted plastics at a particular temperature. The measurement of MFI involves weighing the mass of melted plastic after it is allowed to pass through a capillary die of a specific length and diameter over a timed interval at a constant temperature and pressure. MFI is expressed in grams of polymer per 10 minutes duration of the test. Generally, lower MFI implies higher viscosity and indicates chain extension [24,28,34].

Chain extension and/or branching can also be monitored by the zero-shear viscosity (η_0) of a polymer melt, which is directly related to its molecular weight (M_w) by the Mark-Houwink equation [28]:

$$\eta_0 = k \cdot M_w^a \qquad \text{(Equation 2.2)}$$

with k and a as Mark-Houwink constants.

The MFI test can be used to calculate the zero-shear viscosity value using the following equation [24,23,34]:

$$\eta_0 = \frac{\delta_m \cdot W \cdot R^4}{8 \cdot MFI \cdot L \cdot R_A^2} \qquad \text{(Equation 2.3)}$$

where δ_m is the melt density which is calculated as the ratio of MFI to melt volume rate (MVR), R is the bore radius of the die, R_A is the bore radius of the cylinder where the polymer melts, L is the length of the die and W is the applied dead load.

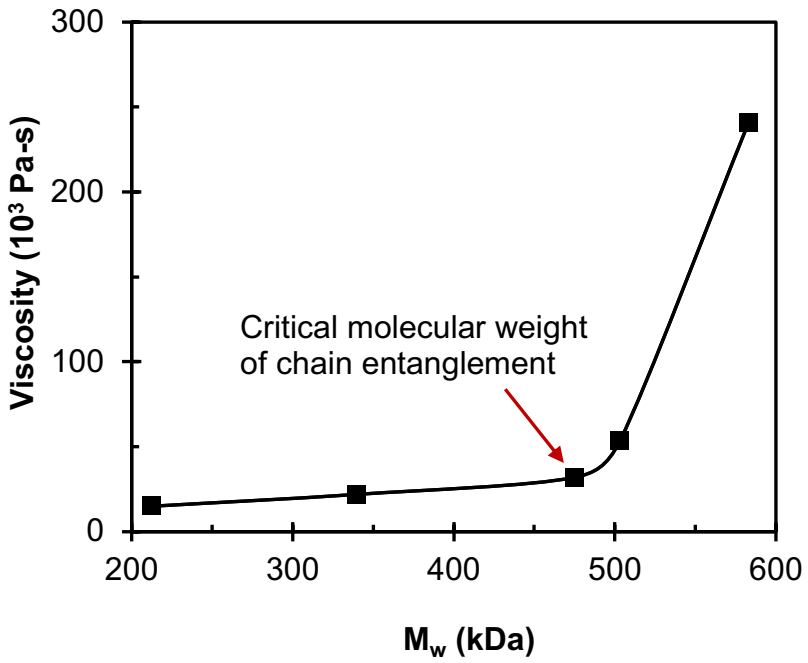

Figure 2.5 Typical plot of zero-shear viscosities determined from the MFI data as a function of weight-average molecular weight of chain extended PLA.

Figure 2.5 shows a typical plot of zero-shear viscosities determined from the MFI data as a function of weight-average molecule weight of chain extended PLA [28]. As seen in the figure, the viscosity increases gradually until a molecular weight value of ~475kDa (in this case) is reached, after which it increases exponentially. This point of inflection (~475kDa, in this case) indicates the critical molecular weight, i.e, the onset of chain entanglements attributable to the high degree of branching [28].

As seen in the figure, the viscosity increases gradually until a molecular weight value of ~475kDa (in this case) is reached, after which it increases exponentially. This point of inflection (~475kDa, in this case) indicates the critical molecular weight, i.e, the onset of chain entanglements attributable to the high degree of branching [28].

2.4.5.2.2 Torque rheometry

As described previously, chain extension and/or branching of a polymer leads to an increase in its viscosity. Since increased viscosity is associated with increased torque, torque rheometry can be used to monitor the torque during polymer processing and thus follow chain extension reactions [50-52].

A typical curve obtained from a Brabender torque rheometer for the torque of PLA as a function of mixing time is shown in Figure 2.6. It can be seen in Figure 2.6 that the torque curve reaches a maximum torque during the initial loading of neat PLA resin into the mixing chamber; indicating that the chamber is filled with resin. Then the torque gradually decreases and reaches a constant value or an equilibrium when the plastic is melted into a homogenous mass [53]. The equilibrium torque (or end torque value) is proportional to the apparent viscosity and molecular weight of the material and depends on polymer chain structure such as branching [50-52]. An

increase in the end torque values indicates an increase in the viscosity and molecular weight due to the formation of longer and/or branched chains [32,44,50-52]. Consequently, the end torque values could be used to monitor the chain extension reaction of a polymer.

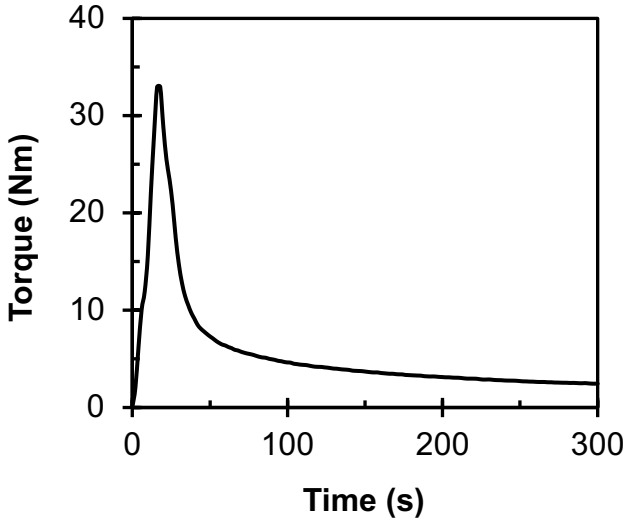

Figure 2.6 Typical curve of torque of neat PLA as a function of time generated by a torque rheometer.

Several researchers have reported an increase in the end torque values of PLA [50], poly (butylene adipate-co-terephthalate) (PBAT) [50] as well as poly (ethylene terephthalate) (PET) [52] on addition of chain extenders.

2.4.5.3 Fourier transform infrared spectroscopy (FTIR)

FTIR is an analytical technique used to identify organic (and in some cases inorganic) materials. This technique measures the absorption of infrared radiation by the sample material versus the incident wavelength. The infrared absorption bands identify molecular components and structures [49].

Molecules with covalent bonds may absorb infrared radiation when a bond in the molecule rotates or vibrates at the same frequency as the incident radiant energy. After absorbing radiation, the molecules have more energy and vibrate at increased amplitude. The frequency absorbed depends on various factors such as the mass of the atoms in the bond, the geometry of the molecule, the strength of the bond, and several other factors. However, it should be noted that molecules must have a change in dipole moment during vibration in order to absorb IR radiation [49].

Figure 2.7 shows a schematic diagram of an infrared spectrophotometer. As shown in the figure, an infrared source such as a silicon carbide element heated to 1200^{o}K (Globar) generates radiation which passes the sample through a Michelson interferometer. A detector measures the intensity of transmitted or reflected light after passing through the sample as a function of its wavelength. The signal obtained from the detector is an interferogram, which is analyzed using Fourier transforms to obtain a single-beam infrared spectrum. The FTIR spectra are usually presented as plots of intensity versus wavenumber (in cm^{-1}) [49].

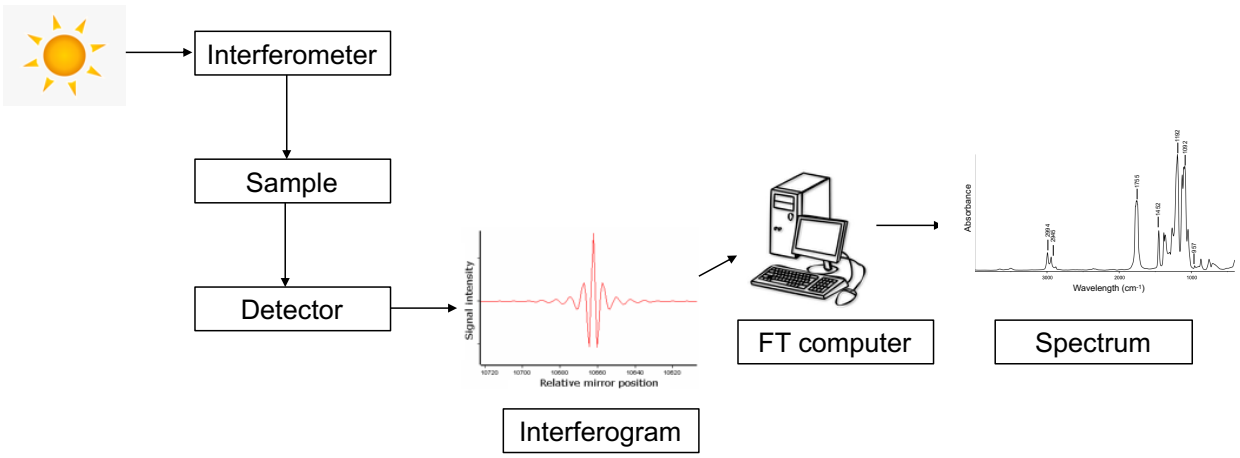

Figure 2.7 Schematic representation of a FTIR instrument.

Figure 2.8 shows typical FTIR spectrum of PLA. The peaks observed at 2994, 2945 and 1452 cm^{-1} correspond to the stretching of C-H in CH_3. Moreover, the peaks at 1755 and 957 cm^{-1} are clearly visible and belong to the stretching of C=O and O-H vibration in PLA's carboxyl group. The cluster of peaks at about 1092 and 1192 cm^{-1} are characteristic of C-O stretching in carboxyl and C-O-C stretch.

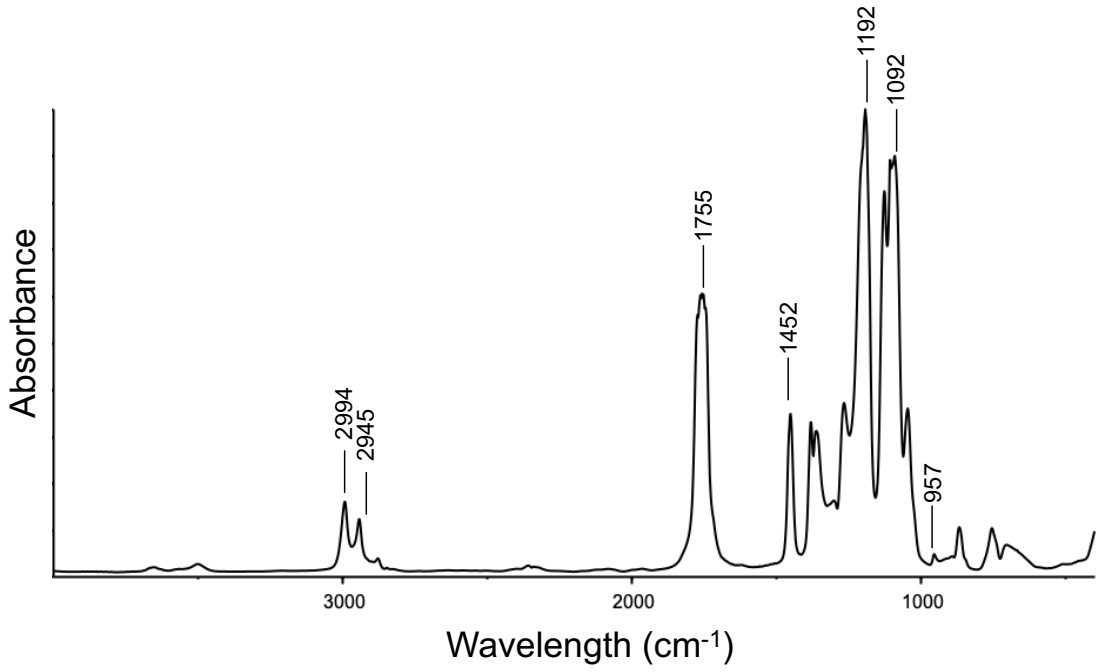

Figure 2.8 Typical FTIR spectrum of PLA.

FTIR spectroscopy can be used to gain an in-depth understanding of chain extension reaction mechanisms. The reaction between multifunctional epoxies and polyesters such as PLA has been extensively studied in the literature [28,45,50,54-56]. PLA has two distinct functional end-groups, carboxyl and hydroxyl, that can react with the epoxy groups in multifunctional epoxies. The reaction proceeds via ring-opening of the epoxide group leading to the formation of new secondary hydroxyl groups and ester linkages when reaction occurs with PLA's carboxyl groups and/or ether linkages with PLA's hydroxyl groups (Figure 2.9) [28,45,50,54-56]. Several researchers have reported the disappearance of epoxy groups in blends of PLA and chain extenders due to their consumption during the ring-opening reaction with PLA [28,45].

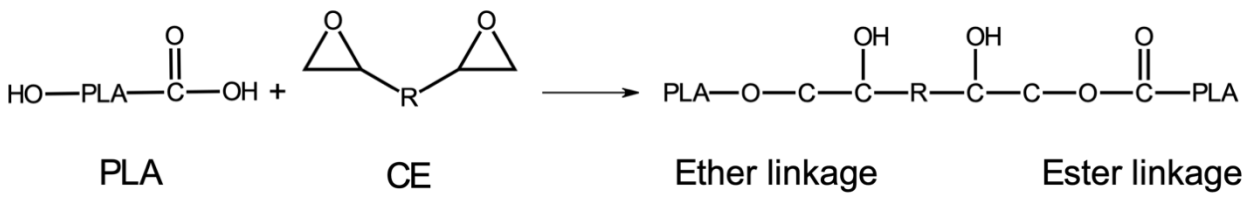

Figure 2.9 Generalized reaction mechanism of a multifunctional epoxy chain extender with the hydroxyl and carboxyl end groups in PLA.

2.4.5.4 Differential scanning calorimetry (DSC)

The degree of crystallinities of PLA can also be evaluated to verify its chain branching. Generally, dense packing of branched polymer chains is difficult, leading to reduced crystallinity. Differential scanning calorimetry (DSC), one of the most commonly used thermal analysis methods, is a calorimetric technique that measures the differences in heat flow between a reference and sample as a function of the sample's temperature. One of the biggest advantages of this technique is that very little or no sample preparation is required. Additionally, the results are quickly and easily generated in the form of a thermogram [49].

In this technique, the reference material (usually air) and sample (5-10 mg) are contained in two different aluminum pans. These pans are placed on heated thermoelectric disks with thermocouples in order to be heated in a controlled manner. The difference in the thermocouple signals is used to measure the differential heat flow to the sample and reference pans [49]. This difference in heat flow is plotted against the sample temperature and is used to estimate thermal transition temperatures such as glass transition temperature (T_g), crystallization temperature (T_c) and melting temperature (T_m). It can additionally be used to estimate the heat of melting (ΔH_m) and heat of cold crystallization (ΔH_c), which can then be used to calculate the degree of crystallinity of the polymer being characterized [49].

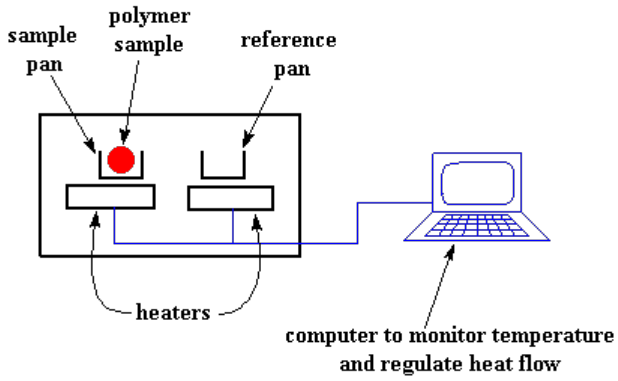

Figure 2.10 Schematic representation of a differential scanning calorimeter [57].

It should be noted that other techniques such as the density gradient method and X-ray diffraction can also be used to measure the density of a polymer.

2.4.5.5 Falling dart impact strength

Chain branching is associated with reduced crystallinity and hence higher impact strength. Therefore, impact strength can be used as an indicator of chain branching [28]. Falling dart impact, using the falling dart impact tester shown in Figure 2.11, is a traditional method for evaluating the impact strength of a plastic film. This test uses a dart dropped from a specific drop height, while varying the weight of the dart. In this test, film samples are clamped at the base of a drop tower, and a dart is inserted into the testing bracket. The dart is then released onto the center of the test specimen, and the test result (pass/fail) is recorded along with the weight of the dart. Fail is generally defined as film rupture so that the dart penetrates through the film and "pass" indicates the situation where the film sustains its integrity to hold the dart [28,58,59]. The 'Bruceton Staircase' process is used to evaluate the data: when the sample passes, the dart weight is increased, whereas the dart weight is decreased if the sample fails. The results are then used to calculate the

impact failure weight, which is defined as the weight for which 50% or more of the test samples will fail under the impact at a given height [59].

Figure 2.11 Falling dart impact tester [59].

2.5 Cellulose nanocrystals (CNCs)

Cellulose nanocrystals (CNCs) are renewable and biodegradable nanomaterials derived from the most abundant natural polymer, cellulose. Their chemical structure is shown in Figure 2.12. These nanomaterials have received significant interest due to their mechanical, optical, chemical, and rheological properties. CNCs are often added to the PLA matrix to increase its crystallinity and improve its barrier and mechanical properties [60-63].

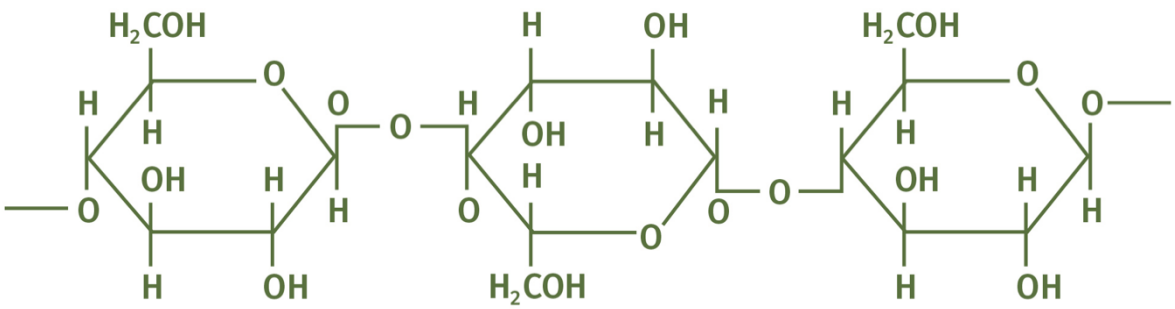

Figure 2.12 Chemical structure of CNC [60].

2.5.1 Production of CNCs

CNCs are extracted from lignocelluloses through a chemical process. In the first step, known as refining, non-cellulose components are segregated from the source material. In the second step, extraction of CNCs takes place by acid hydrolysis, wherein para-crystalline (or disordered) regions are first solubilized, leaving behind the crystalline domains that possess high resistance to acid. The resulting highly crystalline domains are whisker-like and are known as CNCs. Sulfuric and hydrochloric acids are commonly used for the acid hydrolysis, resulting in CNCs with varying dispersibility. CNCs produced from sulfuric acid have an abundance of charged sulfate groups on its surface and are hence readily dispersed in water. On the other hand, CNCs produced from hydrochloric acid are difficult to disperse due to the lack of charge [60-63].

2.5.2 Properties of CNCs

CNCs exhibit good characteristics such as renewability, low density, biocompatibility and biodegradability compared to other inorganic nanoparticles. Their geometrical dimensions can vary widely, with a diameter ranging from 4-25 nm and length ranging from 100-1000 nm [60-63].

The source and extraction method of CNCs influence their size, morphology and crystallinity. On an average, the tensile strength of CNCs is in the range of 7.5-7.7 GPa, which is much more than that of steel wire. Their elastic modulus is ~150 GPa and transverse modulus is in the range of 18-50 GPa [60-63].

The thermal stability of CNCs is important because it is often added to polymer matrices that are processed at temperatures exceeding 200ºC. In general, CNCs have a thermal decomposition temperature of 300ºC, which meets the temperature requirements for processing composite materials[60-63].

CNCs have excellent optical properties. Several researchers have reported that CNC cast films are highly transparent because they have ether and hydroxyl groups as well as carbon-carbon, and carbon-hydrogen bonds which do not absorb light in the visible range (400-700 nm) [60-63].

2.5.3 Use of CNCs in bio-based polymer matrices

Cellulose nanocrystals (CNCs) are recently gaining interest amongst researchers as natural and bio-based nucleating agents [64-70]. Well-dispersed CNCs in a polymer matrix can increase the polymer's crystallinity. Increased crystallinity is associated with improved thermal, mechanical and barrier performance.

Although, well-dispersed CNCs can increase a polymer's crystallinity, their dispersion into the polymer matrix is a challenge. CNC particles tend to agglomerate (Figure 2.13) due to their high surface area to volume ratio when the aqueous medium that they are produced in is eliminated by freeze or spray drying. Moreover, CNC particles are difficult to disperse in non-polar polymers due to their high polarity and strong hydrogen bonding forces [71]. Various approaches such as

solvent-casting and melt-compounding, described in the next section, have been investigated to disperse cellulose nanomaterials such as CNCs into a polymer matrix [64-76].

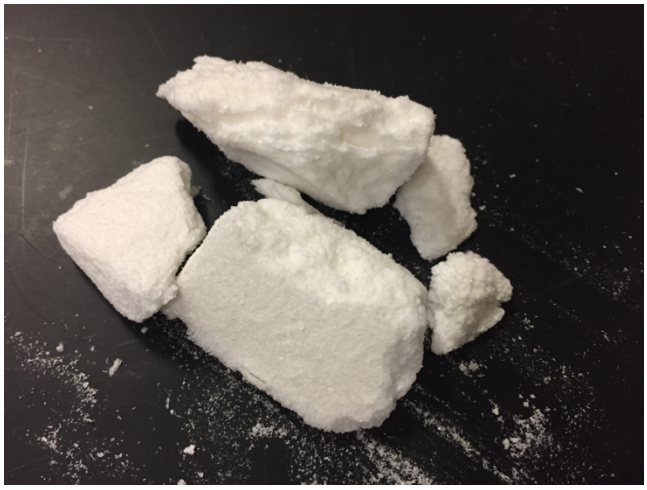

Figure 2.13 Cellulose nanocrystal agglomerations.

2.6 Dispersion of cellulose nanomaterials in polymer matrices

2.6.1 Solvent-casting

The solvent-casting technique involves the dissolution of the polymer and CNCs in a solvent such as water, alcohol, or any organic solvent. The solution is then stirred and cast onto a mold or flat surface (such as petri-dish) where the solvent evaporates, and the dried nanocomposite film can be peeled off (Figure 2.14) [77].

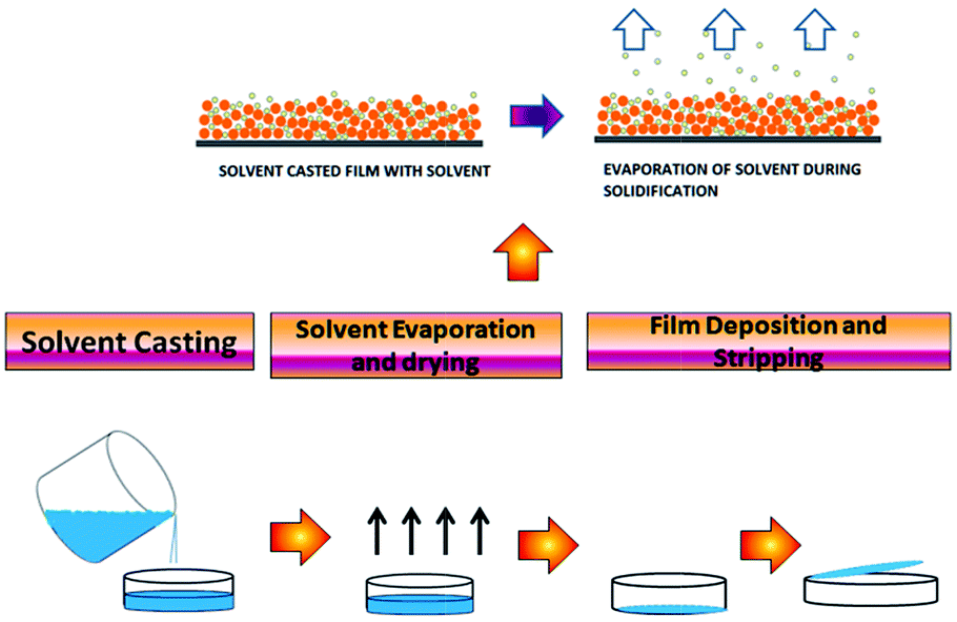

Figure 2.14 Solvent-casting process [77].

Several researchers have used solvent-casting technique to manufacture PLA nanocomposite films with improved barrier performance by adding various amounts of unmodified and modified cellulose nanomaterials [64-67]. In one such effort, the addition of 1% CNCs modified with an acid phosphate ester of ethoxylated nonylphenol (s-CNCs) decreased the oxygen transmission rate (OTR) and water vapor permeability (WVP) of PLA films by 26% and 34%, respectively attributable to the tortuosity effect induced by well dispersed s-CNCs [64]. These results were consistent with those previously reported by Sanchez-Garcia and co-workers for nanocomposite films containing 1% nanowhiskers [66].

2.6.2 Solvent dispersion prior to melt compounding

Polymer/cellulose nanomaterial composites have also been prepared using a two-step process [71]. In the first step, the solvent-casting technique is used to prepare a masterbatch of the cellulose nanomaterial with the polymer matrix. In the second step, the masterbatch is crushed, diluted and dry-mixed with the polymer matrix, melt-compounded in an extruder, and then prepared into samples by techniques such as compression or injection molding. For instance, PLA/5% cellulose nanofiber samples prepared by the described technique had 24% and 21% increase in tensile modulus and tensile strength, respectively. Nonetheless, large standard deviation in the values of tensile modulus reported indicated a non-homogenous dispersion of CNFs in the PLA matrix [71].

Another approach to disperse cellulose nanomaterials into polymer matrices has been examined by investigators where an aqueous suspension of cellulose nanomaterials in a slurry of plasticizer, acetone and water is prepared (Figure 2.15) [72-74]. The prepared suspension is then melt-compounded with polymer pellets in an extruder equipped with a liquid feeder and vents for removal of acetone and water [72-74]. Compression molding, injection molding or extrusion blown-film processes can then be used to prepare samples. In one such study, a masterbatch of PLA, 5% ChNCs and 20% glycerol triacetate plasticizer (GTA) was prepared using the previously described liquid feeding technique in a vented twin-screw extruder. This masterbatch was diluted with PLA and PBAT and mixed with talc to produce films with 1% ChNCs, 6% talc, 9% GTA, 25% PBAT and 59% PLA. The final composites were then blown into films and evaluated for optical, thermal, mechanical and barrier properties amongst others. The researchers found that addition of ChNCs increased the viscosity and melt strength of PLA, thus aiding in the blown film processing of the films. Moreover, the addition of 1% ChNCs increased the tensile modulus, tensile

strength, tear resistance and puncture resistance of the film by 74%, 64%, 80% and 300%, respectively. In contrast, the nanocomposite films did not have improved thermal stability or barrier performance compared to their reference films [74].

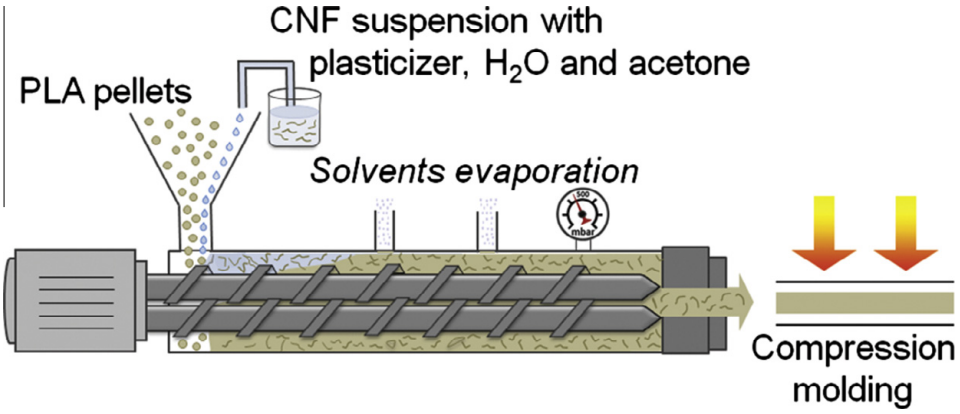

Figure 2.15 Liquid-feeding process [72].

2.6.3 Melt-processing

Past efforts on dispersing cellulose nanomaterials in polymer matrices were focused on solvent-casting techniques (a batch process) instead of melt-processing which is an important processing method for introducing nanocomposite materials in the market where high-volume production is required [78]. However, limited studies have been reported on dispersing cellulose nanomaterials into polymer matrices using melt-processing [25-27,68,69].

The melt-processing technique employs (1) heat to soften the polymer and (2) shear to maximize dispersion of cellulose nanomaterials into the polymer matrix. In this approach, materials pass through melt compounders such as internal batch mixers or single/twin screw extruders one or more times before the final product is obtained [62]. For example , CNCs derived from coffee silverskin were dispersed into a PLA matrix using a twin-screw extruder before being

compression molded into films. These PLA/3% CNC nanocomposite films had higher crystallinity and hence better barrier and mechanical performance compared to their neat PLA counterpart films [68].

2.6.4 Techniques for studying dispersion of CNCs into polymer matrices

Dispersion of CNCs into polymer matrices can be examined using techniques such as microscopy (light, scanning electron and transmission electron) as well as spectroscopy (ultraviolet-visible), amongst others. Since light microscopy and ultraviolet-visible (UV-Vis) spectroscopy were used in this dissertation to observe the dispersion of CNCs into a PLA matrix, these techniques are described in this section of the literature review.

2.6.4.1 Light microscopy

Microscopes such as the one shown in Figure 2.16 are often used to examine the distribution and dispersion of CNCs in a PLA matrix [25,26]. These microscopes, also known as optical microscopes, commonly use visible light and a system of objective lenses to generate magnified images of small objects, allowing the user to observe it by the naked eye. The specimen (PLA/CNC film, in this case) is placed on a stage which is lit by an illumination source placed below it and may be viewed directly through one or two eyepieces on the microscope [79]. A camera is typically used to capture the image. Image processing software can then be used to measure the CNC agglomeration size and quantify their frequency over a specified surface area.

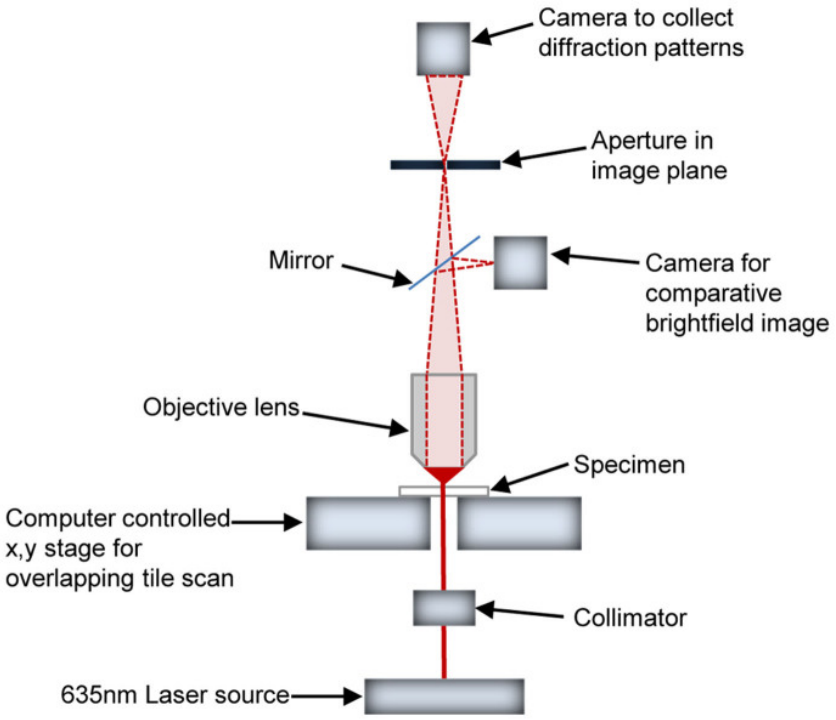

Figure 2.16 Light microscope [80].

2.6.4.2 Ultraviolet-Visible (UV-Vis) Spectroscopy

Transparency can be used as an indicator of the dispersion of nanoparticles in a matrix, if the size of individual nanoparticles is smaller than the wavelength of visible light (400-700 nm) (Figure 2.17) [25,26,72]. In other terms, if nanosize dispersion of CNC in PLA matrix is obtained, the addition of CNCs will not affect the transparency of resulting films, because pure CNC films are highly transparent [25,26,81]. UV-Vis spectroscopy can be used to monitor the transparency of PLA and PLA/CNC nanocomposite films [25,26].

In a UV-Vis spectrophotometer, light is passed through the sample at a specific wavelength in the ultraviolet or visible spectrum [82]. The sample absorbs some of the light and transmits the rest. The absorbed energy either causes the emission of electrons, resulting in a photocurrent or moves electrons into the conduction band of a solid semiconductor, resulting in an increase in

conductivity. Detection devices such as photoelectric transducers, have surfaces that can absorb radiant energy and convert it into an electrical signal. Various software is then used to generate absorption or transmission spectra of samples [49].

Figure 2.17 shows a typical spectra of PLA's light transmission as a function of its wavelength generated by a UV-Vis spectrophotometer. Three zone are clearly visible in the figure: (1) the UV light region from 10-400 nm, (2) visible light from 400-700nm, and the (3) infrared light region from 700 nm onwards (up to 1 mm).

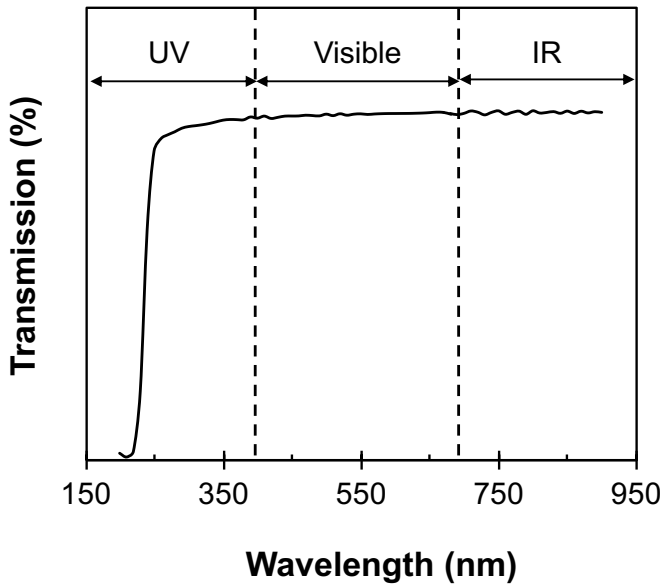

Figure 2.17 Typical spectra of PLA's light transmission as a function of its wavelength generated by a UV-Vis spectrophotometer.

2.7 Barrier performance of PLA/CNC films

As discussed previously, incorporating CNCs into a PLA matrix can improve its barrier performance by (1) increasing PLA's crystallinity and (2) acting as impermeable regions in the matrix. The impermeable regions create a more tortuous diffusion path for the permeant, leading to slower diffusion and hence lower transmission rates [25-27,60,61]. A few techniques to evaluate the barrier performance of PLA and PLA/CNC nanocomposite films are discussed in this section of the literature review. Also, the potential application of these nanocomposite films to extend the shelf-life of food are reviewed.

2.7.1 Barrier measurement

The concept of permeability is normally associated with the quantitative evaluation of the barrier properties of a plastic material. Permeability is defined as the quantification of permeate transmission, gas or vapor, through a resisting material [83]. A good barrier material has low permeability. To measure water vapor or gas permeability of a film sample, the sample is mounted between two chambers of a permeability cell [84]. One chamber holds the permeant such as gas or water vapor. Since there is a permeant concentration difference between the chambers, the permeant diffuses through the film into the second chamber. The quantity of permeant entering the second chamber is measured by a detection method such as infrared spectroscopy, gravimetry, coulometry, manometry or gas-liquid chromatography. Generally, permeability is measured by the following test procedures: (1) isostatic and (2) quasi-isostatic [84].

2.7.1.1 Isostatic method

With the isostatic method of permeability measurement, the pressure in each chamber is held constant (generally atmospheric pressure). One chamber has a continuous supply of permeant which permeates through the film into the other chamber (lower permeant concentration) (Figure 2.18).

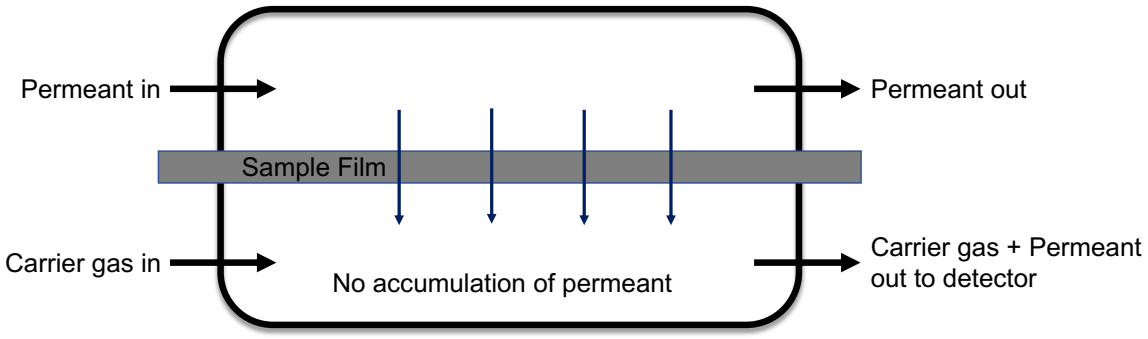

Figure 2.18 Isostatic method of permeability measurement.

The permeated molecules are continuously conveyed (no accumulation) by a carrier gas to the sensor for quantification and the permeant flow versus time is recorded (Figure 2.19), providing measurements in both the unsteady and the steady state regions. In this method, the flow rate of the permeant continues to increase until it becomes constant (steady state). The permeability of the material (P) is then calculated using the following equation:

$$P = \frac{F_{ss} \cdot l}{A \cdot \Delta p} \qquad \text{(Equation 2.4)}$$

where F_{ss} is the flow rate at steady state, l is the thickness of the material, A is the effective area of permeation and Δp is difference in partial pressure of permeant across the sample.

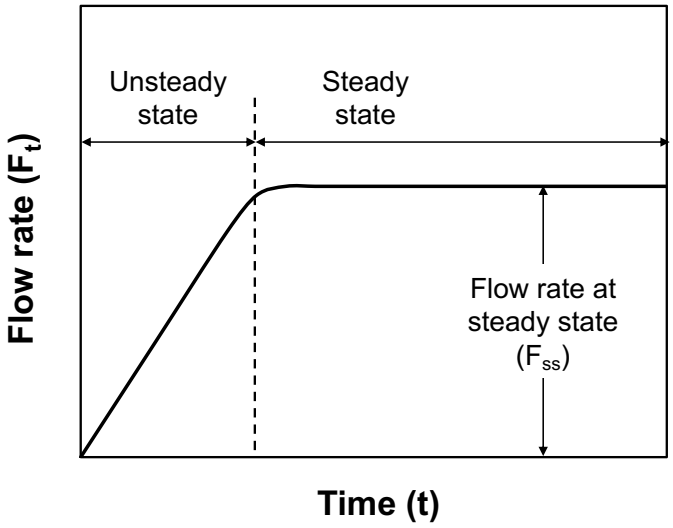

Figure 2.19 Plot of flow rate as a function of time generated by the isostatic method.

Commercially available isostatic testing equipment has been used extensively for measuring the oxygen and carbon dioxide permeability of plastic films [84].

2.7.1.2 Quasi-isostatic method

The main difference between the isostatic and quasi-isostatic methods is that the permeant is allowed to accumulate in the lower-concentration chamber in the quasi-isostatic method. This method of permeability measurement is generally used to measure the water vapor permeability of films (Figure 2.20).

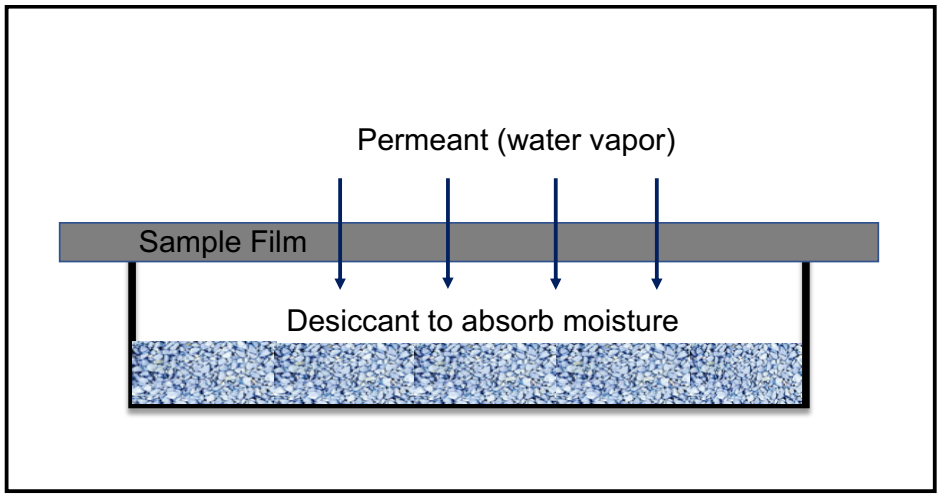

Figure 2.20 Quasi-isostatic method of water vapor permeability measurement.

In this method, the total quantity of accumulated permeant is then determined and plotted as a function of time (Figure 2.21) [84]. The total quantity of permeant increases gradually in the unsteady state and then linearly in the steady state as a function of time. The slope of the linear portion of this plot is directly related to the sample's permeability using the following equation:

$$P = \left(\frac{q}{t}\right)_{ss} \times \frac{l}{A \cdot \Delta p} \qquad \text{(Equation 2.5)}$$

where $(q/t)_{ss}$ is the flow rate at steady state, l is the thickness of the material, A is the effective area of permeation and Δp is difference in partial pressure of permeant across the sample.

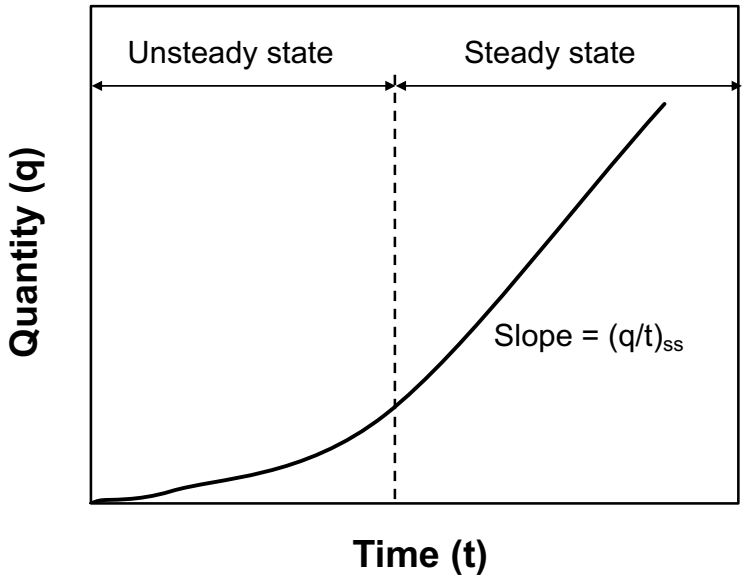

Figure 2.21 Plot of flow rate as a function of time generated by the quasi-isostatic method.

2.8 Shelf-life of moisture-sensitive food

The shelf-life estimation and modelling of a moisture-sensitive product-package systems requires the determination of (1) moisture sorption isotherms for food; (2) barrier properties of films; (3) experimental shelf-life estimation of the product-package system and (4) shelf-life models as shown in Figure 2.22. The following section briefly describes each of these concepts essential for shelf-life determination, except for barrier property estimation which was described in section 2.7 of this dissertation.

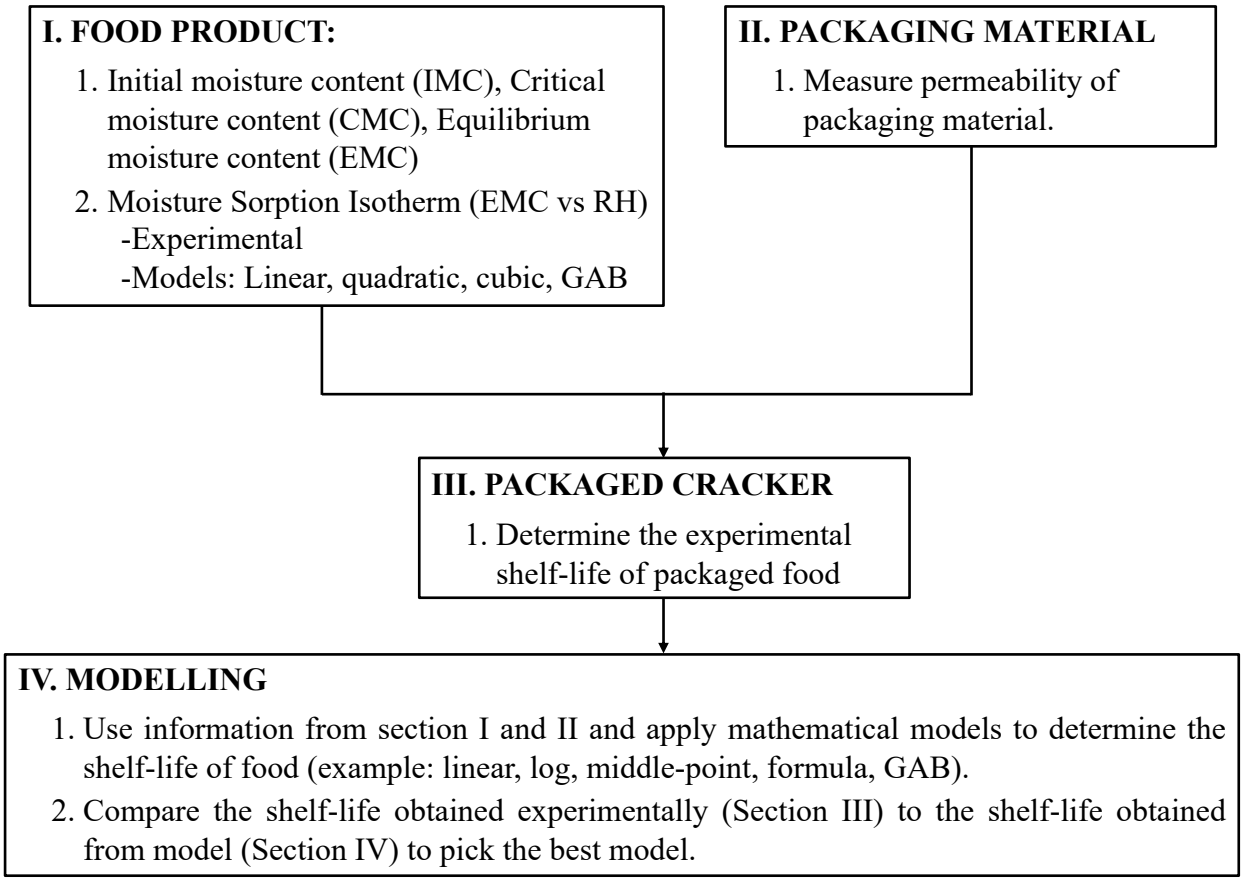

Figure 2.22 Overview of the shelf-life determination process.

2.8.1 Sorption isotherm of a moisture-sensitive food product

2.8.1.1 Background

When a food product is kept in the environment, it may gain or lose moisture depending on whether it has more or less moisture that the surrounding it is kept in. If the product has lesser moisture than its surroundings, it will absorb moisture. It will lose moisture if it has more moisture than that of the surroundings it is kept in. In either case, it will eventually come to an equilibrium with the environment. The corresponding moisture content of the product when it reaches an equilibrium with the environment is known as equilibrium moisture content (EMC). It can be evaluated using the following equation:

$$\text{EMC}\ (\%) = \left[\frac{W_e}{W_i}(\text{IMC} + 1) - 1\right] \times 100 \qquad \text{(Equation 2.6)}$$

where W_e is the weight of the food product at equilibrium (g), W_i is the initial weight of the product (g) and IMC is the initial moisture content calculated as follows:

$$\text{IMC}\ (\%) = \frac{W_i - W_D}{W_D} \times 100 \qquad \text{(Equation 2.7)}$$

where W_i is the initial weight of the product (before drying) (in g) and W_D is the weight of the product after drying (in g) in the oven.

When this EMC is plotted against the water activity of the product at a particular temperature, a moisture sorption isotherm is obtained. Such plots are very useful in determining the stability of the food product and selecting appropriate packaging materials [85,86].

Figure 2.23 shows a sorption isotherm developed for a typical moisture-sensitive food product. It can be divided into three regions: (1) The water in region A represents strongly bound water. Bound water includes structural and monolayer water, which is absorbed by the hydrophilic groups of the food product and is unavailable for chemical reactions. (2) Region B contains water molecules that are bound less firmly than those in region A. These water molecules are present in small capillaries and continuously transition from bound to free water. (3) Region C contains loosely bound free water held in voids, large capillaries and crevices [85,86].

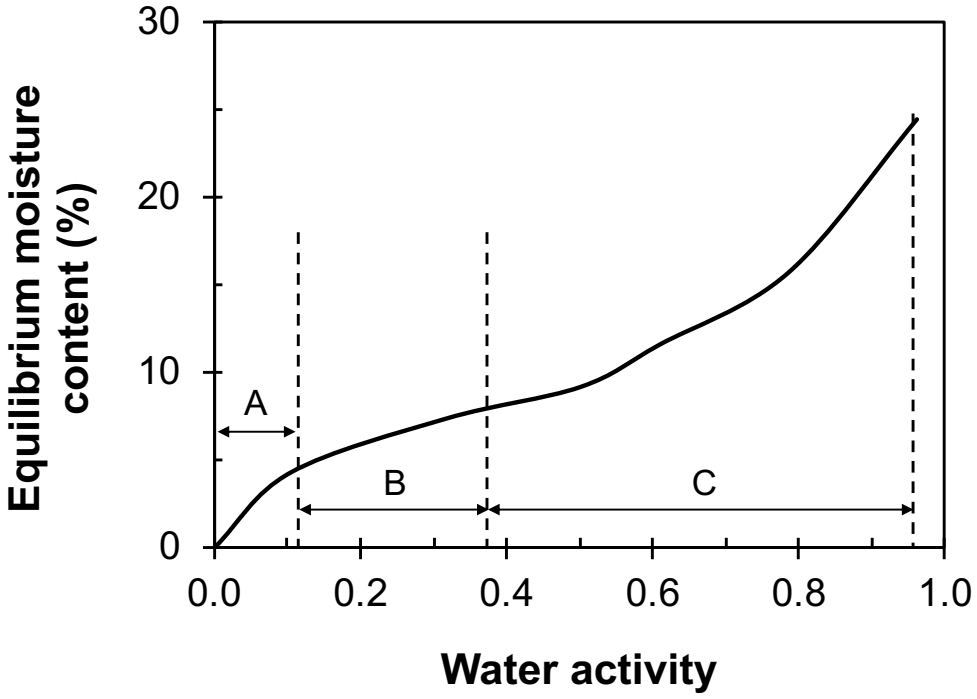

Figure 2.23 Typical moisture sorption isotherm.

Moisture sorption isotherms can be used to predict the quality, shelf-life, stability and moisture changes that can be expected to occur in a product at a particular water activity. They are also useful for determining the drying equipment required in order to preserve food by dehydration methods [85-90].

2.8.1.2 Mathematical models

Since moisture sorption isotherms are considered so important in the packaging and food science industry, many equations and models have been proposed to determine the steady-state relationship between the water activity of a food product and its equilibrium moisture content [85,86]. Linear, quadratic, cubic as well as Guggenheim Anderson de Boer (GAB) models, amongst several others, have been proposed for determining this relationship. It should be noted that even though the linear, quadratic and cubic models have been previously used to fit sorption isotherm data, the GAB model is the most widely accepted one.

2.8.1.2.1 Linear, quadratic and cubic models

Table 2.3 summarizes the equations used for modeling sorption isotherms using the linear, quadratic and cubic models [88,90]. The linear, quadratic and cubic equations listed in Table 2.3 have been used to fit sorption isotherm data for cornflakes [90] as well as salted crackers [88].

Table 2.3 Models to predict moisture sorption isotherms [88,90].

Models	Equations	Definition of terms used in equation.
Linear	$\mathrm{EMC_{pred}} = \mathrm{a} \cdot \mathrm{RH} + \mathrm{b}$	a is the slope of the straight line; b is a constant.
Quadratic	$\mathrm{EMC_{pred}} = \mathrm{a'} \cdot \mathrm{RH}^2 + \mathrm{b'} \cdot \mathrm{RH} + \mathrm{c'}$	a',b' and c' are constants of quadratic equation.
Cubic	$\mathrm{EMC_{pred}} = \mathrm{a''} \cdot \mathrm{RH}^3 + \mathrm{b''} \cdot \mathrm{RH}^2 + \mathrm{c''} \cdot \mathrm{RH} + \mathrm{d''}$	a",b",c" and d" are constants of cubic equation.

2.8.1.2.2 Guggenheim Anderson de Boer (GAB) model

The Guggenheim Anderson de Boer (GAB) model is a refinement of the Brunauer Emmett Teller (BET) and Langmuir theories of physical adsorption and is expressed as the following equation:

$$\mathrm{EMC_{pred}} = \frac{\mathrm{CKa_w W_m}}{(1 - \mathrm{Ka_w}) \cdot (1 - \mathrm{Ka_w} + \mathrm{CKa_w})} \qquad \text{(Equation 2.8)}$$

where $\mathrm{EMC_{pred}}$ is the predicted equilibrium moisture content of the product, C is the Guggenheim constant, K is the correction factor, $\mathrm{W_m}$ is the monolayer saturated water content, and $\mathrm{a_w}$ is the water activity (given as %RH/100).

In order to calculate the C, K and W_m values in equation 2.8, a plot of the experimental values for a_w/EMC as a function of a_w is generated. Figure 2.24 shows a typical plot of a_w/EMC as a function of a_w [91].

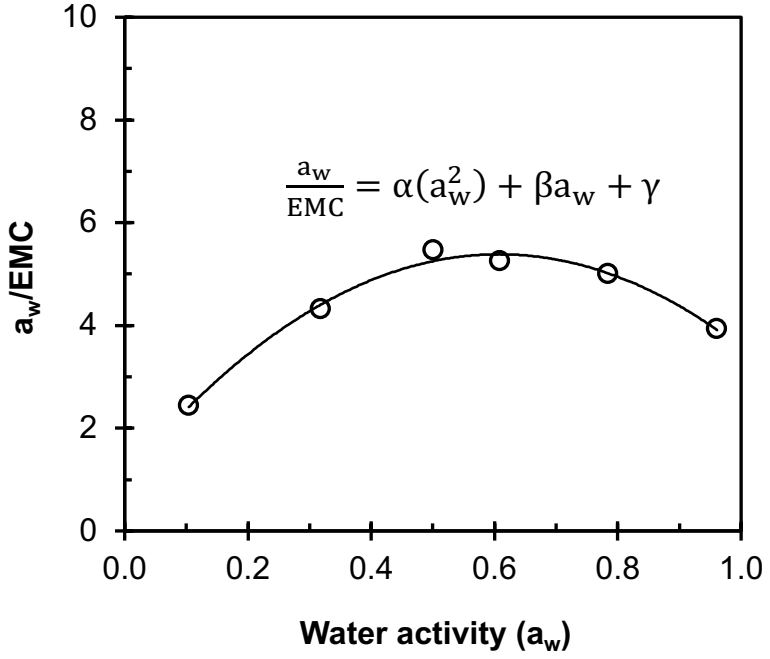

Figure 2.24 A typical plot of the experimental values for a_w/EMC as a function of a_w.

A quadratic trend is then fit to the plot shown in Figure 2.24 using the following equation [86-91]:

$$\frac{a_w}{EMC} = \alpha(a_w^2) + \beta a_w + \gamma \qquad \text{(Equation 2.9)}$$

where α, β and γ are constants of the quadratic equation used to fit the experimental data.

Once the values of α, β and γ are known, the following equation can be used to estimate the values of C [91]:

$$C = \frac{T + \sqrt{T^2 - 4T}}{2} \quad \text{(Equation 2.10)}$$

Where T is given as:

$$T = \frac{\beta^2}{-\alpha\gamma} + 4 \quad \text{(Equation 2.11)}$$

The values of K and W_m can be obtained by solving the following equations simultaneously [91]:

$$\alpha = \frac{k}{W_m}\left[\frac{1}{C} - 1\right] \quad \text{(Equation 2.12)}$$

$$\gamma = \frac{1}{W_m C k} \quad \text{(Equation 2.13)}$$

The major advantages of the GAB model are: (1) it is mathematically simple and easy to interpret because its parameters have a physical meaning in terms of the sorption process; (2) it provides a good description of the sorption behavior of almost all food isotherms with a water activity between 0-0.9; (3) it can be used to describe the temperature effect on isotherms by means of the Arrhenius equation [87]. However, it should be noted that the GAB model underestimates equilibrium moisture content values at high water activity levels (above 0.93) and is thus

unsuitable for a high humidity range [85,86]. This model has been widely used in research to describe the moisture sorption behavior of dry food products like salted [88] and rice crackers [89] as well as cornflakes [90].

2.8.1.2.3 Goodness of fit using root mean square (RMS) value

Since various models exist to predict the sorption isotherm of products, it is important to understand which model fits the data most accurately. The root mean square (RMS) value is one such tool that can help determine if the predicted EMC values generated by models fit the experimental data. It can be calculated as follows [88-90]:

$$\mathrm{RMS} = \left[\sqrt{\frac{\sum_{i=1}^{N} \left(\frac{\mathrm{EMC_{exp}} - \mathrm{EMC_{pred}}}{\mathrm{EMC_{pred}}} \right)^2}{N}} \right] \times 100 \qquad \text{(Equation 2.14)}$$

where EMC_{exp} is the experimental equilibrium moisture content, EMC_{pred} is the equilibrium moisture content predicted by the GAB model, and N is the number of experimental points.

Generally, a low RMS value (below 10%) signifies a good fit of the model to the experimental data [88-90].

2.8.2 Shelf-life of food packaged in films

Shelf-life is defined as the length of time before a food product is considered unacceptable to the consumer. It is important to note that the term “shelf-life” says nothing about the safety of the food product. For instance, a food product that passes its shelf-life does not immediately become unsafe for human consumption. Rather, it no longer conforms to a set of given quality parameters [92]. Shelf-life of a food is influenced by the product itself, packaging materials, food processing methods as well as storage conditions, amongst others [92].

2.8.2.1 Experimental shelf-life determination of product-package system

For moisture sensitive food products, the shelf-life is determined as the time required by the food product to reach its critical moisture content (CMC) from moisture content versus storage time plots. Generally, CMC is determined by sensory evaluation tests as the minimum moisture content at which the product becomes organoleptically unacceptable, for example losing its crispiness [92].

Figure 2.25 shows a typical plot of moisture content vs storage for a moisture sensitive food product (crackers) packaged in a film (PLA) at a constant temperature and relative humidity (RH). As seen in the figure, the food packaged in the film absorbs moisture gradually with increasing time until it reaches a constant value or an equilibrium. The shelf-life of the food product can be obtained from such a plot by drawing a horizontal line parallel to the X-axis (time) at the critical moisture content value. The point on the X-axis at which this line intesects the data trendline is known as the shelf-life.

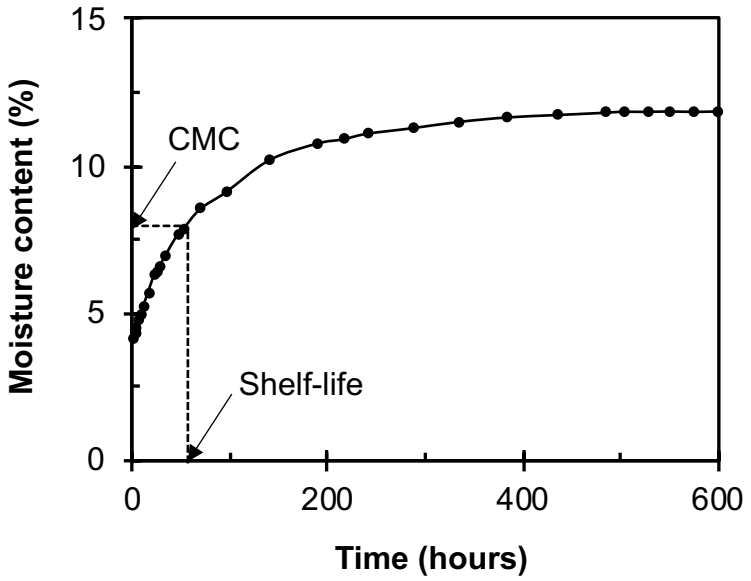

Figure 2.25 Plot of moisture content as a function of time for shelf-life determination.

2.8.2.2 Shelf-life modeling

Shelf-life determination of food product-package systems using experimental techniques can be very time and labour intensive, depending on the type of food product, packaging material and storage conditions. In fact, even slight changes in a product's ingredients and processing, packaging materials, as well as storage environment can drastically change the shelf-life of the system. Since food manufacturers are constantly changing their product-packaging system for superior product performance and cost reduction, shelf-life prediction using mathematical models becomes very crucial for making commercial decisions within tight time constraints. However, it should be noted that all shelf-life simulation models are approximations, and therefore have associated error. In most cases, the expected error is 10-50%, based on the assumptions made [88-92].

Several mathematical models for predicting the shelf-life of a moisture sensitive product packaged in a film have been described in literature. Some of these models, such as the linear, middle-point, logarithmic and GAB model have been described in this section. Table 2.4 lists the models and their respective equations used for the shelf-life prediction of a moisture sensitive product-package system [88-91].

Table 2.4 Models to predict shelf-life of moisture sensitive foods [88-91].

Model	Equation
Linear	$t = \frac{l \cdot W_D \cdot \beta}{P \cdot A \cdot P_s} \ln\left(\frac{a_{wo} - a_{w,t=0}}{a_{wo} - a_{w,t=t}}\right)$
Middle-point	$t = \frac{l \cdot W_D}{P \cdot A \cdot P_s} \sum_{i=1}^{n} \frac{\Delta M_i}{a_{wo} - \left(\frac{a_{w,t=i} + a_{w,t=i+1}}{2}\right)}$
Logarithmic	$t = \frac{l \cdot W_D}{P \cdot A \cdot P_s} \sum_{i=1}^{n} \beta_i \ln\left(\frac{a_{wo} - a_{w,t=i}}{a_{wo} - a_{w,t=i+1}}\right)$
where l is the thickness of the packaging material; W_D is the weight of product in the package; P is the permeability of the packaging material; A is area of the package; P_s is the saturated vapor pressure at food storage temperature; a_{wo} is the water activity at the storage condition (%RH/100); β is the slope of the straight line; $a_{w,t=0}$ is the water activity at initial moisture content; $a_{w,t=t}$ is the water activity at critical moisture content; ΔM_i is moisture content change in each interval "i"; $a_{w,t=i}$ and $a_{w,t=i+1}$ are the water activities at the beginning and end of each interval "i", respectively; and β_i is the slope of the line at each interval "i".	

The linear model for shelf-life prediction is the simplest one. In this model, the sorption isotherm data is modelled linearly in the range of interest (between IMC and CMC). In the middle point method and logarithmic methods, the region of interest is divided into “n” intervals and the value of time needed to change the product’s moisture content between the limits of each interval is calculated. The larger the number of intervals (minimum of three), the smaller the error [88-91]. All of the above models have been used to predict the shelf-life of moisture sensitive food products [88-91]. In one such study, the previously mentioned models were used to predict the shelf-life of salted crackers packaged in commercial low-density polyethylene (LDPE) films [88]. The researchers reported that the linear, middle point and logarithmic models overestimated the experimental shelf-life by 50, 30 and 30%, respectively. The researchers attributed these differences to experimental errors in determining the sorption isotherm and critical moisture content [88].

Although the models mentioned previously have been used to predict the shelf-life of dry foods packaged in films, the GAB equation is the most commonly used model. The shelf-life of a food-package system predicted by the GAB equation can be determined as follows [91]:

$$t = \frac{H}{\varepsilon \emptyset} \quad \text{(Equation 2.15)}$$

where H, ε and ϕ are given as:

$$H = M_f - M_i + \frac{2W_m C}{\varepsilon} \ln\left(\frac{\varepsilon M_f - 2W_m C}{\varepsilon M_i - 2W_m C}\right) \quad \text{(Equation 2.16)}$$

$$\varepsilon = (1 - C)(2Ka_{wo} - 2) \quad \text{(Equation 2.17)}$$

$$\emptyset = \frac{A \cdot P \cdot P_s}{2K \cdot (1 - C) \cdot l \cdot W_D} \quad \text{(Equation 2.18)}$$

where C, W_m and K are GAB constants (described in section 2.8.1.2.2), M_f and M_i are the critical and initial moisture contents of the food, a_{wo} is the water activity at the storage condition (%RH/100), A is area of the package, P is the permeability of the packaging material, P_s is the saturated vapor pressure at food storage temperature, l is the thickness of the packaging material; W_D is the weight of product in the package.

The GAB model has been used to predict the shelf-life of several dry food products with approximately 40-50% differences between the experimental and predicted shelf-life [88,89]. These differences were attributed to the possible spoilage of food due to factors such as food structure and composition, besides moisture content. It should be noted that GAB models work best when the shelf-life of the food depends on its moisture content only.

REFERENCES

REFERENCES

1. Hartmann, M.H. and Kaplan D.L., Biopolymers from renewable resources, Springer -Verlag, Berlin, pp. 367-411 (1998).

2. Lee, S.Y., Kang, I.A., Doh, G.H., Yoon, H.G., Park, B.D., and Wu, Q., Thermal and mechanical properties of wood flour/talc-filled polylactic acid composites: effect of filler content and coupling treatment, Journal of Thermoplastic Composite Materials, 21 (3): 209-23 (2008).

3. Pilla, S., Gong, S., O'Neill, E., Rowell, R.M., and Krzysik, A.M., Polylactide-pine wood flour composites, Polymer Engineering and Science, 48: 578-87 (2008).

4. Oksman, K., Skrifvars, M., and Selin, J.F., Natural fibers as reinforcement in polylactic acid (PLA) composites, Composites Science and Technology, 63: 1317-24 (2003).

5. Lasprilla, A.J., Martinez, G.A., Lunelli, B.H., Jardini, A.L., and Rubens, M.F., Poly-lactic acid synthesis for application in biomedical devices-a review, Biotechnology Advances, 30 (1): 321-328 (2012).

6. Gupta, B., Revagade, N., and Hilborn, J., Poly (lactic acid) fiber: an overview, Progress in Polymer Science, 32 (4): 455-482 (2007).

7. Adsul, M.G., Varma, A.J., and Gokhale, D.V., Lactic acid production from waste sugarcane bagasse derived cellulose, Green Chemistry, 9 (1): 58-62 (2007).

8. Datta, R., Tsai, S.P., Bonsignore, P., Moon, S.H., and Frank, J.R., Technological and economic potential of poly (lactic acid) and lactic acid derivatives, FEMS Microbiology Reviews, 16(2-3): 221-231 (1995).

9. Jardini, A.L., and Lopes, M.S., Synthesis and characterizations of poly (lactic Acid) by ring-opening polymerization for biomedical applications, Chemical Engineering Transactions, 38: 331-336 (2014).

10. Porter, K.A., Ring opening polymerization of lactide for the synthesis of poly (lactic acid), State of Illinois (2006).

11. Garlotta, D., A literature review of poly (lactic acid), Journal of Polymers and the Environment, 9(2): 63-84 (2001).

12. Gupta, A.P. and Kumar, V., New emerging trends in synthetic biodegradable polymers–polylactide: a critique, European Polymer Journal, 43(10): 4053-4074 (2007).

13. Masutani, K. and Kimura, Y., Poly(lactic acid) science and technology: processing, properties, additives and applications, The Royal Society of Chemistry, Cambridge, pp. 1-36 (2014).

14. Avérous, L. and Pollet, E., Environmental silicate nano-biocomposites, Springer-Verlag, London, pp. 13-39 (2012).

15. Smith, R., Biodegradable polymers for industrial applications, Woodhead; CRC Press, Cambridge, pp 37-42 (2005).

16. Urayama, H., Moon, S.I., and Kimura, Y., Microstructure and thermal properties of polylactides with different L- and D-unit sequences: Importance of the helical nature of the L-sequenced segments, Macromolecular Materials and Engineering, 288: 137-143 (2003).

17. Perego, G. and Cella, G.D., Poly(lactic acid) synthesis, structures, properties, processing, and applications, John Wiley & Sons, Inc., New Jersey, pp 141-154 (2010).

18. Auras, R., Harte, B., and Selke, S., An overview of polylactides as packaging materials, Macromolecular Biosciences, 4: 835-864 (2004).

19. Auras, R., Harte, B., Selke, S., and Hernandez, R., Mechanical, physical, and barrier properties of poly (lactide) films, Journal of Plastic film and Sheeting, 19(2): 123-135 (2003).

20. Cygan, Z., Improving processing and properties of polylactic acid, Plastic Trends, 20: 49 (2009).

21. Almenar, E. and Auras, R., Poly(lactic acid) synthesis, structures, properties, processing, and applications, John Wiley & Sons, Inc., New Jersey, pp 155-180 (2010).

22. Yam, K.L., The Wiley encyclopedia of packaging technology, John Wiley & Sons, Inc., New Jersey, pp 551-555 (2009).

23. Dorgan, J.R., Poly(lactic acid) synthesis, structures, properties, processing, and applications, John Wiley & Sons, Inc., New Jersey, pp 125-139 (2010).

24. Karkhanis, S.S., Stark, N.M., Sabo, R.C., and Matuana, L.M., Blown film extrusion of poly(lactic acid) without melt strength enhancers, Journal of Applied Polymer Science, 134(34): 45212 (2017).

25. Karkhanis, S.S., Stark, N.M., Sabo, R.C., and Matuana, L.M., Performance of poly(lactic acid)/cellulose nanocrystal composite blown films processed by two different compounding approaches, Polymer Engineering and Science, 58(11): 1965-1974 (2017).

26. Karkhanis, S.S., Stark, N.M., Sabo, R.C., and Matuana, L.M., Water vapor and oxygen barrier properties of extrusion-blown poly(lactic acid)/cellulose nanocrystals nanocomposite films, Composites Part A: Applied Science and Manufacturing, 114: 204-211 (2018).

27. Matuana, L.M., Karkhanis, S.S., Stark, N.M., and Sabo, R.C., Cellulose Nanocrystals as barrier performance enhancer of extrusion-blown PLA films for food applications, Biotech, Biomaterials and Biomedical - TechConnect Briefs, 3: 1-4 (2016).

28. Karkhanis, S.S. and Matuana, L.M., Extrusion blown films of poly(lactic acid) chain-extended with food grade multifunctional epoxies, Polymer Engineering and Science, 59(11): 2211-2219 (2019).

29. Salvidar-Guerra, E. and Vivaldo-Lima, E., Perego, G., Handbook of polymer synthesis., characterization and processing, John Wiley & Sons, Inc., New Jersey, pp 225-247 (2013).

30. Frenz, V., Villalobos, M., Awojulu, A.A, Edison, M., van der Meer, R., Multifunctional polymers as chain extenders and compatibilizers for polycondensates and biopolymers, SPE Antec 2008-Milwaukee, Wisconsin, 1682-1686 (2008).

31. Meng, Q., Heuzey, M.C., and Carreau, P.J., Control of thermal degradation of polylactide/clay nanocomposites during melt processing by chain extension reaction, Polymer Degradation and Stability, 97(10): 2010-2020 (2012).

32. Jaszkiewicz, A., Bledzki, A. K., & Meljon, A., Online observations and process analysis of chain extended polylactides during injection moulding, Polymer Degradation and Stability, 101(1): 65-70 (2014).

33. Vijayarajan, S., Selke, S.E.M., and Matuana, L.M., Continuous blending approach in the manufacture of epoxidized soybean-plasticized poly(lactic acid) sheets and films, Macromolecular Materials and Engineering, 299(5): 622-630 (2014).

34. Xing, C. and Matuana, L.M., Epoxidized soybean oil-plasticized poly (lactic acid) films performance as impacted by storage, Journal of Applied Polymer Science, 133(12): 43201 (2016).

35. Mallet, B., Lamnawar, K., and Maazouz, A., Improvement of blown film extrusion of poly(lactic acid): structure-processing-properties relationships, Polymer Engineering and Science, 54(4): 840-857 (2014).

36. Mallet, B., Lamnawar, K., and Maazouz, A., Compounding and melt strengthening of poly(lactic acid): shear and elongational investigations for forming process, Key Engineering Materials, 554-557: 1751-1756 (2013).

37. Mihai, M., Huneault, M.A., and Favis, B.D., Rheology and extrusion foaming of chain-branched poly(lactic acid), Polymer Engineering and Science, 50(3): 629-642 (2010).

38. Matuana, L.M., and Diaz, C.A., Study of cell nucleation in microcellular poly(lactic acid) foamed with supercritical CO_2 through a continuous-extrusion process, Industrial and Engineering Chemistry Research, 49(5): 2186-2193 (2010).

39. Al-Itry, R., Lamnawar, K., and Maazouz, A., Improvement of thermal stability, rheological and mechanical properties of PLA, PBAT and their blends by reactive extrusion with functionalized epoxy, Polymer Degradation and Stability, 97(10): 1898-1914 (2012).

40. Lim, L.T., Cink, K., and Vanyo, T., Poly(lactic acid) synthesis, structures, properties, processing, and applications, John Wiley & Sons, Inc., New Jersey, pp 191-215 (2010).

41. Pilla, S., Kim, S.G., Auer, G.K., Gong, S., and Park, C.B., Microcellular extrusion-foaming of polylactide with chain-extender, Polymer Engineering and Science, 49(8): 1653-1660 (2009).

42. Di, Y., Iannace, S., Di Maio, E., and Nicolais, L., Reactively modified poly (lactic acid): properties and foam processing, Macromolecular Materials and Engineering, 290(11): 1083-1090 (2005).

43. Tuominen, J., Kylmä, J., and Seppala, J., Chain extending of lactic acid oligomers. 2. increase of molecular weight with 1,6-hexamethylene diisocyanate and 2,2′-bis(2-oxazoline), Polymer 43 (1): 3-10 (2002).

44. Dong, W., Zou, B., Yan, Y., Ma, P., & Chen, M., Effect of chain-extenders on the properties and hydrolytic degradation behavior of the poly(lactide)/poly(butylene adipate-co-terephthalate) blends, International Journal of Molecular Sciences, 14(10): 20189-20203 (2013).

45. Wang, Y., Fu, C., Luo, Y., Ruan, C., Zhang, Y., and Fu, Y., Melt synthesis and characterization of poly(L-lactic acid) chain linked by multifunctional epoxy compound, Journal Wuhan University of Technology, Materials Science Edition, 25(5): 774-779 (2010).

46. Frenzen, P.D., Majchrowicz, T.A., Buzby, J.C., and Imhoff, B., Consumer acceptance of irradiated meat and poultry products (No. 33616), United States Department of Agriculture, Economic Research Service (2000).

47. Brun, E., Expert forecast on emerging chemical risks related to occupational safety and health, Office for Official Publications of the European Communities, Luxemburg, pp. 33-76 (2009).

48. Wu, C. S. (2003). Handbook of size exclusion chromatography and related techniques: revised and expanded, Marcel Dekker, New York, pp 1-23 (2003).

49. Robinson, J.W., Frame, E.M.S., and Frame II, G.M., Undergraduate instrumental analysis, Marcel Dekker, New York (2005).

50. Arruda, L.C., Magaton, M., Bretas, R.E.S., and Ueki, M.M., Influence of chain extender on mechanical, thermal and morphological properties of blown films of PLA/PBAT blends, Polymer Testing, 43: 27-37 (2015).

51. Liu, J., Lou, L., Yu, W., Liao, R., Li, R., and Zhou, C., Long chain branching polylactide: structures and properties, Polymer, 51(22): 5186-5197 (2010).

52. Cavalcanti, F.N., Teofilo, E.T., Rabello, M.S., and Silva, S.M.L., Chain extension and degradation during reactive processing of PET in the presence of triphenyl phophite, Polymer Engineering and Science, 47(12): 2155-2163 (2007).

53. Tee, Y.B., Talib, R.A., Abdan, K., Chin, N.L., Basha, R.K., and Yunos, K.F.M., Toughening poly(lactic acid) and aiding the melt-compounding with bio-sourced plasticizers, Agriculture and Agricultural Science Procedia, 2: 289-295 (2014).

54. Ojijo V. and Ray, S.S., Super toughened biodegradable polylactide blends with non-linear copolymer interfacial architecture obtained via facile in-situ reactive compatibilization, Polymer, 80: 1-17 (2015).

55. Tanaka, Y. and Kakiuchi, H., J., Study of epoxy compounds . part vi . curing reactions of epoxy resin and acid anhydride with amine , acid , alcohol , and phenol as catalysts, Journal of Polymer Science: Part A, 2: 3405-3430 (1964).

56. Wang, X., Mi, J., and Zhou, H., J., Transition from microcellular to nanocellular chain extended poly (lactic acid)/ hydroxyl-functionalized graphene foams by supercritical CO_2, Journal of Materials Science, 54(5): 3863-3877 (2019).

57. Polymer Science Learning Center, Differential Scanning Calorimetry, Retrieved from Polymer Science Learning Center: https://pslc.ws/macrog/dsc.htm. Accessed on August 30, 2020.

58. Liu, Y. and Matuana, L.M., Surface texture and barrier performance of poly(lactic acid)-cellulose nanocrystal extruded-cast films, Journal of Applied Polymer Science, 136(22): 47594 (2019).

59. Falling dart impact testing per ASTM D1709 and ISO 7765, Retrieved from G2MT laboratories: https://www.g2mtlabs.com/falling-dart-impact-testing-astm-d1709-iso-7765-1/. Accessed on August 30, 2020.

60. Stark, N.M., Opportunities for cellulose nanomaterials in packaging films: a review and future trends, Journal of Renewable Materials, 4(5): 313-326 (2016).

61. George, J. and Sabapathi, S.N., Cellulose nanocrystals: synthesis, functional properties, and applications, Nanotechnology, Science and Applications, 8: 45-54 (2015).

62. Mokhena, T.C., Sefadi, J.S., Sadiku, E.R., John, M.J., Mochane, M.J., and Mtibe, A., Thermoplastic processing of PLA/cellulose nanomaterials composites, Polymers, 10(12): 1363 (2018).

63. Moon, R.J., Martini, A., Nairn, J., Simonsen, J., and Youngblood, J., Cellulose nanomaterials review: Structure, properties and nanocomposites, Chemical Society Reviews, 40(7): 3941-3994 (2011).

64. Fortunati, E., Peltzer, M., Armentano, I., Torre, L., Jimenez, A., and Kenny, J. M., Effects of modified cellulose nanocrystals on the barrier and migration properties of PLA nano-biocomposites, Carbohydrate Polymers, 90(2): 948-956 (2012).

65. Espino-Pérez, E., Bras, J., Ducruet, V., Guinault, A., Dufresne, A., and Domenek, S., Influence of chemical surface modification of cellulose nanowhiskers on thermal, mechanical, and barrier properties of poly(lactide) based bionanocomposites, European Polymer Journal, 49: 3144-3154 (2013).

66. Sanchez-Garcia, M.D. and Lagaron, J.M., On the use of plant cellulose nanowhiskers to enhance the barrier properties of polylactic acid, Cellulose, 17: 987-1004 (2010).

67. Yu, H.Y., Zhang, H., Song, M.L., Zhou, Y., Yao, J., and Ni, Q.Q., From cellulose nanosperes, nanorods to nanofibers: various aspect ratio induced nucleation/reinforcing effects on polylactic acid for robust-barrier food packaging, ACS Applied Materials and Interfaces, 9(50): 43920-43938 (2017).

68. Sung, S.H., Chang, Y., and Han, J., Development of polylactic acid nanocomposite films reinforced with cellulose nanocrystals derived from coffee silverskin, Carbohydrate Polymers, 169: 495-503 (2017).

69. Dhar, P., Gaur, S.S., Soundararajan, N., Gupta, A., Bhasney, S.M., Milli, M., Kumar, A., and Katiyar, V., Reactive extrusion of polylactic acid/cellulose nanocrystal films for food packaging applications: influence of filler type on thermomechanical, rheological, and barrier properties, Industrial and Engineering Chemistry Research, 56(16): 4718-4735 (2017).

70. Pei, A., Zhou, Q., and Berglund, L.A., Functionalized cellulose nanocrystals as biobased nucleation agents in poly(l-lactide) (PLLA) - crystallization and mechanical property effects, Composites Science and Technology, 70(5): 815-821 (2010).

71. Jonoobi, M., Harun, J., Mathew, A.P., and Oksman, K., Mechanical properties of cellulose nanofiber (CNF) reinforced polylactic acid (PLA) prepared by twin screw extrusion, Composites Science and Technology, 70(12): 1742-1747.

72. Herrera, N., Mathew, A.P., and Oksman, K., Plasticized polylactic acid/cellulose nanocomposites prepared using melt-extrusion and liquid feeding: mechanical, thermal and optical properties, Composites Science and Technology, 106: 149-155 (2015).

73. Herrera, N., Salaberria, A.M., Mathew, A.P., and Oksman, K., Plasticized polylactic acid nanocomposite films with cellulose and chitin nanocrystals prepared using extrusion and compression molding with two cooling rates: Effects on mechanical, thermal and optical properties, Composites Part A: Applied Science and Manufacturing, 83: 89-97 (2016).

74. Herrera, N., Roch, H., Salaberria, A.M., Pino-Orellana, M.A., Labidi, J., Fernandes, S.C., Radic, D., Leiva,A., and Oksman, K., Functionalized blown films of plasticized polylactic acid/chitin nanocomposite: Preparation and characterization, Materials and Design, 92: 846-852 (2016).

75. Bondeson, D. and Oksman, K., Polylactic acid/cellulose whisker nanocomposites modified by polyvinyl alcohol, Composites Part A: Applied Science and Manufacturing, 38: 2486-2492 (2007).

76. Shi, Q., Zhou, C., Yue, Y., Guo, W., Wu, Y., and Wu, Q., Mechanical properties and in vitro degradation of electrospun bio-nanocomposite mats from PLA and cellulose nanocrystals, Carbohydrate Polymers, 90(1): 301-308 (2012).

77. Katiyar, N. and Balasubramanian, K., Nano-heat-sink thin film composite of PC/three-dimensional networked nano-fumed silica with exquisite hydrophobicity, *RSC Advances*, **5**(6): 4376-4384 (2015).

78. Oksman, K., Aitomaki, Y., Mathew, A.P., Siqueira, G., Zhou, Q., Butylina S., Tanpichai, S., Zhou, X., Hooshmand, S., Review of the recent developments in cellulose nanocomposite processing, Composites Part A: Applied Science and Manufacturing, 83: 2-18 (2016).

79. Olympus, Types of optical miscroscopes, Retrieved from Olympus: https://www.olympus-ims.com/en/microscope/terms/feature10/. Accessed on August 30, 2020.

80. Marrison, J., Marriott, P., and O'Toole, P., Ptychography-a label free, high-contrast imaging technique for live cells using quantitative phase information, Scientific Reports, 3: 2369 (2013).

81. Zhou, Y., Fuentes-Hernandez, C., Khan, T.M., Liu, J.C., Hsu, J., Shim, J.W., Dindar, A., Youngblood, J.P., Moon, R.J., and Kippelen, B., Recyclable organic solar cells on cellulose nanocrystal surface, Scientific Reports, 3: 1536 (2013).

82. Volchko, J., Visible light spectrum: from a lighting manufacturer's perspective, Retrieved from Lumitex: https://www.lumitex.com/blog/visible-light-spectrum. Accessed on August 30, 2020.

83. Siracusa V., Food packaging permeability behaviour: a report, International Journal of Polymer Science, 2012: 1-11 (2012).

84. Rosato, M.G. and Rosato, D.V., Plastics design handbook, Springer, New York (2001).

85. Robertson, G.L., Food packaging: principles and practice, CRC press, Boca Raton (2013).

86. Andrade P,R.D., Lemus M,R., and Perez C,C.E., Models of sorption isotherms for food: uses and limitations, Vitae, 18(3): 325-334 (2011).

87. van den Berg, C., Properties of water in foods, Springer, New York, pp 119-131 (1985).

88. Rachtanapun, P., Shelf life study of salted crackers in pouch by using computer simulation models, Chiang Mai Journal of Science, 34(2): 209-218 (2007).

89. Sirpatrawan, U., Shelf-life simulation of packaged rice crackers, Journal of Food Quality, 32(2): 224-239 (2009).

90. Azanha, A.B. and Faria, J.A.F., Use of mathematical models for estimating the shelf-life of cornflakes in flexible packaging, Packaging Technology and Science, 18(4): 171-178 (2005).

91. Robertson, G.L. and Lee, D.S., Comparison of linear and GAB isotherms for estimating the shelf life of low moisture food packaged in plastic films, Journal of Food Engineering, 291: Article 110317 (2021).

92. Kilcrast, D. and Subramaniam, P., Food and beverage stability and shelf life, Woodhead Publishing, Cambridge (2011).

Chapter 3

EXPERIMENTAL

3.1 Materials

Poly(lactic) acid (PLA 4044D) with a melt flow rate of 3.95 g/10 min (190ºC, 2.16 kg) and density of 1.24 g/cm^3, obtained from NatureWorks® LLC (Minnetonka, MN) was used as the resin in this study [1-3]. Two grades of epoxy-functionalized, FDA-approved polymeric chain extenders (CE), Joncryl ADR® 4468 and 4400 in the solid flake form were used, with characteristics and listed in Table 3.1. Freeze-dried cellulose nanocrystals were obtained from Forest Products Laboratory (2012-FPL-CNC-043). These CNCs were produced by dissolving wood pulp using the sulfuric acid process with a procedure described elsewhere [4]. They have diameters around 5 nm and lengths around 100-300 nm [5].

Table 3.1 Properties of chain extenders.

Properties	**Chain extender grades**	
	4468	4400
Epoxy equivalent weight (g/mol)	310	485
Molecular weight (g/mol)	7,250	7,100
Specific gravity, 25°C	1.08	1.08

3.2 Sample manufacturing

The following section describes the sample compounding and film manufacturing.

3.2.1 Preparation of PLA/CE composites

Firstly, experiments were performed in a torque rheometer to evaluate the effectiveness and efficiency of two multifunctional epoxy CE grades in chain extending PLA. PLA pellets and the two grades of CE listed in Table 3.1 were oven-dried at 50°C for at least 24 hours to remove moisture before compounding. Compounding of PLA pellets with both grades of multifunctional epoxies took place in an electrically heated 60 ml three-piece internal mixer/measuring head (3:2 gear ratio) with counter-rotating roller style mixing blades (C.W. Brabender Instruments, South Hackensack, NJ) at 200°C for 5 minutes with the rotor speed set at 35 rpm. A 5.6 kW (7.5 hp) Intelli-Torque Plasti-Corder torque rheometer (C.W. Brabender Instruments) powered the mixer [1,6,7]. The multifunctional epoxy loading varied from 0.25 to 1 wt%, with an increment of 0.25 wt%. From this experiment, the torque and stock temperature data were recorded as function of mixing time and analyzed to assess the effectiveness of these chain extenders and identify the most efficient one.

Secondly, the feasibility of utilizing the most efficient CE in extrusion-blown PLA film processing was assessed by dry-blending it at various concentrations (0 to 1 wt%) with PLA in a high-intensity mixer (Blender MX1050XTS from Waring Commercial, Calhoun, GA, USA) at 22,000 rpm for 10 s [1,2,8]. The compounded formulations in pellet form were gravity-fed into the hopper of a 19 mm single-screw extruder (C.W. Brabender Instruments) with a length-to-diameter ratio of 30:1 and blown into films as previously described [1-3,8-10]. Starting from the hopper to the die, the temperature profile of the extruder was set at 200-200-200-200°C. The

speeds of the extruder's rotational screw and the pull-up rollers for film take off were set at 35 rpm and 40 rpm, respectively, while an air pressure of 0.517 kPa (0.075 psi) was used to inflate the film to a blow-up ratio of 5, leading to ~0.027 mm thick films, measured by digital micrometer [1-3,8-10].

3.2.2 Preparation of PLA/CNC composites

The CNCs were pre-blended in a high intensity mixer at 22,000 rpm for approximately 1 minute to reduce their size from the received cake to a fine powder. PLA pellets and CNCs were oven-dried at 50^{o}C for at least 24 hours to remove moisture before compounding through the following two different approaches of incorporating CNCs into the PLA matrix.

3.2.2.1 Direct dry-blending (DB)

The direct dry-blending of varying amounts of CNCs (0; 0.5; 1; 1.5 and 2 wt%) into PLA was carried out in a high intensity mixer at 22,000 rpm for approximately 1 minute. The compounded materials were then used to manufacture blown film as described below.

From the preliminary work for the direct dry-blending process, 1 wt% CNC was determined as the ideal concentration and was used for the next section (Section 3.2.2.2 Melt blending) [8].

3.2.2.2 Melt blending process (MB)

Mixing temperature, speed and time affect the dispersion of additives into polymer matrices [11]. Blending of CNCs with PLA took place in an electrically heated 60 ml three-piece internal mixer/measuring head (3:2 gear ratio) with counter-rotating roller style mixing blades

(C.W. Brabender Instruments, South Hackensack, NJ) at 160ºC for 3 minutes with the rotor speed set at 30 rpm. A 5.6 kW (7.5 hp) Intelli-Torque Plasti-Corder Torque Rheometer (C.W. Brabender Instruments, South Hackensack, NJ) powered the mixer. These processing conditions were optimized in our preliminary study. As previously mentioned, the CNC loading was fixed at 1 wt%, which was determined as the ideal concentration from our preliminary work [8]. The compounded materials were frozen for at least 24 hours and then pulverized using a Thomas-Wiley Laboratory Mill-Model 4 (A.H. Thomas Co., Philadelphia, PA) with a screen mesh size of 2 mm and then blown into a film as described in the following sections.

3.2.2.3 PLA/CNC film manufacturing

Neat PLA pellets and the compounded materials (CNC filled PLA processed by direct dry- and melt-blending) described above were blown into films using a 19 mm single screw extruder (C.W. Brabender Instruments, South Hackensack, NJ), powered by a 3.73 kilowatt (5 hp) Prep Center® D52 (C.W. Brabender Instruments, South Hackensack, NJ). The extruder had a length-to-diameter ratio of 30:1 and was fitted with an annular die of diameter 25.4 mm and die opening of 0.889 mm. A venting single-stage mixing screw (2.63:1 compression ratio) with a torpedo screw tip (35 degrees) was used during processing. Starting from the hopper to the die, the temperature profile of the extruder was set at 180-180-180-180ºC. The rotational screw speed of the extruder was set at 35 rpm whereas the speed of take-up rollers for drawing the film upward was set at 40 rpm. An internal air pressure of 0.517 kPa (0.075 psi) was used to inflate the film. The blow-up ratio of the film, defined as the ratio of the diameter of the final tubular film to the diameter of the annular die, was calculated as 5. The average thickness was measured as ~0.027 mm at 10 random locations along the film using a digital micrometer (model 49-70 from TMI, Ronkonkoma, NY, USA) with a resolution of 0.001 mm [1-3,8,9].

3.3 Property evaluation

3.3.1 Fourier transform infrared spectroscopy (FTIR)

3.3.1.1 FTIR of PLA/CE blends

Chain extension reactions between PLA and CE in blends containing various amounts of chain extenders compounded in an internal mixer were studied through Fourier transform infrared spectroscopy using a Shimadzu IR Affinity 1S infrared spectrophotometer (Shimadzu Corporation, Kyoto, Japan) in attenuated total reflectance (ATR) mode. Each spectrum was obtained with triangle apodization using 64 scans in the range of 4000-400 cm^{-1}, at a wavelength resolution of 4 cm^{-1} [1]. The spectra were smoothened with the boxcar smooth method using 7 smooth points and truncated from 500-2000 cm^{-1} to study the region of interest using WinFIRST software from Thermo Nicolet (Madison, WI). The compounded materials were compression molded into disks before analysis.

3.3.1.2 FTIR of PLA and PLA/1% CNC composite films prepared by both DB and MB processes

Infrared spectra of PLA and PLA/1% CNC composite films prepared by both direct dry- and melt blending processes were collected using the aforementioned spectrophotometer to verify their mechanism of degradation. Spectra of films were obtained using conditions previously described. Films of similar thickness (~ 0.018 mm) were dried for 24 hours in an oven at 50^{o}C prior to testing. The thickness of samples was kept constant to allow comparison of different spectra since the peak intensity of a FTIR absorption band is dependent on the path length of infrared light, i.e., sample's thickness.

The peak heights (peak intensity) were analyzed without smoothening or baseline correction. The peak intensity at 957 cm^{-1}, assigned to the O-H vibrations in carboxyl groups, a potential product of chain scission of PLA, was chosen to calculate the carboxyl index for each film [1,12,13]. This peak was normalized using the intensities of reference peaks at 2994 cm^{-1} and 2945 cm^{-1}, corresponding to stretching vibrations of C-H in saturated hydrocarbons, because they changed the least during thermal degradation due to processing. The carboxyl index for each film was calculated using the following equation [1,12,13]:

$$\text{Carboxyl index} = \frac{I_{957}}{I_x} \qquad \text{(Equation 3.1)}$$

where I_{957} is the peak intensity at 957 cm^{-1} and I_x is the peak intensity of reference peak at 2994 cm^{-1} or 2945 cm^{-1}. Samples were tested in triplicates [1].

3.3.2 Gel permeation chromatography

The number average (M_n), weight average molecular weight (M_w) and viscosity average molecular weight (M_v) of PLA, PLA/CE and PLA/CNC films; PLA/CE materials compounded in an internal mixer; as well as unprocessed PLA pellets and PLA pellets subjected to direct dry- and melt-mixing were measured by GPC using a Waters instrument (Waters 1515, Waters, Milford, MA) equipped with a series of HR Styragel® columns (HR4, HR3, HR2 (300*7.8 mm (I.D)) and a Refractive Index (RI) detector (Waters 2414, Waters, Milford, MA). The test was conducted at a flow rate of 1 ml/min at 35°C using the Mark-Houwink corrected constant K = 0.000174 ml/g and α = 0.736 for PLA solution in ACS Reagent Grade (99.99% pure) tetrahydrofuran (THF). Polystyrene (PS) standards ranging between 2.9×10^3 to 3.64×10^6 daltons (Da) were used for

calibration. Approximately 20 mg of sample was dissolved in 10 ml of THF. The samples were then filtered and transferred into 2 ml glass vials. A syringe was used to inject 100µl samples from the vial into the GPC. The detector and column were maintained at 35ºC. The obtained data was analyzed using the Breeze software (version 3.30 SPA, 2002) (Waters, Milford, MA, USA). Samples were tested in triplicates [1,3].

3.3.3 Melt flow index (MFI)

The melt flow index (MFI) and melt density (δ_m) of PLA as well as PLA/CE blends compounded in an internal mixer were measured using a Melt Indexer (model LMI 4000) supplied by Dynisco Polymer Testing (Franklin, MA). Methods A and B outlined in ASTM 1238 were employed simultaneously to measure the MFI and melt volume rate (MVR). Three replicates for each sample were tested at 190ºC with a dead load of 2.16 kg. This information was then used to calculate the δ_m of the samples using the following equation [9,10]:

$$\delta_m = \frac{MFI}{MVR} \qquad \text{(Equation 3.2)}$$

The MFI and δ_m were then used to obtain the zero-shear viscosity (η_0) using the following equation [9,10]:

$$\eta_0 = \frac{\delta_m \cdot W \cdot R^4}{8 \cdot MFI \cdot L \cdot R_A^2} = 4.8547 \times \frac{\delta_m \cdot W}{MFI} \qquad \text{(Equation 3.3)}$$

where R (1.0475 mm) is the bore radius of the die, R_A (4.775 mm) is the bore radius of the cylinder where the polymer melts, L (8 mm) is the length of the die and W (2160 g) is the applied dead load.

3.3.4 Differential scanning calorimetry (DSC)

Differential scanning calorimetry (DSC) was performed on at least three samples (each weighing 6-10 mg) of PLA, PLA/CE and PLA/CNC films as well as PLA/CE materials compounded in an internal mixer using a Q100 instrument (TA Instruments, New Castle, DE) in accordance with ASTM D3418. The DSC cell was purged with liquid nitrogen flowing at 70 ml/min. Each test employed 6-10 mg of sample tested with a set of heating and cooling cycles. The samples were heated from 25°C to 200°C at a ramp rate of 10°C/min and held at 200°C for 5 minutes to erase their thermal history. Subsequently, the samples were cooled to 25°C and reheated to 200°C at the same ramp rate. The glass transition temperature (T_g), cold crystallization temperature (T_c), melt peak temperature (T_m), enthalpy of the cold crystallization process (ΔH_c) and melting peaks (ΔH_m) were determined using the software Universal Analysis 2000, V4.5 (TA Instruments, Delaware). The percentage crystallinity (% χ_c) was calculated from both, the first and second heat scans using the following equation [1-3,9,10,14,15]:

$$\%\chi_c = \frac{\Delta H_m - \Delta H_c}{\Delta H_m^{\infty} \times [1 - (\%\text{wt CNC}/100)]} \times 100 \qquad \text{(Equation 3.4)}$$

where %wt CNC is the total weight percentage of CNC (1 wt%). The melt enthalpy of a spherulite of infinite size (ΔH_m^{∞}) used for PLA was 93 J/g [1-3,9,10,14,15]. Six samples were tested for each material.

3.3.5 Thermogravimetric analysis (TGA)

Non-isothermal and isothermal TGA measurements of the neat PLA and PLA/CNC composite films were performed using a Q500 thermogravimetric analyzer (TA Instruments, New Castle, DE) on samples weighing between 6-10 mg. For non-isothermal TGA, the samples (in triplicates) were heated from 25^{o}C to 700^{o}C at a ramp rate of 10^{o}C/min under nitrogen atmosphere (40 ml/min). In contrast, the samples were heated to 180^{o}C at a rate of 180^{o}C/min and held isothermal for 300 minutes under the same nitrogen atmosphere for isothermal TGA [1].

3.3.6 Light microscopy

PLA and PLA/CNC composite films were observed using an Olympus BX41 optical microscope (Olympus, Center Valley, PA) equipped with a camera (Olympus Qcolor3). Additionally, the films were also observed using a Keyence VHX-600E (Keyence Corporation, Osaka, Japan) microscope equipped with a Keyence VH-Z100R lens to monitor the distribution and dispersion of CNCs into the PLA film [1-3].

3.3.7 Ultraviolet-visible (UV-Vis) spectroscopy

A UV-Visible spectrophotometer Perkin-Elmer Lambda 25 (Perkin-Elmer Instruments, Beaconsfield, UK) was used to record the transmittance of PLA and PLA/CNC composite films. The UV-Visible spectra were obtained over a wavelength range of 200 to 900 nm at a scan rate of 240 nm/min. For each spectrum, the average light transmission value reported was estimated by averaging the percent light transmission values in the visible range, i.e., from 380 to 720 nm wavelength. Three replicates were tested [1-3].

3.3.8 Residence time of PLA/CE blends in the extruder

The residence times of chain-extended PLA compounds in the single-screw extruder were estimated from their residence time distribution (RTD) curves. These RTD curves for PLA/CE blends were obtained by introducing carbon black as a tracer into the feed stream of the extruder during blown film manufacture using processing conditions previously described. A constant amount of carbon black (50 mg) was directly fed into the single screw extruder instantaneously once the films were inflated to a stable blow-up ratio of 5. Films were collected every 15 s and tracer concentrations in the films determined using a UV-Vis spectrophotometer (Perkin-Elmer Lambda 25, Perkin-Elmer Instruments, Beaconsfield, UK), until the black color imparted by the tracer visually disappeared (approximately 30 minutes). Since carbon black absorbs light throughout the visible light range (380-720 nm), UV-Vis spectra were obtained over a randomly selected wavelength range of 480-520 nm at a scan rate of 120 nm/min but the tracer contents were determined at a fixed wavelength of 500 nm [1,2,16-18]. The obtained tracer concentrations were plotted as a function of sampling times for each film to develop its RTD curve.

3.3.9 Falling dart impact strength

Impact strength of the films was determined using Labthink FDI-01 Falling Dart Impact Tester (Labthink International, Inc., Medford, MA, USA) in agreement with method A described in ASTM D1709 with slight modifications. A customized 10 g dart with diameter of 38.2 mm was dropped from a height of 0.33 m (13 in) onto four layers of the film specimens secured by clamp rings with an inside diameter of 76.2 mm. The films were then assessed as fail or non-fail. “Failure” refers to the film rupture allowing the full penetration of the dart through the films, and “non-failure” indicates the films sustain the integrity to hold the dart. Testing followed a stair-step

approach with the increment of dart weight of 5 g, meaning that the weight of the dart increased by 5 g if "non-fail" occurred or decreased by 5 g in case of film failure. Each test required the occurrence of at least ten fails and ten non-fails to complete and generated the failure weight as a measurement of impact strength. This study employed at least three test replicates for each film composition [19].

3.3.10 Water vapor permeability (WVP)

The water vapor transmission rate (WVTR) of the PLA/CNC films was measured gravimetrically, according to the desiccant method in ASTM E 96. Film samples, in replicates of at least 5, were mechanically sealed onto 3/4" depth vapometer cup assemblies, weighed and placed in a controlled humidity chamber set at various temperature and relative humidity (RH) conditions as described below. The cups were removed from the chamber and weighed to the nearest 0.0001 g after 24 hours to determine the amount of water vapor permeating through the film and being absorbed by the desiccant (anhydrous calcium sulfate). The change in the weight of cups was used to calculate the water vapor transmission rate (WVTR) as follows [1,2,8]:

$$\mathrm{WVTR} = \frac{\Delta \mathrm{W}/\mathrm{t}}{\mathrm{A}} \qquad \text{(Equation 3.5)}$$

where ΔW is the weight gain of the cups at time t (24 hours); and A is the effective area of exposed film (31.67×10^{-4} m^2).

For the PLA and PLA/CNC (DB) films, the influence of temperature was studied using four different temperatures (10°C, 17°C, 23°C and 31°C) at a constant RH of 85%, whereas the

effect of RH content was evaluated at 23°C in the range of 50% to 85% with 7% increments, both testing conditions generating different partial water vapor pressures [2].

The obtained WVTR values were normalized by the thickness (l) and difference in partial pressure of permeant across the sample (Δp) to calculate the WVP:

$$WVP = \frac{WVTR \times l}{\Delta p} = \frac{WVTR \times l}{p_1 - p_2} = \frac{WVTR \times l}{P_{sat} \cdot (RH_{out} - RH_{in})} \quad \text{(Equation 3.6)}$$

where p_1 and p_2 are the partial vapor pressures of the permeant (water vapor) on the outside and inside of the test film, respectively and can be given as $p_1 = P_{sat} \cdot RH_{out}$ and $p_2 = P_{sat} \cdot RH_{in}$, respectively. RH_{out} and RH_{in} are the relative humidities of the external (testing RH) and internal side (≈ 0%) of the film; and P_{sat} is the saturated vapor pressure at the test temperature. For the temperatures tested, the saturated vapor pressures were 1227 Pa, 1938 Pa, 2812 Pa and 4498 Pa at 10°C, 17°C, 23°C and 31°C, respectively.

3.3.11 Oxygen permeability (OP)

Oxygen transmission rate (OTR) of PLA and PLA/CNC films was measured using VAC-V2 Gas Permeability Tester (Labthink International, Medford, MA, USA) in accordance with the procedures outlined in ASTM D3985. The influence of temperature was studied from 17°C to 50°C at 0% RH. At least three replicates were tested for each film sample [2]. The OP was calculated from OTR values as follows:

$$OP = \frac{OTR \times l}{\Delta p} \quad \text{(Equation 3.7)}$$

where l is the thickness; Δp is difference in partial pressure of permeant (oxygen) across the sample (101,325 Pa).

3.4 Shelf-life of crackers packaged in direct dry-blended PLA/1% CNC films

3.4.1 Moisture sorption isotherm of crackers

3.4.1.1 Initial moisture content (IMC)

Six aluminum dishes were weighed using the Ohaus Discovery Analytical Balance (Ohaus Corp., Parsippany, NJ) without the product (crackers). About 2-3 grams of the saltine crackers were crushed, placed into the aluminum dishes and weighed again. The aluminum dishes with the crackers were then placed into an oven for drying at 100 ± 2°C for 48 hours until a constant weight was achieved. The dishes were re-weighed to determine the weight loss of the product. The initial moisture content (IMC) on dry basis was calculated using the following equation [20-22]:

$$MC\ (\%) = \frac{W_i - W_D}{W_D} \times 100 \quad \text{(Equation 3.8)}$$

where W_i is the initial weight of the product (before drying) (in g) and W_D is the weight of the product after drying (in g) in the oven.

3.4.1.2 Equilibrium moisture content (EMC)

Six different saturated salt solutions were used in desiccators to provide constant relative humidity (RH) conditions ranging from 10% to 96% (Table 3.2). These desiccators were further placed in an oven set to 25°C to maintain a constant temperature. Six samples of approximately 2-3 grams of saltine crackers were put in aluminum dishes and placed in each of the six desiccators containing different saturated salt solutions (various RH conditions). The samples were allowed to equilibrate for a period of at least two weeks until there was no discernable weight gain. The EMC of the samples was then calculated using the following equation [20-22]:

$$\text{MC}\ (\%) = \left[\frac{W_e}{W_i}(\text{IMC} + 1) - 1\right] \times 100 \qquad \text{(Equation 3.9)}$$

where W_e is the weight of crackers at equilibrium (g), W_i is the initial weight of crackers (g) and IMC is the initial moisture content calculated from Equation 3.8.

The moisture sorption isotherm was constructed as a plot of the EMC values of the crackers as a function of their storage RH [20-22].

Table 3.2 Theoretical and measured relative humidity (RH) conditions generated in desiccators with saturated salt solutions.

Salt	%RH at 25°C	
	Theoretical	**Measured**
Lithium chloride	11.3	10.4 ± 0.8
Magnesium chloride	32.8	31.8 ± 1.8
Magnesium nitrate	52	50.1 ± 3.5
Sodium nitrite	65	61.1 ± 3.5
Ammonium chloride	78.8	78.5 ± 5.3
Potassium nitrate	93.6	96.1 ± 5.9

3.4.2 Shelf-life of crackers packaged in PLA and PLA/CNC films

Film samples (PLA and PLA/1% CNC direct dry-blended) were mechanically sealed onto the previously described vapometer cup assemblies containing approximately 10 grams of crushed crackers and placed into the desiccators set at various RH conditions. The desiccators were then placed in an oven set at 25°C to maintain a constant temperature. The vapometer cup assemblies were weighed periodically over a one-month period to determine the percent moisture gain until the equilibrium moisture content (EMC) was reached (steady state).

From the data, plots of moisture content versus storage time were generated [23]. The product's shelf-life, i.e., the time required by the crackers to reach its critical moisture content (CMC), was determined from moisture content versus storage time plots. Generally, CMC is determined according to the sensory evaluation as the minimum moisture content at which the

product becomes organoleptically unacceptable, for example losing its crispiness. Critical moisture content values of 6.1% for wheat crackers [24]; 6.8% for rice crackers (21.09% fat, 6.31% protein, 68.39% total carbohydrate) [21]; as well as 10% and 8% for lean and rich crackers, respectively [25,26] have been reported in the literature based on the sensory evaluation for crackers; rice crackers; and crackers, respectively. Nevertheless, a CMC value of 8% was adopted in this study, an average between the CMC values of 6% and 10% reported in the literature for wheat crackers [21,24-26].

3.5 Statistics

Means were compared by the analysis of variance (ANOVA) and least significant differences (LSD) tests at 5% level of significance using IBM SPSS Statistics 24 (Armonk, NY).

REFERENCES

REFERENCES

1. Karkhanis, S.S., Stark, N.M., Sabo, R.C., and Matuana, L.M., Performance of poly(lactic acid)/cellulose nanocrystal composite blown films processed by two different compounding approaches, Polymer Engineering and Science, 58(11): 1965-1974 (2017).

2. Karkhanis, S.S., Stark, N.M., Sabo, R.C., and Matuana, L.M., Water vapor and oxygen barrier properties of extrusion-blown poly(lactic acid)/cellulose nanocrystals nanocomposite films, Composites Part A: Applied Science and Manufacturing, 114: 204-211 (2018).

3. Karkhanis, S.S. and Matuana, L.M., Extrusion blown films of poly(lactic acid) chain-extended with food grade multifunctional epoxies, Polymer Engineering and Science, 59(11): 2211-2219 (2019).

4. Reiner, R.S. and Rudie, A.W., Production and Applications of Cellulose Nanomaterials, TAPPI Press, Peachtree Corners, pp. 21-24 (2013).

5. Postek, M.T., Vladar, A., Dagata, J., Farkas, N., Ming, B., Wagner, R., Raman, A., Moon, R.J., Sabo, R., and Wegner, T.H., Development of the metrology and imaging of cellulose nanocrytsals, Measurement Science and Technology, 22(1): 024005 (2011).

6. Faruk, O. and Matuana, L.M., Nanoclay reinforced HDPE as a matrix for wood-plastic composites, Composites Science and Technology, 68(9): 2073-2077 (2008).

7. Matuana, L.M. and Kim, J.W., Fusion characteristics of rigid PVC/wood-flour composites by torque rheometry, Journal of vinyl additive and technology, 13(1): 7-13 (2007).

8. Matuana, L.M., Karkhanis, S.S., Stark, N.M., and Sabo, R.C., Cellulose Nanocrystals as barrier performance enhancer of extrusion-blown PLA films for food applications, Biotech, Biomaterials and Biomedical - TechConnect Briefs, 3: 1-4 (2016).

9. Karkhanis, S.S., Stark, N.M., Sabo, R.C., and Matuana, L.M., Blown film extrusion of poly(lactic acid) without melt strength enhancers, Journal of Applied Polymer Science, 134(34): 45212 (2017).

10. Vijayarajan, S., Selke, S.E.M., and Matuana, L.M., Continuous blending approach in the manufacture of epoxidized soybean-plasticized poly(lactic acid) sheets and films, Macromolecular Materials and Engineering, 299(5): 622-630 (2014).

11. Mayoral, B., Lopes, J., and McNally, T., Influence of processing parameters during small-scale batch melt mixing on the dispersion of MWCNTs in a poly(propylene) matrix, Macromolecular Materials and Engineering, 299(5): 609-621 (2014).

12. Stark, N.M and Matuana, L.M., Surface chemistry changes of weathered HDPE/wood-flour composites studied by XPS and FTIR spectroscopy, Polymer Degradation and Stability, 86(1): 1-9 (2004).

13. Fechine, G.J.M., Rabello, M.S., Souto Maior, R.M., and Catalani, L.H., Surface characterization of photodegraded poly(ethylene terephthalate). The effect of ultraviolet absorbers, Polymer, 45(7): 2303-2308 (2004).

14. Xing, C. and Matuana, L.M., Epoxidized soybean oil-plasticized poly(lactic acid) films performance as impacted by storage, Journal of Applied Polymer Science, 133(12): 43201 (2016).

15. Battegazzore, D., Bocchini, S., and Frache, A., Crystallization kinetics of poly(lactic acid)-talc composites, Express Polymer Letters, 5(10): 849-858 (2011).

16. Wang, J., Thurber, C., Bishop, M., Monaenkova, D., Marchbanks, E., Kim, H., Keene, E., and Chen, X., Study of residence time distribution for a blown film line using inline uv-vis spectroscopy and optical imaging on a film bubble, SPE Antec 2017–Anaheim, California, 1168-1174 (2017).

17. Wesholowski, J., Berghaus, A., and Thommes, M., Inline determination of residence time distribution in hot-melt-extrusion, Pharmaceutics, 10(2): 49 (2018).

18. Levinson, R., Berdahl, P., and Akbari, H., Solar spectral optical properties of pigments- Part I: model for deriving scattering and absorption coefficients from transmittance and reflectance measurements, Solar Energy Materials and Solar Cells, 89(4): 319-349 (2005).

19. Liu, Y. and Matuana, L.M., Surface texture and barrier performance of poly(lactic acid)-cellulose nanocrystal extruded-cast films, Journal of Applied Polymer Science, 136(22): 47594 (2019).

20. Rachtanapun, P., Shelf life study of salted crackers in pouch by using computer simulation models, Chiang Mai Journal of Science, 34(2): 209-218 (2007).

21. Sirpatrawan, U., Shelf-life simulation of packaged rice crackers, Journal of Food Quality, 32(2): 224-239 (2009).

22. Azanha, A.B. and Faria, J.A.F., Use of mathematical models for estimating the shelf-life of cornflakes in flexible packaging, Packaging Technology and Science, 18(4): 171-178 (2005).

23. Matuana, L.M., Karkhanis, S.S., Stark, N.M., and Sabo,R.C., Potential of PLA/CNC films for improving the shelf life of a dry food product [MSU Invention Disclosure], Case number TEC2018-0131, Filed on April 6, 2018.

24. Hao, F., Lu, L., and Wang, J., Finite element simulation of shelf life prediction of moisture-sensitive crackers in permeable packaging under different storage conditions, Journal of Food Processing and Preservation, 40(1): 37-47 (2016).

25. Kaletunc, G. and Breslauer, K.J., Characterization of cereals and flours: properties, analysis and applications, Marcel Dekker, Inc, New York, pp. 151-171 (2003).

26. Amemiya, J. and Menjivar, J.A., Mechanical properties of cereal-based food cellular systems, American Association of Cereal Chemists, 77th Annual Meeting, Minneapolis, Abstract 207 (1992).

Chapter 4

RESULTS AND DISCUSSION

4.1 Extrusion blown films of poly(lactic acid) chain-extended with food grade multifunctional epoxies

The title and content of section 4.1 were published in Polymer Engineering and Science, 59(11): 2211-2219 (2019). doi: https://doi.org/10.1002/pen.25224. This paper was co-authored by L.M. Matuana.

The main objective of this section was to investigate the effectiveness and efficiency of two food-grade multifunctional epoxies with varying reactivities in chain extending and branching PLA, improving its processability through the blown film extrusion process and improving the ductility of PLA films (*specific objective #1*) [1].

4.1.1 Effectiveness and efficiency of multifunctional epoxy grades in chain extending PLA

Torque rheometry can be used to follow the chain extension reaction of PLA with CE since an increase in torque is associated with chain extension [2-4].

Typical curves obtained from the Brabender torque rheometer for the torque and stock temperature of PLA as a function of mixing time are shown in Figure 4.1. It can be seen that stock temperature reduces when the material is loaded and then increases above the set temperature of 200ºC to reach 211ºC due to shear generated by the mixer when the material is kneaded by the rotor blades [5].

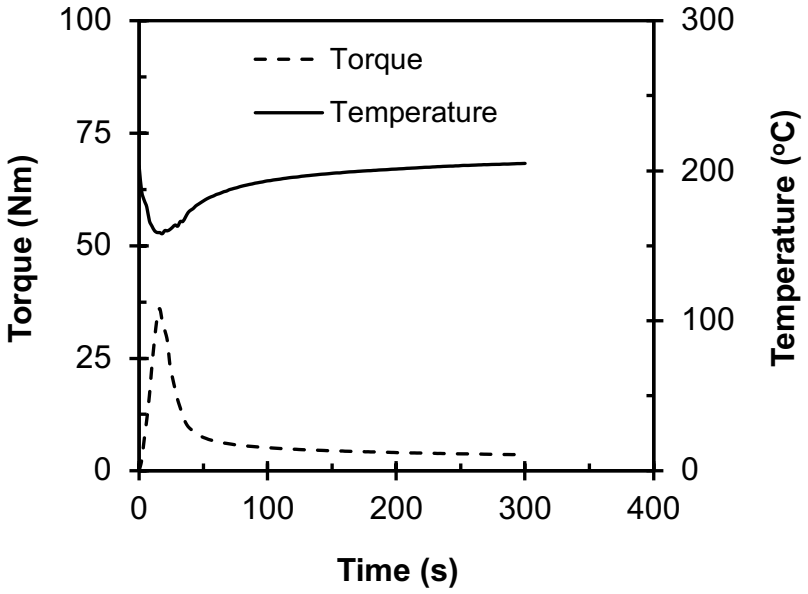

Figure 4.1 Typical curves of torque and stock temperature of neat PLA as a function of time generated by a torque rheometer.

Similar results were obtained for PLA blended with various CE contents for both grades of CE [Figure 4.2 (a) and (b)]. As expected, the stock temperature vs time curves of all PLA/CE blends overlapped during processing and did not change with CE content or grade [Figure 4.2 (a) and (b)]. It can also be seen in Figure 4.1 that the torque curves reach a maximum torque during the initial loading of neat PLA resin into the mixing chamber; indicating that the chamber is filled with resin. Then the torque gradually decreases and reaches a constant value or an equilibrium when the plastic is melted into a homogenous mass [5]. Similar curves were obtained for PLA/CE blends [Figure 4.2 (c) and (d)].

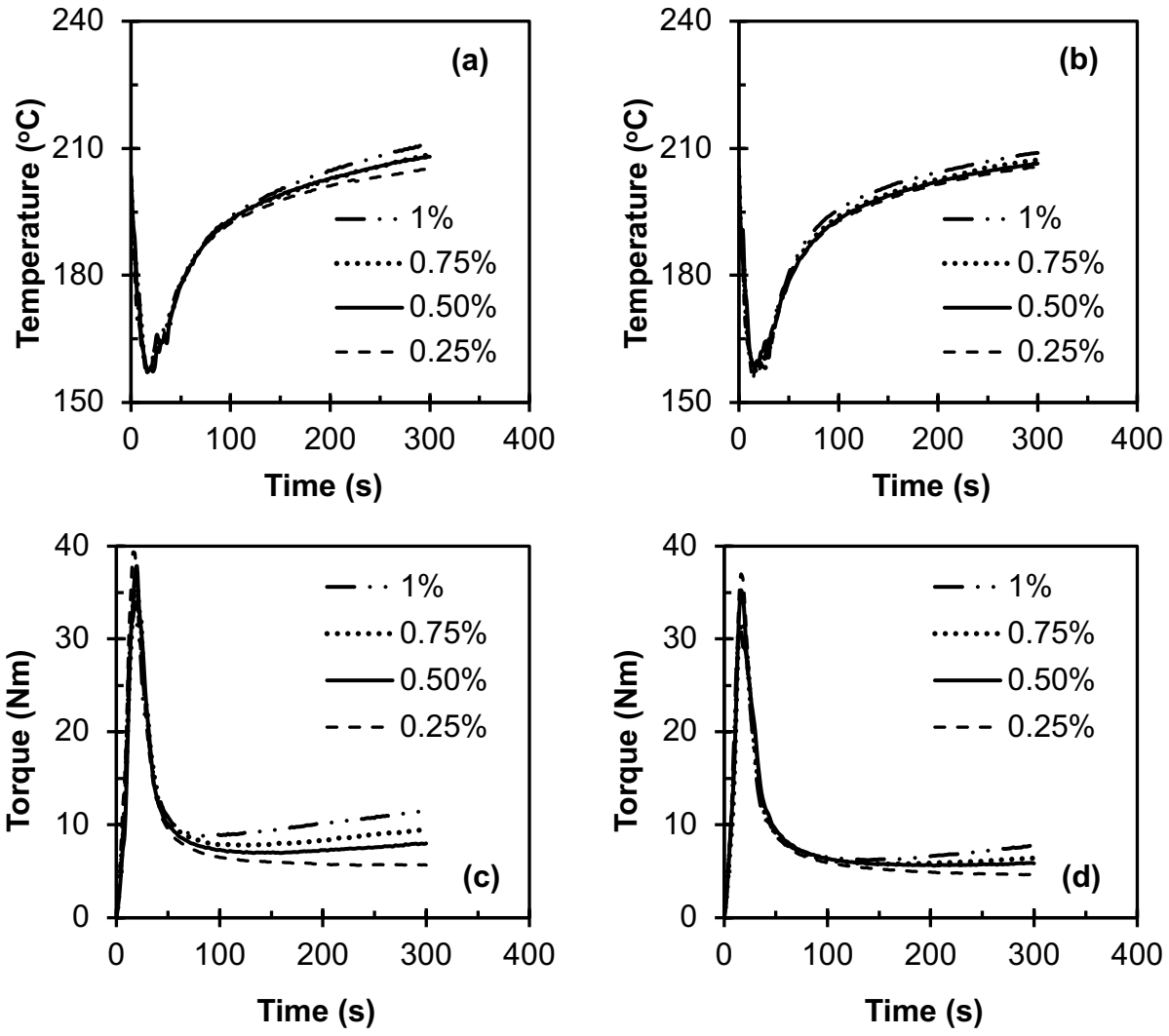

Figure 4.2 Typical curves of stock temperature and mixing torque of PLA blends with CE 4468 [(a) and (c)] as well as CE 4400 [(b) and (d)] as a function of time generated by a torque rheometer.

From these curves, the times required to reach 200°C were recorded (Table 4.1). A residence time of at least 120 s is recommended by the manufacturer for the reaction of these CE to be over 99% complete at 200°C. Since the total processing time was held constant at 300 s, the residence times provided to PLA/multifunctional epoxy samples at a minimum of 200°C were calculated by the difference between the total mixing times and the times taken to reach 200°C (Figures 4.1 and 4.2) and the results are tabulated in Table 4.1. The experimental residence times for complete chain extension reaction between PLA and both multifunctional epoxy grades exceeded the time recommended by the manufacturer, irrespective of the CE content, clearly indicating that the reaction was over 99% complete. Since the stock temperature continued to increase above the recommended 200°C due to shear generated during processing, it is believed that this increased heat could have accelerated the chain extension reaction between the PLA and CE.

Table 4.1 Mixing time of PLA with both grades of multifunctional epoxies in torque rheometer.

CE (%)	**Time to reach 200°C (s)**		**Total time at 200-211°C (s)**	
	4468	4400	4468	4400
0.25	162.3 ± 22.1	170.0 ± 3.5	137.7 ± 22.1	130.0 ± 3.5
0.5	161.7 ± 10.0	173.7 ± 7.5	138.3 ± 10.0	126.3 ± 7.5
0.75	159.7 ± 4.5	167.3 ± 8.1	140.3 ± 4.5	132.7 ± 8.1
1	152.3 ± 11.0	152.0 ± 11.8	147.7 ± 11.0	148.0 ± 11.8

The average values of the time to reach 200°C decreased with CE content whereas an opposite trend was observed for the average values of the total time at 200-211°C, which increased with CE content, irrespective of CE type (Table 4.1). Comparison between the two chain extender grades with different epoxy equivalent weights indicated that the CE with lower epoxy equivalent weight (CE 4468) experienced slightly shorter times to reach 200°C, i.e., longer total times at 200-211°C than the counterpart with high epoxy equivalent weight (CE 4400) (Table 4.1). Generally, more viscous materials generate higher shear in a mixer when they are kneaded by the rotor blades of the mixer. This additional shear contributes to increased heat, resulting in shorter times to reach the set-point temperature. As the CE content increased, the viscosity of the materials increased, leading to increased shear which contributed to raised temperatures, resulting in reduced times to reach 200°C, irrespective of the CE grade. Moreover, the CE grade with lower epoxy equivalent weight resulted in higher shear due to its higher reactivity and thus reached 200°C in shorter time compared to its counterpart with higher epoxy equivalent weight, regardless of CE content. The increased viscosity of the materials due to the addition of CE and the difference between the reactivities of the two CE grades will be further discussed in the following sections.

The reaction between multifunctional epoxies and polyesters such as PLA has been extensively studied in the literature [4,6-9]. PLA has two distinct functional end-groups, carboxyl and hydroxyl, that can react with the epoxy groups in multifunctional epoxies. The reaction proceeds via ring-opening of the epoxide group leading to the formation of new secondary hydroxyl groups and ester linkages when reaction occurs with PLA's carboxyl groups and/or ether linkages with PLA's hydroxyl groups (Figure 4.3) [4,6-9]. Fourier transform infrared spectroscopy (FTIR) was used to gain an in-depth understanding of these reaction mechanisms.

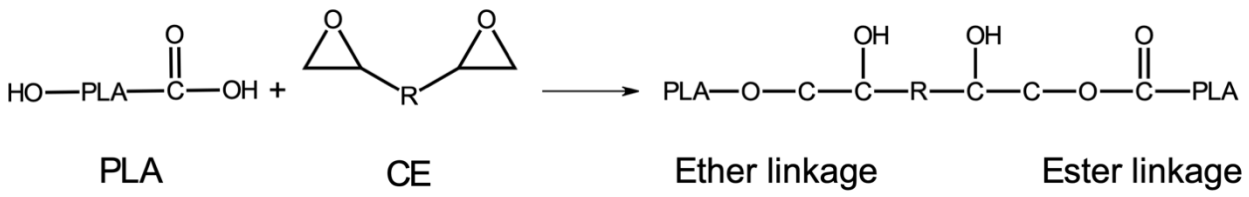

Figure 4.3 Generalized reaction mechanism of a multifunctional epoxy chain extender with the hydroxyl and carboxyl end groups in PLA.

The FTIR spectra of neat PLA, CE 4468, and PLA/CE blends compounded in an internal mixer are illustrated in Figure 4.4. Table 4.2 summarizes the band assignments for the wavenumbers of peaks found in these spectra to their corresponding functional groups [6,7,10]. Two distinct trends were observed. Firstly, the peaks at 844, 905 and 1250 cm^{-1} in CE 4468 spectrum, assigned to the C-O stretching of epoxy group, disappeared in the spectra of PLA compounded with CE, regardless of CE content (Figure 4.4). This result indicates that the CE reacted with PLA through ring-opening reaction of epoxy groups as illustrated in Figure 4.3 [6,7]. Secondly, the peaks present at 1489 and 1597 cm^{-1} in CE 4468 (Figure 4.4), corresponding to C-C stretching in phenyl group (Figure 4.5), merged into a broad shoulder in PLA/CE compounds at 1513-1547 cm^{-1} (Figure 4.4). It should be noted that the phenyl groups in CE 4468 do not participate in the reaction with PLA and could hence be used to detect the presence of CE in the blends since these groups are absent in neat PLA. Thus, the formation of a broad shoulder from 1513-1547 cm^{-1} in the blends confirmed the presence of CE. As expected, this broad shoulder seemed to intensify as the CE content increased into PLA matrix probably due to more phenyl groups in the blends with higher CE contents.

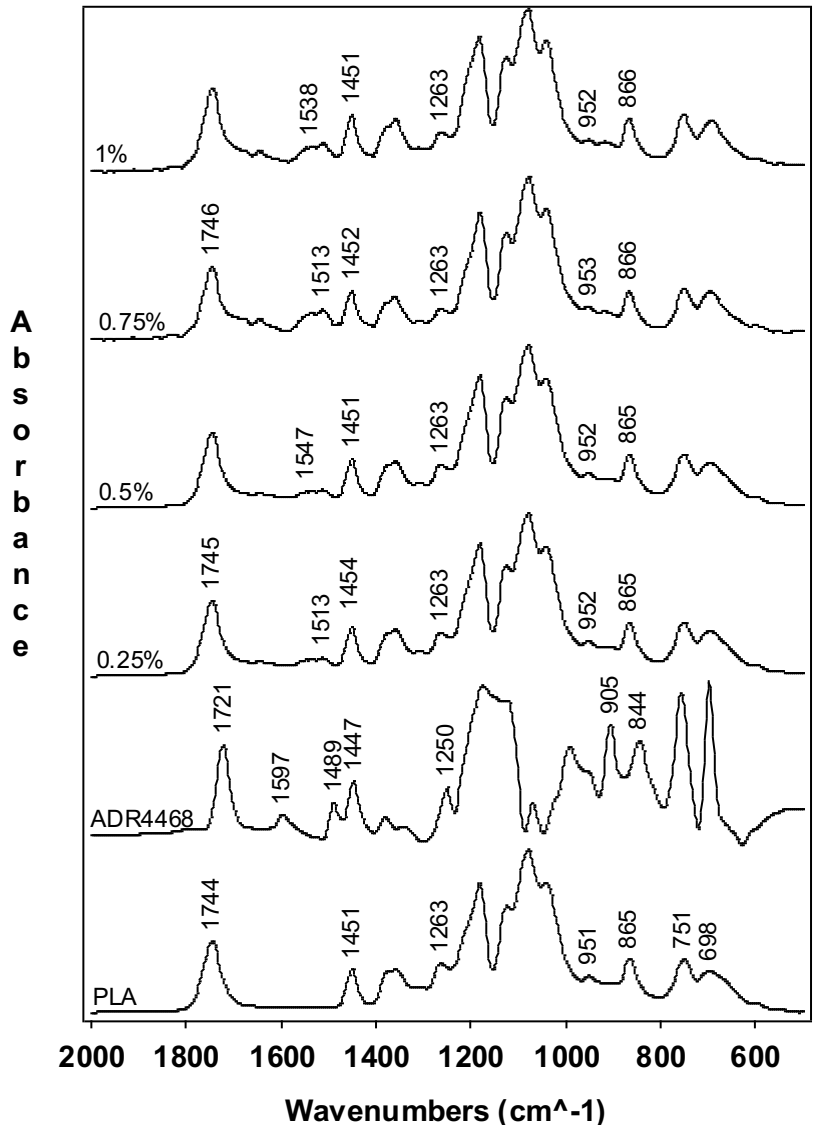

Figure 4.4 Infrared spectra of PLA, CE 4468, and PLA blended with different CE contents in an internal mixer. Absorbance in the y-axis is in arbitrary units.

Table 4.2 Band assignments for the wavenumbers of peaks used in FTIR analysis and corresponding functional groups.

Wavenumber (cm^{-1})			**Peak assignments**
PLA	CE 4468	PLA blends with 0.25, 0.5, 0.75 and 1% CE	
1744	1721	~1745	Stretching of C=O
-	1489, 1597	1513-1547	Stretching of C-C in phenyl
1451	1447	~1451	Scissoring of CH_3
1263	-	1263	Stretching of C-O in carboxyl and C-O-C stretch
-	1250	-	Stretching of C-O in epoxy
951	-	~952	Rocking of CH_3 and stretching of C-C
-	844, 905	-	Stretching of C-O in epoxy
865	-	~865	Stretching of C-O-C

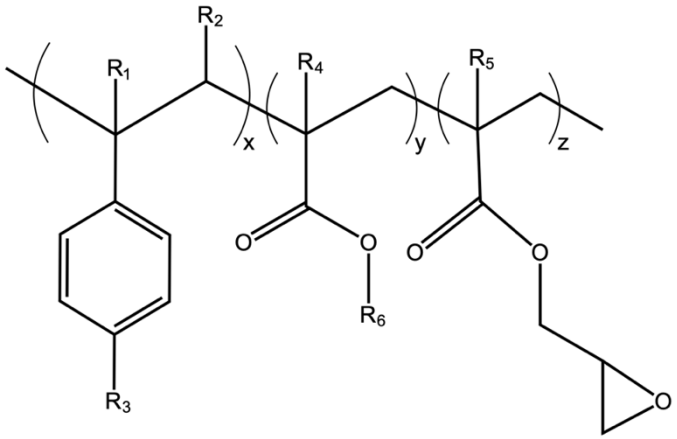

Figure 4.5 Generalized reaction mechanism of a multifunctional epoxy chain extender with the hydroxyl and carboxyl end groups in PLA.

The equilibrium torque taken at 300 s in Figures 4.1 and 4.2 (end torque value) is proportional to the apparent viscosity and molecular weight of the materials and depends on polymer chain structure such as branching [2-4]. An increase in the end torque values indicates an increase in the viscosity and molecular weight due to the formation of longer and/or branched chains [2-4,11,12]. Consequently, the end torque values could be used to monitor the chain extension reaction of a polymer.

Figure 4.6 illustrates the end torque values of PLA chain-extended with low and high epoxy equivalent weight multifunctional epoxies obtained from their torque vs mixing time curves (Figure 4.2) to determine their effectiveness and efficiency in chain extending PLA. Both multifunctional epoxies chain-extended PLA effectively since they significantly increased the end torque during mixing. However, the efficiency of the multifunctional epoxy grades as chain extenders varied and was dependent on the epoxy equivalent weights. Chain extender's efficiency is defined as the contribution to increase the end torque of the blend per unit of chain extender [13] as expressed in the following equation:

$$\text{CE efficiency} = \frac{\text{End torque}}{\text{CE content}} \qquad \text{(Equation 4.1)}$$

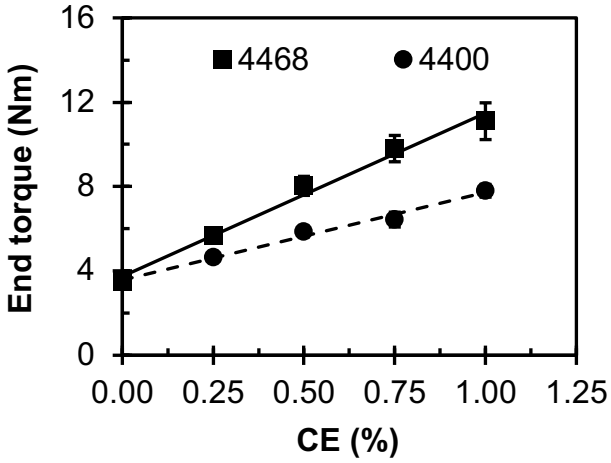

Figure 4.6 End torque of PLA chain-extended with low (CE 4468) and high (CE 4400) epoxy equivalent weight multifunctional epoxies as a function of their contents.

It is evident from Figure 4.6 that the additive with lower epoxy equivalent weight (CE 4468) was more efficient in increasing the end torque of PLA compared to its counterpart with high epoxy equivalent weight (CE 4400) due to the smaller amount of CE needed to increase the end torque at a similar value. For example, by drawing a horizontal line parallel to the X-axis (chain extender content) at an arbitrary end torque value (e.g., 8 Nm in Figure 4.6), the data can produce two intersection points [13]. The first intersection point detected at lower chain extender content for CE 4468 (0.5%) and the next seen at higher chain extender content for CE 4400 (1%), which clearly indicates the higher efficiency of CE 4468 in chain extending PLA, as expected from equation 4.1 [13]. This result can be explained by the lower equivalent weight of CE 4468, resulting in more epoxy groups per chain and thus higher reactivity. Since the efficiency of CE

with a lower epoxy equivalent weight (CE 4468) was higher than its counterpart with high epoxy equivalent weight (CE 4400), it was then selected for further studies.

Chain extension of PLA with the most efficient grade of CE (CE 4468) was further confirmed by the values of molecular weights and dispersity indices of PLA and PLA/CE blends (Table 4.3). The addition of CE increased the number (M_n), weight (M_w) and viscosity (M_v) average molecular weights, as well as polydispersity index (DI) of PLA, due to the formation of longer and/or branched chains. Similar results have been reported for PLA chain-extended with other non-food grades of multifunctional epoxies [6,12,14] and polyethylene terephthalate chain-extended with 1,6-Diisocyanatohexane [15], amongst others.

Table 4.3 Molecular weights, dispersity indices and melt flow index values of PLA chain-extended with CE 4468.

CE (%)	Molecular weight (kg/mol)			DI	MFI (g/10 mins)
	M_n	M_w	M_v		
0	123 ± 5	212 ± 6	198 ± 6	1.7 ± 0.0	11.51 ± 0.30
0.25	139 ± 3	340 ± 34	296 ± 25	2.4 ± 0.2	5.94 ± 0.03
0.5	157 ± 4	475 ± 44	407 ± 59	3.0 ± 0.4	1.62 ± 0.00
0.75	181 ± 12	503 ± 14	433 ± 9	2.8 ± 0.3	0.22 ± 0.00
1	221 ± 10	583 ± 28	469 ± 15	2.6 ± 0.1	0.05 ± 0.00

As previously mentioned, chain extension and/or branching can also be monitored by the zero-shear viscosity (η_0) of a polymer melt, which is directly related to its molecular weight (M_w) by the Mark-Houwink equation:

$$\eta_0 = k \cdot M_w^a \quad \text{(Equation 4.2)}$$

with k and a as Mark-Houwink constants.

Figure 4.7 shows a plot of zero-shear viscosities determined from the MFI data (Table 4.3) as a function of weight-average molecular weights (M_w) of PLA compounded with different contents of CE (Table 4.3) in an internal mixer. The viscosity increased with molecular weight at different extents below and above a molecular weight value of 475 kDa, which corresponds to CE content of 0.5% (Table 4.3). Below 475 kDa, increasing the molecular weight of PLA/CE blends from 212 to 475 kDa gradually increased their viscosities from 1,086 to 7,270 Pa-s, respectively. This trend is not clearly seen in Figure 4.7 due to a wide range of viscosity values on the y-axis, which was overcome by truncating and displaying this range of the graph as an insert. In contrast, a sharp increase in viscosity was observed above 475 kDa, where the viscosity of the blends increased from 7,270 to 240,727 Pa-s when the molecular weight varied from 475 kDa to 583 kDa, respectively. This point of inflection indicates the critical molecular weight, i.e, the onset of chain entanglements attributable to the high degree of branching. Dalsin and co-workers reported a similar trend for atactic polypropylene wherein a weak dependence of zero-shear viscosity on its molecular weight was reported until a critical molecular weight of 8.5 kDa, after which the zero-shear viscosity increased exponentially with increasing molecular weight [16].

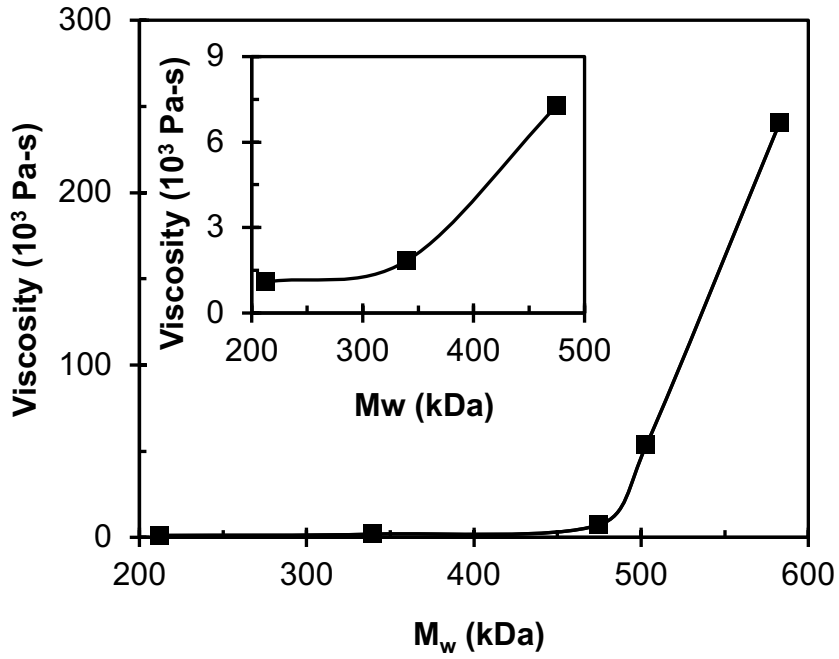

Figure 4.7 Zero-shear viscosities as a function of weight-average molecular weights of PLA/CE blends processed in an internal mixer. Insert shows the viscosity vs. molecular weight trend of these blends at low zero-shear viscosity values.

The degree of crystallinities of PLA and its blends were also evaluated to corroborate chain branching (Figure 4.8) observed through the molecular weight and viscosity data. Generally, dense packing of branched polymer chains is difficult, leading to reduced crystallinity. As expected, the addition of CE into the PLA matrix reduced its degree of crystallinity indicating branching and confirming chain extension, consistent with the trend reported in literature [17].

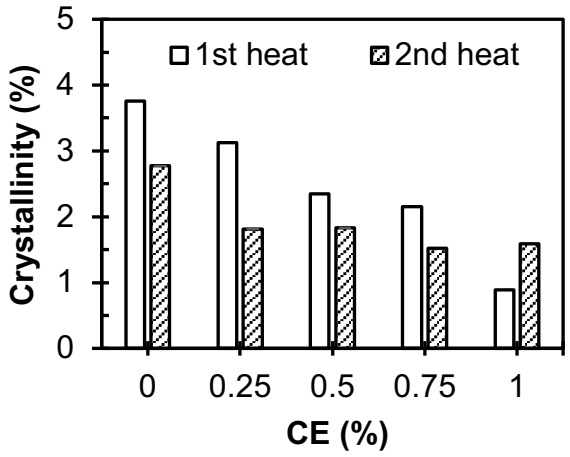

Figure 4.8 Effect of CE content on the crystallinity of PLA processed in an internal mixer.

4.1.2 Extrusion-blown chain-extended PLA films

The feasibility of utilizing the identified most efficient CE grade (CE 4468) in extrusion-blown PLA film processing was assessed by dry-blending it with PLA first and then attempting film manufacturing. The melt stock temperature and pressure at the die generated during processing of the blends with various CE concentrations (up to 1 wt%) were recorded and listed in Table 4.4.

Table 4.4 Processing parameters recorded during extrusion-blown film and residence times as a function of CE 4468 content in PLA.

CE (%)	Melt temperature[a] (°C)	Pressure[a] (10^4 Pa)	Residence time[b] (s)	Peak time[b] (s)	End time[b] (s)
0	211 ± 0	465 ± 3	-	-	-
0.25	211 ± 0	496 ± 33	132 ± 6	156 ± 10	246 ± 6
0.5	211 ± 0	571 ± 10	176 ± 24	228 ± 30	290 ± 28
0.75	NOT PROCESSABLE				
1					

[a]Average values of at least 45 data points.
[b]Average values of three replicates.

The melt experienced a stock temperature higher than the recommended 200°C (Table 4.4) due to shear generated during processing. Notice that film manufacture was feasible only with blends containing up to 0.5% CE, becoming unprocessable above this content due to the increased viscosity at this critical molecular weight for chain entanglement (Figure 4.7), indicated by the increased melt pressure during processing (Table 4.4). The melt pressure in the extruder (Table 4.4), suggestive of the blend's shear stress, increased with increasing chain extender content attributable to the chain extension reaction between the PLA and CE [3,11,12]. The increased molecular weight (Table 4.5) and decreased crystallinity (Figure 4.9) of PLA films with chain extender content corroborated the chain extension and branching of PLA. As expected, these results were similar to those obtained for PLA/CE blends processed in the internal mixer (Table 4.3 and Figure 4.8).

Table 4.5 Molecular weights and dispersity indices of PLA films chain-extended with CE 4468.

CE (%)	Molecular weight (kDa)			DI
	M_n	M_w	M_v	
0	105 ± 7	183 ± 2	170 ± 1	1.7 ± 0.1
0.25	112 ± 5	232 ± 2	208 ± 2	2.1 ± 0.1
0.5	127 ± 9	243 ± 16	219 ± 12	1.9 ± 0.3
0.75	NOT PROCESSABLE			
1				

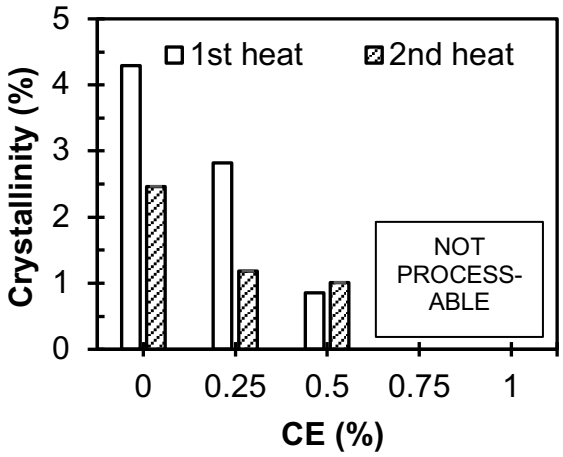

Figure 4.9 Effect of CE content on the crystallinity of PLA films.

To ensure that the melts experienced the recommended 200°C within 120 s for 99% reaction to occur between PLA and CE, the residence times of processable blends inside the extruder were recorded. Figure 4.10 shows typical residence time distribution (RTD) curves of PLA films blended with 0.25 and 0.5% CE. The residence time, peak time and end time were the three parameters extracted from each RTD curve generated (Table 4.4). The residence time is defined as the first time at which a tracer signal of 5% of the maximum peak height was detected. It relates to the minimum exposure time and duration for PLA to react with CE in the extruder. The peak time, where the maximum signal occurred, represents the average transit or mean processing time. The end time, the time for detection of the last signal of 5% of the maximum peak height, is linked to the maximum time the blends resided in the extruder [18,19].

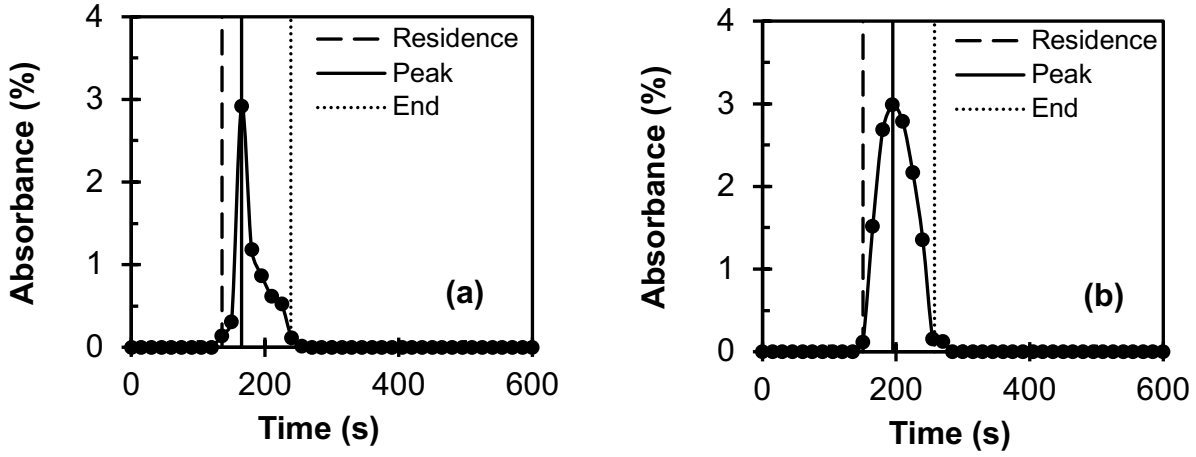

Figure 4.10 Typical residence time distribution curves of PLA with (a) 0.25% CE and (b) 0.5% CE.

PLA/CE blends experienced residence times longer than the recommended 120 s at 200°C, suggesting 99% completion of reaction. The residence time of PLA blended with 0.5% CE was longer than its counterpart with 0.25% (Table 4.4), due to its higher viscosity (Figure 4.7), which provided more resistance to flow resulting in slower movement of the blend through the extruder; thus higher peak and end times (Table 4.4 and Figure 4.10). It is also worth mentioning that the maximum time that the materials stayed in the extruder (end time) was more than twice the 120 s and the melt experienced a temperature of 11°C above the 200°C recommended by the manufacturer (Table 4.4 and Figure 4.10). This clearly indicates that the blends were exposed to extrusion processing conditions (heat and time) that favored chain extension reactions in the films.

4.1.3 Effect of chain extender content on the dart impact strength of PLA films

Figure 4.11 shows the failure mass, indicative of the falling dart impact strength of PLA films chain-extended with various amounts of CE 4468 (low epoxy equivalent weight). Chain extension of PLA film was found beneficial in overcoming its brittleness. As seen in Figure 4.11, the impact strength of PLA film increased almost linearly with the chain extender content, implying that the film became more ductile by branching the polymer chain and reducing its crystallinity (Figure 4.9). Interestingly, the addition of only 0.5% chain extender into the PLA films increased its failure mass by ~56%, due to the chain extension reaction. These results validate the need for chain extenders to reduce the brittleness of PLA films even though neat PLA films without any chain extenders have been successfully manufactured in this and our previous studies [10,20,21].

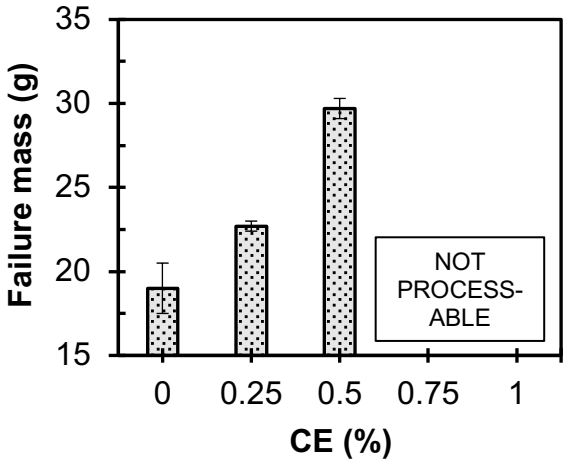

Figure 4.11 Effect of CE content on the failure mass of PLA films.

4.2 Performance of poly(lactic acid)/cellulose nanocrystal composite blown films processed by two different compounding approaches

The title and content of section 4.2 were published in Polymer Engineering and Science, 58(11): 1965-1974 (2017). doi: https://doi.org/10.1002/pen.24806. This paper was co-authored by N.M. Stark, R.C. Sabo and L.M. Matuana.

The main objective of this section was to compare the performance of PLA/CNC blown films prepared by the melt-blending and direct dry-blending techniques in terms of particle dispersion, optical, thermal, molecular weight and barrier properties to identify the most effective blending approach (*specific objective #2*) [10]. It should be noted that for all results presented in this section, the CNC loading was fixed at 1%, which was determined as the ideal concentration in our preliminary study.

4.2.1 Effect of blending process on CNC dispersion and PLA's optical properties

CNC distribution and dispersion in the PLA matrix were examined using light microscopy (Figure 4.12). In this study, CNC dispersion was defined as the degree of breaking up of CNC agglomerates, whereas CNC distribution was a measure of how uniformly the CNCs were distributed throughout the PLA matrix [22]. As seen in Figure 4.12, homogenous distribution of CNCs in the PLA matrix was achieved, irrespective of the blending technique. However, some agglomerates were still visible, indicative of not well-dispersed CNCs in the matrix. The difference in CNC dispersion in the direct dry-blended and melt-blended films was not apparent from the obtained images. Therefore, UV-Vis spectroscopy was performed to further investigate the dispersion of CNCs into the PLA matrix (Figure 4.13).

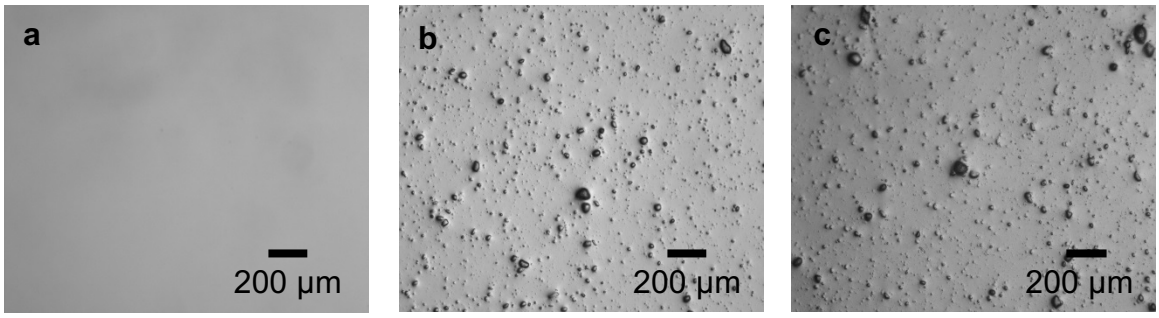

Figure 4.12 Light microscope of (a) PLA, (b) PLA/1% CNC (DB) and (c) PLA/1% CNC (MB) films.

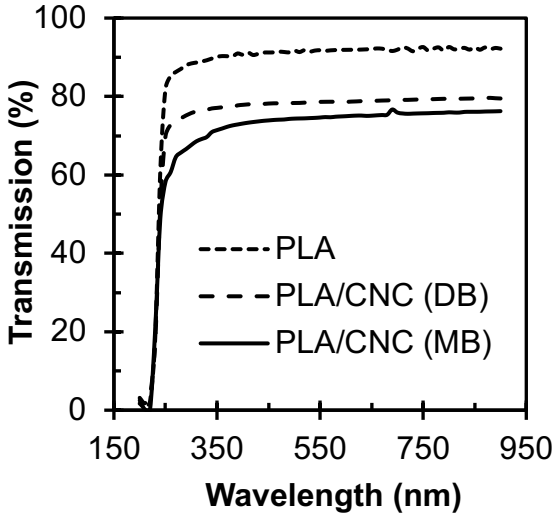

Figure 4.13 Effects of CNC addition and blending process on the transparency of PLA and PLA/CNC composite films.

Transparency can be used as an indicator of the dispersion of nanoparticles in a matrix, if the size of individual nanoparticles is smaller than the wavelength of visible light (380-700 nm) [23]. In other terms, if nanosize dispersion of CNC in PLA matrix is obtained, the addition of CNCs will not affect the transparency of resulting films, because pure CNC films are highly transparent [24]. The UV-Vis spectroscopy results for neat PLA and PLA/CNC composite films prepared by the direct dry- and melt-blending approaches are illustrated in Figure 4.13. The average light transmission values for neat PLA, PLA/CNC direct dry-blended (DB) and PLA/CNC melt-blended (MB) films in the visible region were calculated as described in the experimental section and reported as 91.5 ± 0.8%, 78.5 ± 3.3% and 74.5 ± 0.9%, respectively. These results show that the light transmission of neat PLA decreased significantly by adding 1% CNCs, irrespective of the blending technique (Figure 4.13). Reduced transparency of PLA due to the addition of CNCs, irrespective of the blending method, implied that nanoscale dispersion did not fully occur and some micrometer sized agglomerations could still be present. The light microscope images showing agglomerations of CNCs (Figure 4.12) corroborate the UV-Vis results (Figure 4.13). Generally, nanoparticle agglomeration sizes larger than the incident wavelength of light tend to scatter light and reduce light transmission [23]. Although there is still need for improvement to completely eliminate agglomerations, a transparency in the range of 75-78% was achieved in this study, demonstrating that reasonably good transparency remains despite limited dispersion. It is worth mentioning that the difference in average light transmission values of direct dry-blended PLA/CNC films (78.5 ± 3.3%) and melt-blended PLA/CNC films (74.5 ± 0.9%) were not significantly different, implying that blending methods yielded films of similar transparency.

4.2.2 Effects of CNC addition and blending process on PLA's thermal properties

Thermogravimetric analysis (TGA) was performed to evaluate the effects of CNC addition and blending approaches on the thermal decomposition of PLA. The non-isothermal TGA and differential thermogravimetric (DTG) curves of PLA and PLA/CNC composite films are illustrated in Figure 4.14 (a) and (b). There was no noticeable significant difference in the onset temperatures of decomposition (~ 315^{o}C) measured on addition of 1% CNCs, irrespective of the blending process used. Similar results were reported by Lizundia and co-workers for PLA-grafted CNCs at 1 wt% [25]. It is evident from Figure 4.14 (a) that the decomposition of all films started at temperatures of ~315^{o}C and reached their maximum decompositions at ~364^{o}C. The decomposition of PLA above 200^{o}C has been reported by various researchers and could be attributed to hydrolysis of ester bonds in the main chain, unzipping depolymerization reactions catalyzed by residual polymerization catalysts, oxidative random main-chain scission as well as inter and intra- molecular transesterification reactions leading to the formation of low molecular weight monomers and oligomeric esters [26-29]. Figure 4.14 (c) shows the TGA measurements performed under isothermal conditions at 180^{o}C for 300 minutes for PLA and PLA/CNC nanocomposite films. The addition of CNCs by both the direct dry- and melt-blending processes did not affect the decomposition of PLA films at the processing temperature used in this study to manufacture blown films. The weight loss for all films was around 1% even after holding the films at 180^{o}C for 300 minutes.

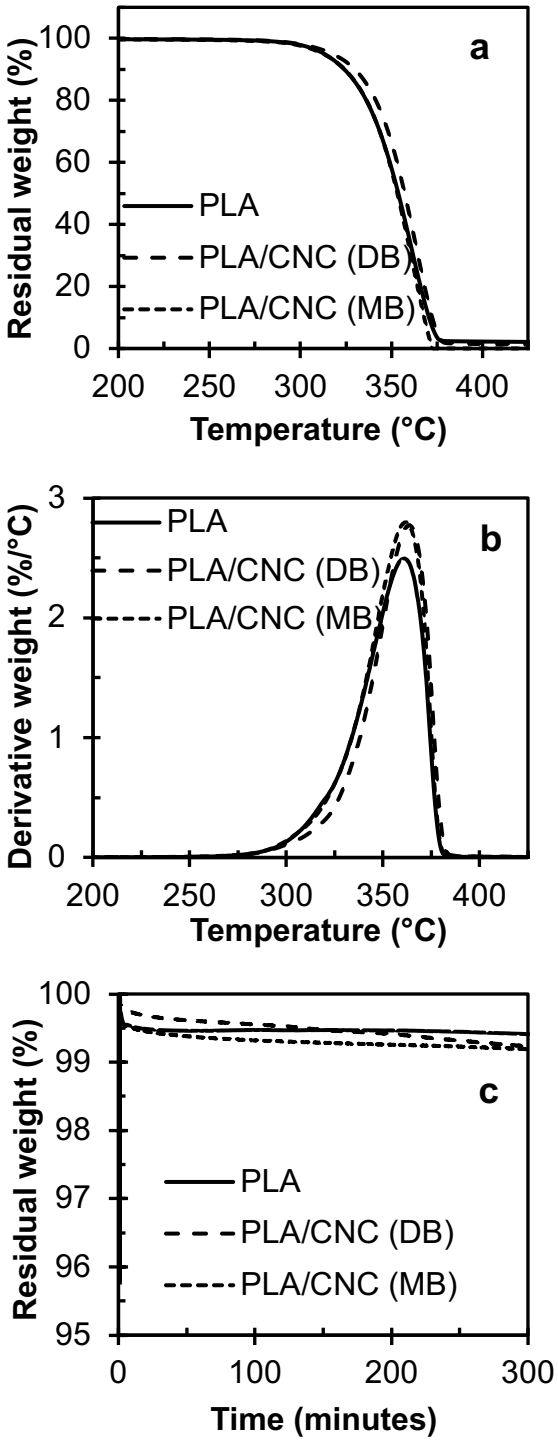

Figure 4.14 (a) Non-isothermal thermograms, (b) Non-isothermal DTG and (c) Isothermal thermograms of PLA and PLA/CNC composite films.

Table 4.6 lists the thermal transition temperatures (T_g, T_c and T_m) and degree of crystallinity ($\%\chi_c$) from the first and second DSC heating scans measured for PLA as well as PLA/CNC composite films manufactured by the direct dry- and melt-blending techniques. In this study, the first heating scan was used to assess the film's thermal properties in the as-molded condition whereas the second heating scan was used to evaluate the material's intrinsic properties after erasing its thermal history. In both the first and second heating scans, no notable changes were observed in the T_g of the PLA films on addition of CNC, irrespective of the blending technique. Intermolecular interaction and chain flexibility can cause a change in a material's T_g [30]. As expected, the low concentration of added CNCs did not significantly change the PLA's chain flexibility nor intermolecular interaction and consequently had no noteworthy effect on its T_g. In contrast, the T_c values of direct dry-blended and melt-blended PLA/CNC films in the first and second heating scans were significantly lower than that of neat PLA (control films), indicating faster crystallization due to the nucleation effect of CNCs, as expected from the heterogeneous nucleation theory [31]. The nucleation rate (N), according to the heterogeneous nucleation theory is given as follows [31]:

$$N \cong N_o \times \exp\left(\frac{-C}{\Delta T}\right) \qquad \text{(Equation 4.3)}$$

Where N_o is the pre-factor, and ΔT and C are given as follows:

$$\Delta T = T_m^o - T_c \qquad \text{(Equation 4.4)}$$

$$C = \frac{4 \cdot \sigma \cdot \sigma_e \cdot T_m^o}{k \cdot T \cdot \Delta h} \qquad \text{(Equation 4.5)}$$

where T_m^o is the equilibrium melting temperature, T_c is the cold crystallization temperature, σ and σ_e are the end and lateral surface free energies, k is the Boltzmann's constant, T is the temperature and Δh is the enthalpy of fusion.

Table 4.6 DSC analysis for PLA as well as direct dry-blended (DB) and melt-blended (MB) PLA/1% CNC films.

Materials	T_g (°C)[A]		T_c (°C)[A]		T_m (°C)[A]		χ_c (%)[A]	
	1st heat	2nd heat	1st heat	2nd heat	1st heat	2nd heat	1st heat	2nd heat
PLA	63.2 ± 2.9[a]	61.0 ± 0.4[a]	117.0 ± 3.1[a]	124.9 ± 1.2[a]	149.9 ± 0.3[a]	151.0 ± 0.5[a]	4.5 ± 0.1[a]	1.5 ± 0.4[a]
PLA + 1% CNC (DB)	63.3 ± 3.0[a]	60.8 ± 0.2[a]	113.9 ± 2.1[b]	122.7 ± 1.2[b]	149.2 ± 0.3[a]	150.4 ± 0.4[a]	5.4 ± 0.8[b]	4.5 ± 0.4[b]
PLA + 1% CNC (MB)	64.5 ± 0.3[a]	61.1 ± 0.7[a]	111.7 ± 0.2[c]	113.2 ± 0.1[c]	147.7 ± 0.2[b]	148.0 ± 0.1[b]	4.6 ± 0.3[a]	4.4 ± 0.2[b]

[A]Same superscript letters within the same column are not significantly different based on the ANOVA results at 5% significance level.

As equations 4.3 and 4.4 suggest, a lower cold crystallization temperature results in higher nucleation rate and faster crystallization. Thus, the lower T_c of PLA/CNC composite films obtained in this study was accompanied by significantly higher crystallinity compared to neat PLA films in the second heat curve confirming that CNCs acted as efficient nucleating agents. Similar results have been reported for PLA nanocomposites with CNCs [25,32-35], microcrystalline cellulose (MCC) [36], cellulose nanofibers [37], and plasticized PLA with MCC [38]. It is also worth mentioning that a significantly lower T_c was observed for the melt-blended (MB) PLA/CNC films compared to their direct dry-blended (DB) counterparts because of the faster crystallization of shorter polymer chains resulting from degradation of the melt-blended PLA/CNC films, leading to a lower T_c. However, this reduced T_c, indicating nucleating action of the degradation products in the melt-blended films was not accompanied by a further increase in crystallinity. GPC (described in the next section) was performed to confirm the degradation of melt-blended PLA/CNC films. The T_m of direct dry-blended PLA/CNC films remained unchanged as compared to neat PLA in the first and second heating curves. In contrast, the melt-blended PLA/CNC films had a significantly lower T_m, which was attributed to the degradation of these films. Generally, degradation of films is accompanied by a reduction in molecular weight leading to reduced chain length and chain entanglement. Shorter and less entangled chains require less energy to slide past each other and melt at lower temperatures.

4.2.3 Effects of CNC addition and blending process on the degradation of PLA

As discussed above, the T_c and T_m results (Table 4.6) revealed that the extra heat and mechanical shear experienced in the melt-blending process degraded the melt-blended PLA/CNC films. GPC was performed to evaluate PLA degradation during compounding and the results are shown in Table 4.7. The addition of CNCs through the direct dry-blending process did not affect

the M_n of PLA films, whereas their addition through the melt-blending process decreased the M_n of PLA films. The mechanical shear generated at 22,000 rpm during the direct dry-blending process had no significant effect on the M_n of direct dry-blended PLA/CNC compounds. However, the M_n of PLA/CNC films produced by the melt-blending process was significantly lower than their direct dry-blended counterparts and neat PLA, which can be attributed to the additional heat exposure of these compounds during the melt-blending process in a three-piece mixer prior to blown film extrusion. In contrast, the M_w and M_v of PLA films remained unaffected on the addition of CNCs by both blending approaches. The PLA and PLA/CNC composite films were processed using the same processing conditions of blown film extrusion and the only difference between these films was their pre-processing (or blending). Thus, it was acceptable to assume that the reduction in M_n for the melt-blended films occurred during the blending process. To confirm that the degradation of PLA/CNC composite films was occurring exclusively during the blending process prior to blown film extrusion, neat PLA pellets processed through direct dry- and melt-blending approaches were tested by GPC without manufacturing into films. The GPC results of unprocessed PLA pellets, PLA (DB) and PLA (MB) are shown in Table 4.7. The M_n of melt-blended PLA was significantly lower than that of unprocessed PLA pellets implying that PLA degraded during the melt-blending process, whereas the M_n of direct dry-blended PLA remained unaffected by the direct dry-blending process. The same trend was observed for the PLA/CNC composite films confirming that degradation of PLA was occurring during the melt-blending process due to additional heat exposure, prior to blown film extrusion.

Table 4.7 Molecular weights of PLA, direct dry-blended PLA/CNC (DB) and melt-blended PLA/CNC (MB) films as well as unprocessed PLA pellets, and PLA pellets subjected to DB and MB processes.

Materials	**M_n (kg/mol)[A]**	**M_w (kg/mol)[A]**	**M_v (kg/mol)[A]**	**# chain scission (10^{-6} mol/kg)**
Films				
PLA	142 ± 3[a]	272 ± 10[a]	252 ± 8[a]	-
PLA + 1% CNC (DB)	138 ± 3[a]	272 ± 4[a]	251 ± 4[a]	213
PLA + 1% CNC (MB)	126 ± 7[b]	267 ± 13[a]	246 ± 11[a]	915
Pellets				
PLA	158 ± 7[a]	310 ± 13[a]	287 ± 12[a]	-
PLA (DB)	147 ± 11[a]	299 ± 7[a,b]	276 ± 7[a]	509
PLA (MB)	130 ± 9[b]	282 ± 17[b]	259 ± 15[b]	1399

[A]Same superscript letters within the same column of films or pellets are not significantly different based on the ANOVA results at 5% significance level.

The degradation of PLA is very complex and can occur by various mechanisms, including random main chain scission reactions and hydrolysis [28,29,39]. Hydrolytic degradation results in drastic reduction in average molecular weight. Nevertheless, since the reduction in M_n was not very prominent, the dominating mechanism of degradation was more likely to be chain scission and not hydrolysis [28]. The number of chain scissions for the PLA/CNC composite films calculated using the following equation [40,41]:

$$\#\ \text{chain scissions} = \frac{1}{M_n(\text{composite})} - \frac{1}{M_n(\text{PLA})} \qquad \text{(Equation 4.6)}$$

Where M_n (composite) is the number average molecular weight of PLA/CNC (DB) or PLA/CNC (MB) films and M_n (PLA) is the number average molecular weight of PLA films. Equation 4.6 was also used to calculate the chain scission of PLA (DB) and PLA (MB) where M_n (composite) is the number average molecular weight of PLA (DB) or PLA (MB) compounds and M_n (PLA) is the number average molecular weight of unprocessed PLA pellets.

The number of chain scissions is listed in Table 4.7. Unsurprisingly, the PLA/CNC melt-blended films and PLA (MB) had more chain scissions compared to their direct dry-blended counterparts, indicating that the melt-blended composites degraded more during the melt-blending process due to the additional heat experienced during this process. These findings corroborate the T_c and T_m results (Table 4.6) that indicated degradation of the PLA/CNC melt-blended composites.

It was of interest to further investigate the mechanism of degradation occurring in the PLA/CNC composite films. A literature review revealed that in case of polyesters, chain scission can occur via β-C-H transfer reaction (Figure 4.15), leading to a decrease in molecular weight and

generation of vinyl terminated ester and carboxyl end-group [28,39,42,43]. The presence of carboxyl end-groups, which designates degradation, can be detected by FTIR spectroscopy [44,45]. Infrared spectra of neat PLA and PLA/CNC composite films prepared by both blending processes are shown in Figure 4.16. Table 4.8 lists the band assignments for the wavenumbers of peaks found in these spectra to their corresponding functional groups [28,46-52].

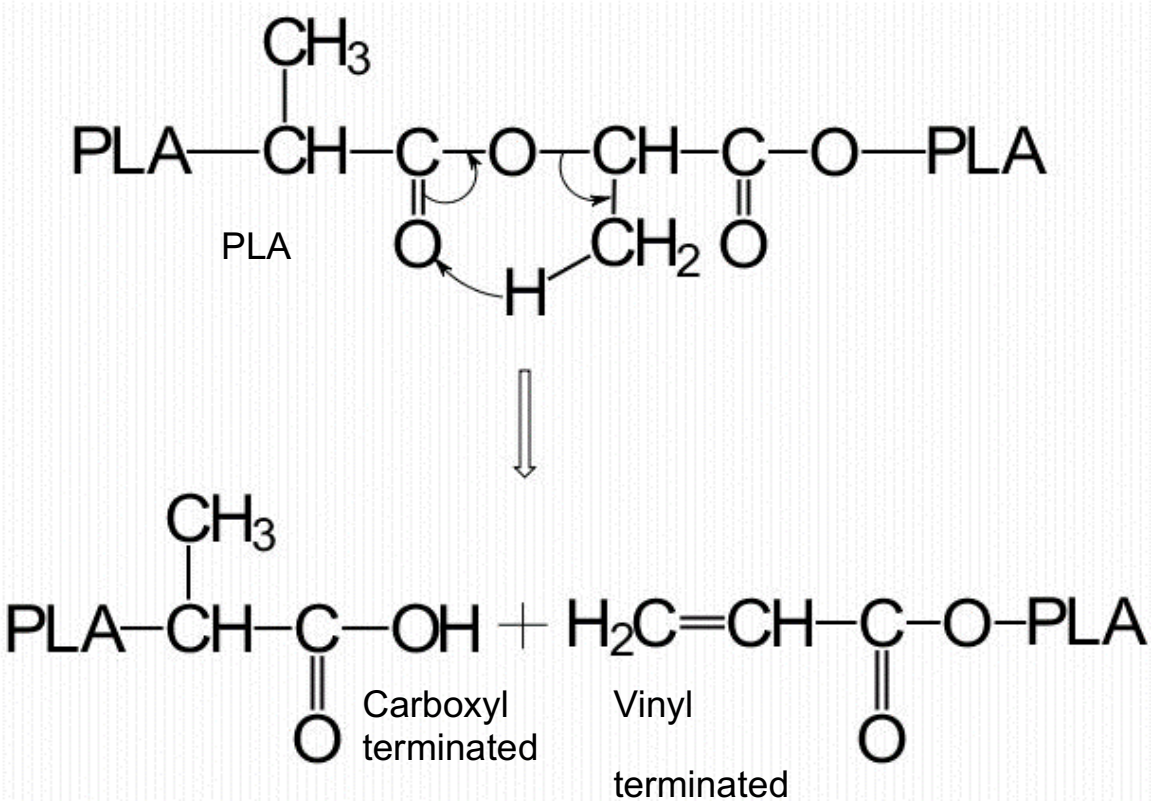

Figure 4.15 Proposed β-C-H transfer mechanism for degradation of PLA.

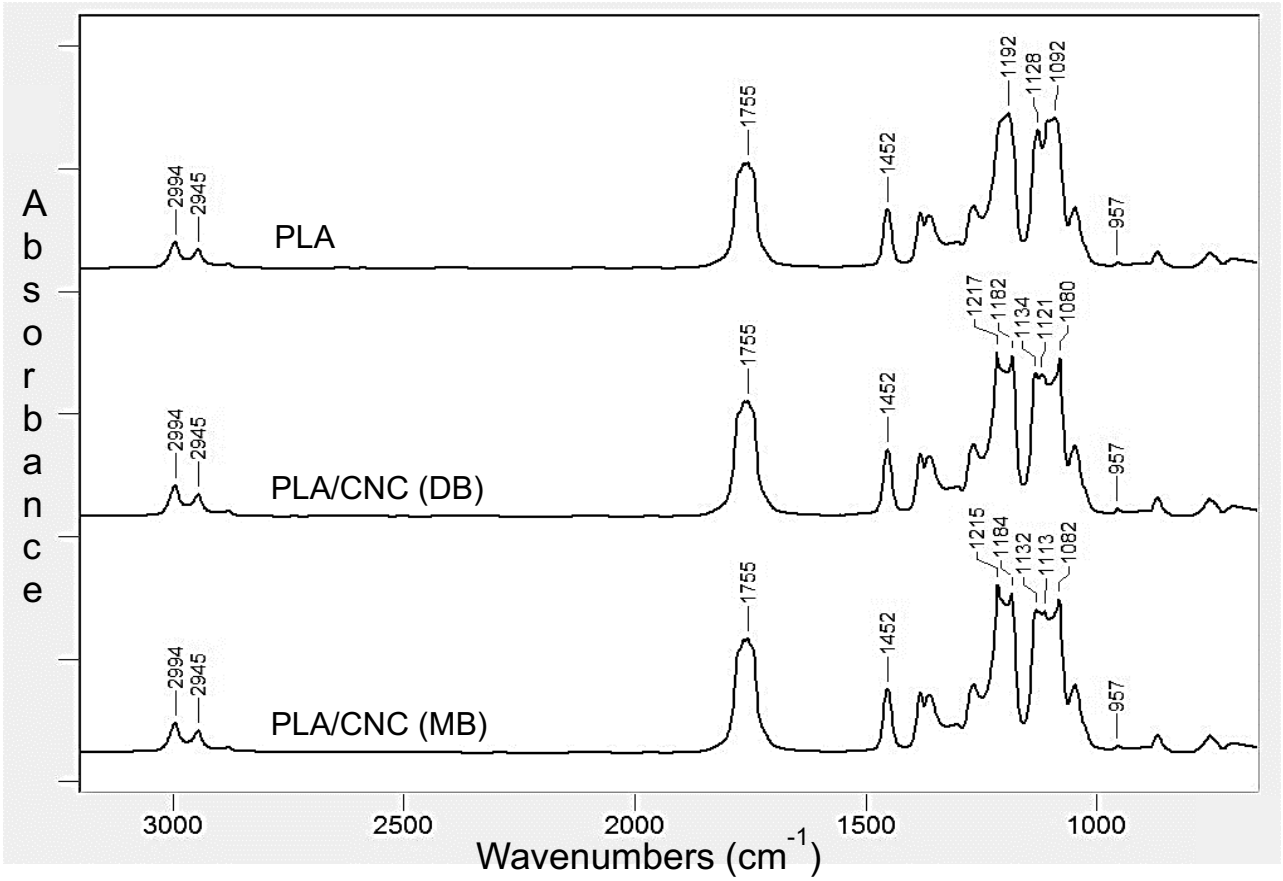

Figure 4.16 Infrared spectra of PLA and PLA/CNC composite films prepared by direct dry (DB)- and melt-blending (MB) processes.

Table 4.8 Band assignments for the wavenumbers of peaks used in FTIR analysis and corresponding functional groups [6,36,50-55].

Wavenumber (cm^{-1})			**Peak assignments**
PLA	PLA/CNC (DB)	PLA/CNC (MB)	
2994, 2945	2994, 2945	2994, 2945	Stretching of C-H in CH_3
1755	1755	1755	Stretching of C=O
1452, 1382, 1364	1452, 1382, 1364	1452, 1382, 1364	Stretching of C-H in CH_3
1267, 1192, 1128, 1092, 1047	1267, 1217, 1182, 1134, 1121, 1080, 1047	1267, 1215, 1184, 1132, 1113, 1082, 1047	Stretching of C-O in carboxyl and C-O-C stretch
957	957	957	O-H vibration in carboxyl
870	870	870	Amorphous phase of PLA
756	756	756	Crystalline phase of PLA

The major differences between the spectrum of PLA film and the spectra of PLA/CNC films were observed in the region between 1045-1270 cm^{-1}, associated with C-O and C-O-C stretching. The peak present at 1192 cm^{-1} in neat PLA split into two peaks at 1217 cm^{-1} and 1182 cm^{-1} in the PLA/CNC (DB) films, and 1215 cm^{-1} and 1184 cm^{-1} in the PLA/CNC (MB) films. Additionally, the sharp peak at 1128 cm^{-1} in PLA films split into two broader peaks in the composite films [1134 cm^{-1} and 1121 cm^{-1} in PLA/CNC (DB); 1132 cm^{-1} and 1113 cm^{-1} in PLA/CNC (MB)]. The broad peak in PLA at 1092 cm^{-1} became sharper and shifted to lower wavelengths in the range of 1080-1082 cm^{-1} for the composite films. These changes could indicate degradation of the PLA/CNC composite films because ester linkages in PLA's main chain cleave to form carboxyl end-groups, as illustrated in Figure 4.15. However, since the region between 1045-1270 cm^{-1} is assigned to both, C-O stretch from carboxyl groups and C-O-C stretching vibrations, it was difficult to use its intensity or area to accurately quantify the formation of carboxyl end-groups. Thus, the intensity of the peak at 957 cm^{-1}, assigned specifically to the O-H vibrations in carboxyl groups, was considered more appropriate to monitor the carboxyl group formation by calculating the carboxyl index (equation 3.1). An increase in carboxyl index would indicate the presence of additional carboxyl end-groups generated due to main chain scission by the proposed degradation mechanism (Figure 4.15).

The carboxyl indices of PLA and PLA/CNC composite films are illustrated in Figure 4.17. PLA/CNC composite films have higher carboxyl indices compared to PLA, indicating that chain scission occurred during both, the direct dry- and melt-blending processes by the proposed degradation mechanism (Figure 4.15). However, the PLA/CNC melt-blended films have higher carboxyl index than their direct dry-blended counterparts suggesting that more chain scissions occurred for these films, in corroboration with the GPC results.

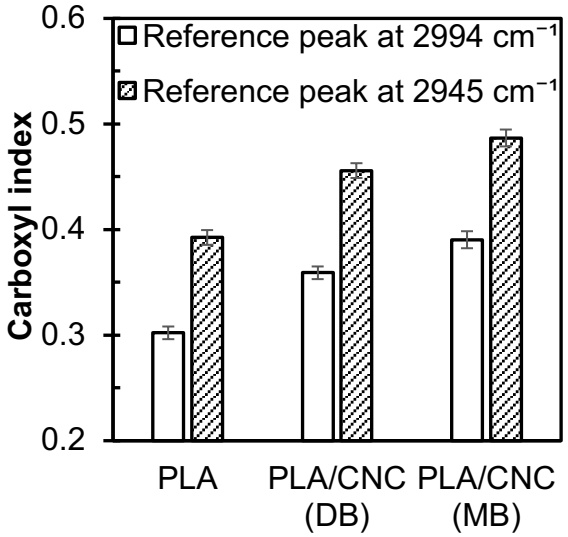

Figure 4.17 Carboxyl indices using the intensities of reference peaks at 2994 cm^{-1} and 2945 cm^{-1} of PLA, PLA/1% CNC (DB) and PLA/1% CNC (MB) films.

4.2.4 Effects of CNC addition and blending process on the WVTR and OTR of PLA

The incorporation of 1% CNCs into the PLA matrix improved its water and oxygen barrier performance, irrespective of the blending process (Table 4.9). This improved barrier performance of PLA/CNC composite films can be attributed to the presence of highly crystalline cellulose nanocrystals which act as impermeable regions in the matrix. The impermeable regions create a more tortuous diffusion path for the permeant, leading to slower diffusion and hence lower transmission rates [53-55].

Table 4.9 WVTR and OTR of PLA as well as direct dry-blended (DB) and melt-blended (MB) PLA/1% CNC films.

Materials	**WVTR at 38°C and 85% RH (10^{-7} kg/m^2·s)[A]**		**OTR at 23°C and 0% RH (10^{-10} kg/m^2·s)[A]**	
	Average	% Decrease	Average	% Decrease
PLA	584.9 ± 49.5^a	-	442.3 ± 87.4^a	
PLA + 1% CNC (DB)	409.7 ± 21.3^b	30	178.9 ± 23.1^b	60
PLA + 1% CNC (MB)	442.9 ± 25.9^c	24	270.1 ± 77.4^c	39

[A]Same superscript letters within the same column are not significantly different based on the ANOVA results at 5% significance level.

Nonetheless, it should be mentioned that the WVTR and OTR of PLA/CNC melt-blended films was higher than their direct dry-blended counterparts due to thermal degradation of these films as demonstrated by DSC (Table 4.6), GPC (Table 4.7) and FTIR (Figure 4.17) results. From obtained WVTR and OTR results, direct dry-blending appeared to be the better approach for incorporating CNCs into the PLA matrix to enhance its water and oxygen barrier properties.

4.3 Water vapor and oxygen barrier properties of extrusion-blown poly(lactic acid)/cellulose nanocrystals nanocomposite films

The title and content of section 4.3 were published in Composites Part A: Applied Science and Manufacturing, 114: 204-211 (2018). doi: https://doi.org/10.1016/j.compositesa.2018.08.025. This paper was co-authored by N.M. Stark, R.C. Sabo and L.M. Matuana.

The main objective of this section was to evaluate the effects of CNC addition level and environmental testing conditions on the barrier properties of PLA/CNC films as well as their thermal and optical properties. The ultimate goal of this section of the study was to gain an in-depth understanding of the mechanisms governing improvement in barrier properties, to model and to establish relationships between environmental testing conditions and barrier properties as well as to optimize the CNC content (specific objective #3) [21]. It should be noted that for all results presented in this section, the direct dry-blending process was used to incorporate CNCs into the PLA matrix because it appeared to be the better approach compared to the melt-blending technique as determined in the previous section.

4.3.1 Effect of CNC content on water vapor permeability (WVP) and oxygen permeability (OP) of films

Figure 4.18 illustrates the effect of CNC content on the water vapor permeability (WVP) and oxygen permeability (OP) of PLA films. The WVP and OP decreased as the CNC concentration increased up to 1% and remained constant thereafter. Significant improvements of approximately 39% and 74% in WVP and OP, respectively, were observed by adding only 1% CNC into PLA matrix. This improved barrier performance of the nanocomposite films is likely due to the presence of highly crystalline CNCs which acted as efficient nucleating agent resulting in higher degree of crystallinity (Figure 4.19) as well as impermeable regions in the matrix [10,46,55-57]. Other investigators have reported similar results for PLA nanocomposites with CNCs [10,25,32,33,35], microcrystalline cellulose [36], and cellulose nanofibers [37].

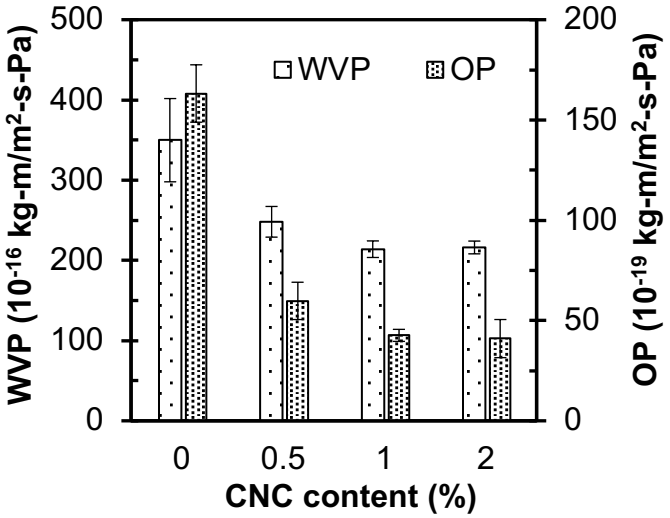

Figure 4.18 Effect of CNC content on the WVP (23°C and 85% RH) and OP (23°C and 0% RH) of PLA films.

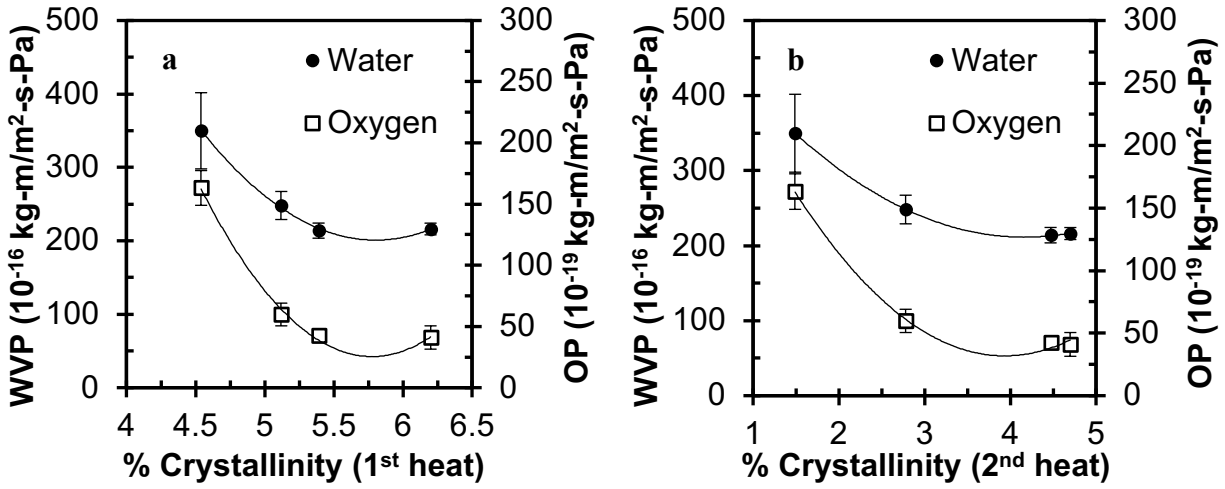

Figure 4.19 WVP and OP of PLA and PLA/CNC nanocomposite films as a function of crystallinity obtained from (a) 1st heat and (b) 2nd heat. In the 1st heat the crystallinities were 4.5 ± 0.1; 5.1 ± 1.0; 5.4 ± 0.8; and 6.2 ± 0.2 whereas in the 2nd heat they were 1.5 ± 0.4; 2.8 ± 0.4; 4.5 ± 0.4; and 4.7 ± 0.4 for PLA with 0; 0.5; 1; and 2% CNC, respectively.

Because the permeant does not readily diffuse through crystallites [55,57], it is believed that the presence of nucleated crystals and CNCs increases the effective travel paths for water vapor and oxygen movements through the nanocomposites, making the path length more tortuous, which reduces the diffusion process, thus lowering permeation as reported by others [10,53,56,57].

Interestingly, the values of WVP and OP negatively correlated with the degree of crystallinity (Figure 4.19) in the as-molded PLA films (1st heat) as well as their intrinsic crystallinity (2nd heat), in reasonable agreement with the work of Shogren [58] who asserted an improvement of 50% or higher in WVP of amorphous PLA by crystallizing it through annealing at 130°C for 10 minutes in a vacuum oven. Similarly, the WVP of another biopolymer, poly(β-hydroxybutyrate-co-hydroxy-valerate) (PHBV) with various valerate contents (6, 12, and 18%),

correlates well with the crystallinity. As valerate content of PHBV decreases, the crystallinity increases and WVP decreases. In other terms, highly crystalline PHBV with low valerate content (PHBV-6) had lower values of WVP in the range of temperatures investigated (6-49^{o}C) [58]. Several other investigators have also reported negative correlation between the degree of crystallinity and WVP as well as OP values of PLA and its nanocomposites with cellulose nanomaterials manufactured using solvent-casting techniques [56,59-61]. In one such study, Sanchez-Garcia and Lagaron demonstrated that PLA's crystallinity increased slightly from 9.1% to 10.7% by adding 3% solvent-exchanged cellulose nanowhiskers resulting in a significant decrease of 49% in WVP values of PLA [59]. In another study, the addition of 3% unmodified and 3% surfactant modified CNCs increased PLA's crystallinity from 5.5% to 6.2% and 8.7%, respectively leading to reductions of 16% and 17% in WVP of PLA, respectively and 21% and 25% in OP of PLA, respectively [60]. Similarly, Oksman and Petersson confirmed the negative correlation between crystallinity and OP values by reporting a 240% increase in PLA's OP on addition of 5% swollen microcrystalline cellulose (S-MCC) due to the combined effects of decreased crystallinity of nanocomposite films compared to PLA and low S-MCC/PLA interactions leading to a straight and less tortuous path for the gas molecules to travel [61].

The maximum increase in crystallinity occurred at 1% CNCs (see Figure 4.19 caption), a CNC content that correlates very well with the optimum improvement in the barrier properties of the films (Figure 4.18). It should be mentioned that the addition of more than 1% CNCs did not improve the crystallinity of PLA further (see Figure 4.19 caption) probably due to the retarded crystal growth caused by CNC agglomerations at high loading levels [35,62].

Consequently, nanocomposite films with different CNC contents (0.5; 1 and 2%) were examined under a digital microscope to monitor CNC agglomerations at high loading levels (Figure 4.20). A plot of the CNC agglomeration frequency as a function of their diameters is also shown. Homogenous distribution of CNCs was achieved in the PLA matrix, regardless of the CNC content. However, some agglomerates indicated by the micrometer-sized particle diameters recorded in Figure 4.20 (a-c) were still visible suggesting that nanoscale dispersion was not achieved as previously reported [10]. As expected, the PLA films with 2% CNCs slightly had higher number of particles with size 10μm or larger compared to the other concentrations [Figure 4.20 (d)].

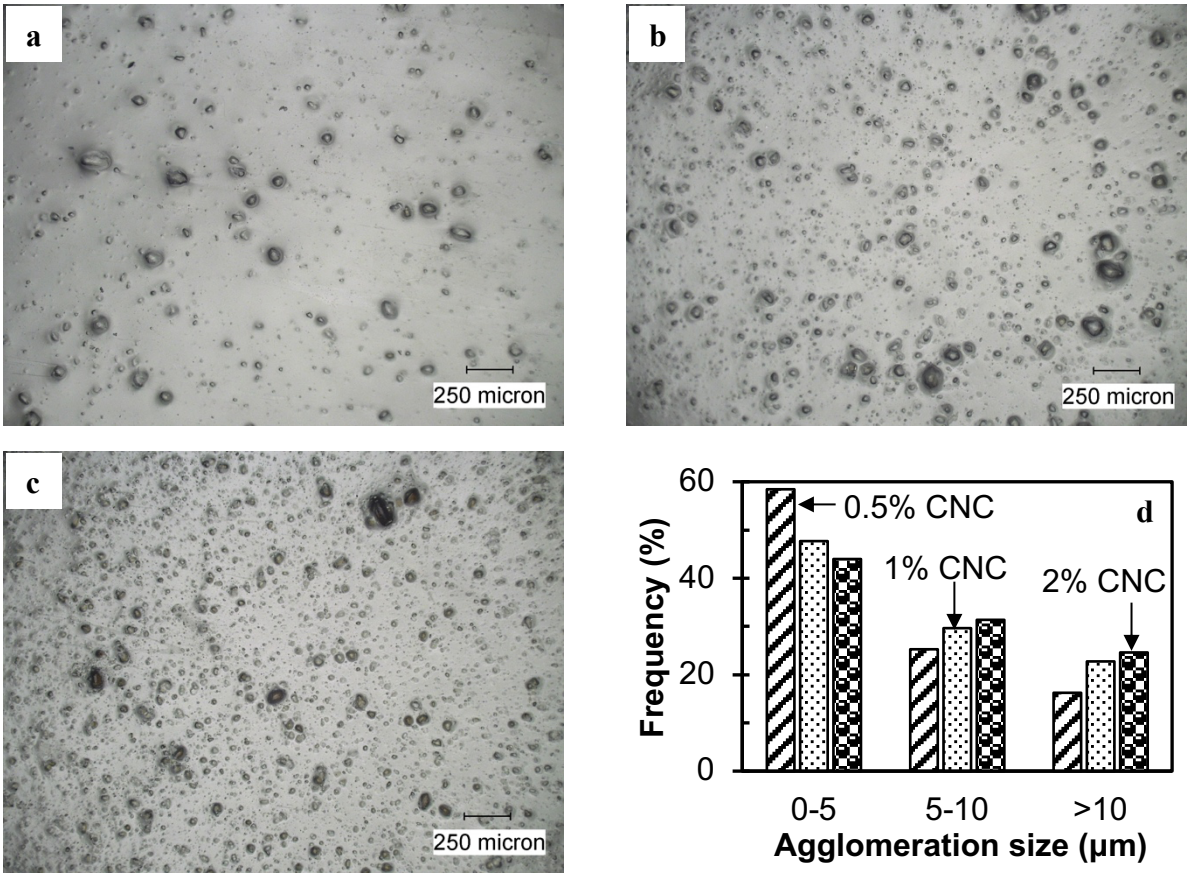

Figure 4.20 Digital microscope images of PLA films with various CNC contents of (a) 0.5%; (b) 1%; and (c) 2% as well as (d) CNC agglomeration frequency as a function of their diameters in the nanocomposite films.

Due to limited CNC dispersion, the light transmission of PLA films in the visible light wavelength range (380-720 nm) decreased by adding CNCs into the films, irrespective of the CNC content (Figure 4.21). This deleterious effect could be attributed to the presence of nucleated crystals and micrometer-sized CNC agglomerations larger than the incident wavelength of light (nanometer) in the nanocomposite films, which scatter light [10,23,63]. The transparency of PLA films decreased from ~92% to ~86% with the addition of 0.5% CNCs, further decreased to ~78% with the addition of 1% CNCs and then levelled off with further addition of CNCs. Remarkably, the decreased light transmission of PLA films on the addition of CNCs did not affect their visual clarity (Figure 4.22). It should be mentioned that the addition of CNCs into PLA reduced the light transmittance in the UV region of the spectra (250-380 nm) indicating that CNCs blocked light in this region, making the nanocomposite films attractive materials for packaging applications requiring UV light protection as reported by others for PLA nanocomposites with CNFs [23], CNCs [63,64] and S-MCCs [61].

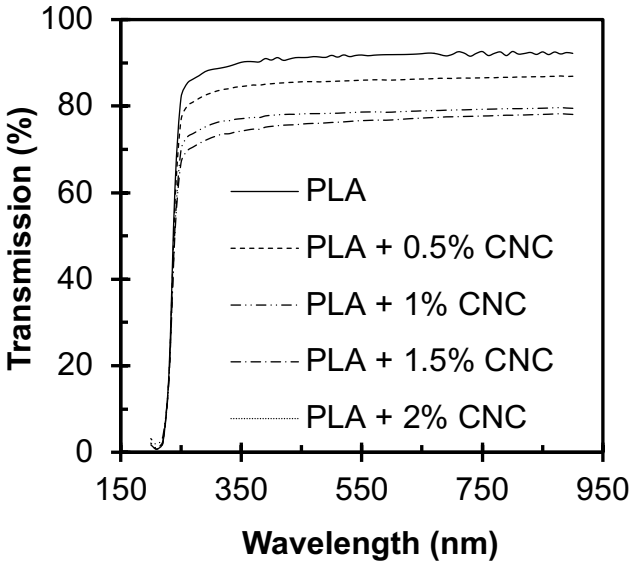

Figure 4.21 Effect of CNC content on the transparency of PLA films.

Figure 4.22 Visual clarity of PLA and PLA/CNC nanocomposite films.

4.3.2 Effect of CNC content on water vapor permeability (WVP) and oxygen permeability (OP) of films

Consider first the effects of CNC addition and testing temperature on the WVP [Figure 4.23 (a)] and OP [Figure 4.23 (b)] of PLA films. Increasing the temperature of the system led to an exponential decrease in the WVP but an exponential increase in OP for PLA and PLA/CNC nanocomposite films in agreement with results reported by other investigators [58,65-67]. However, the WVP decreased as the CNC content increased up to 1% and remained constant thereafter, irrespective of the testing temperature [Figure 4.23 (a)]. Since the optimum improvement in WVP was observed at 1% CNC content [Figure 4.23 (a)], the OP dependence on temperature was evaluated for neat PLA and PLA/1% CNC nanocomposite films only [Figure 4.23 (b)]. Overall, the nanocomposite films had better water and oxygen barrier properties than neat PLA counterparts, regardless of testing temperature due in part to the increased crystallinity (Figure 4.24), which validates the negative correlation between the barrier properties (WVP and OP) and crystallinity discussed earlier.

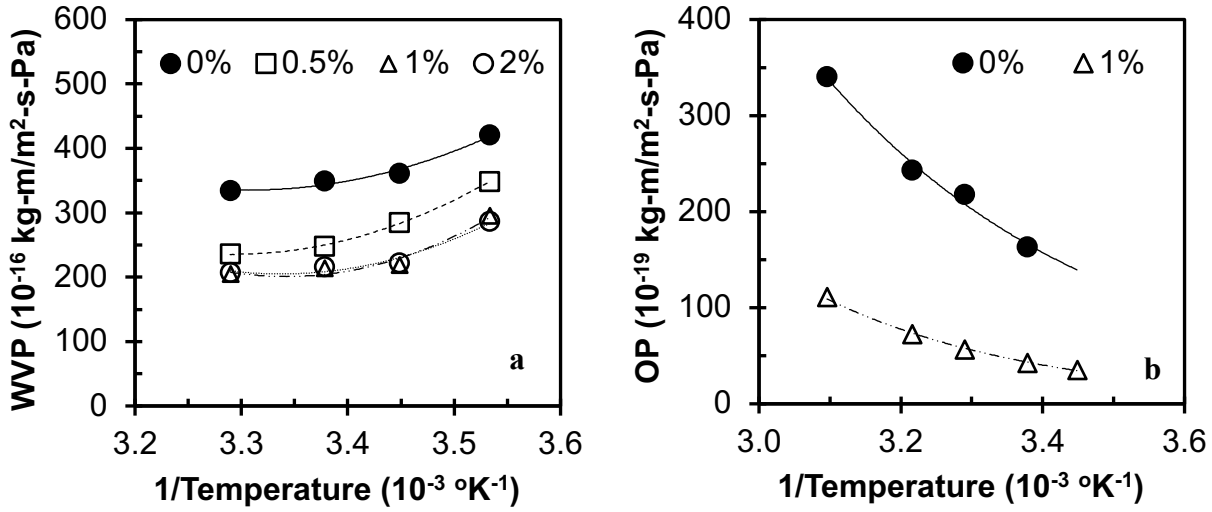

Figure 4.23 Effects of (a) CNC content and testing temperature on the WVP of PLA films at 85% RH and (b) CNC addition and testing temperature on the OP of PLA films at 0% RH.

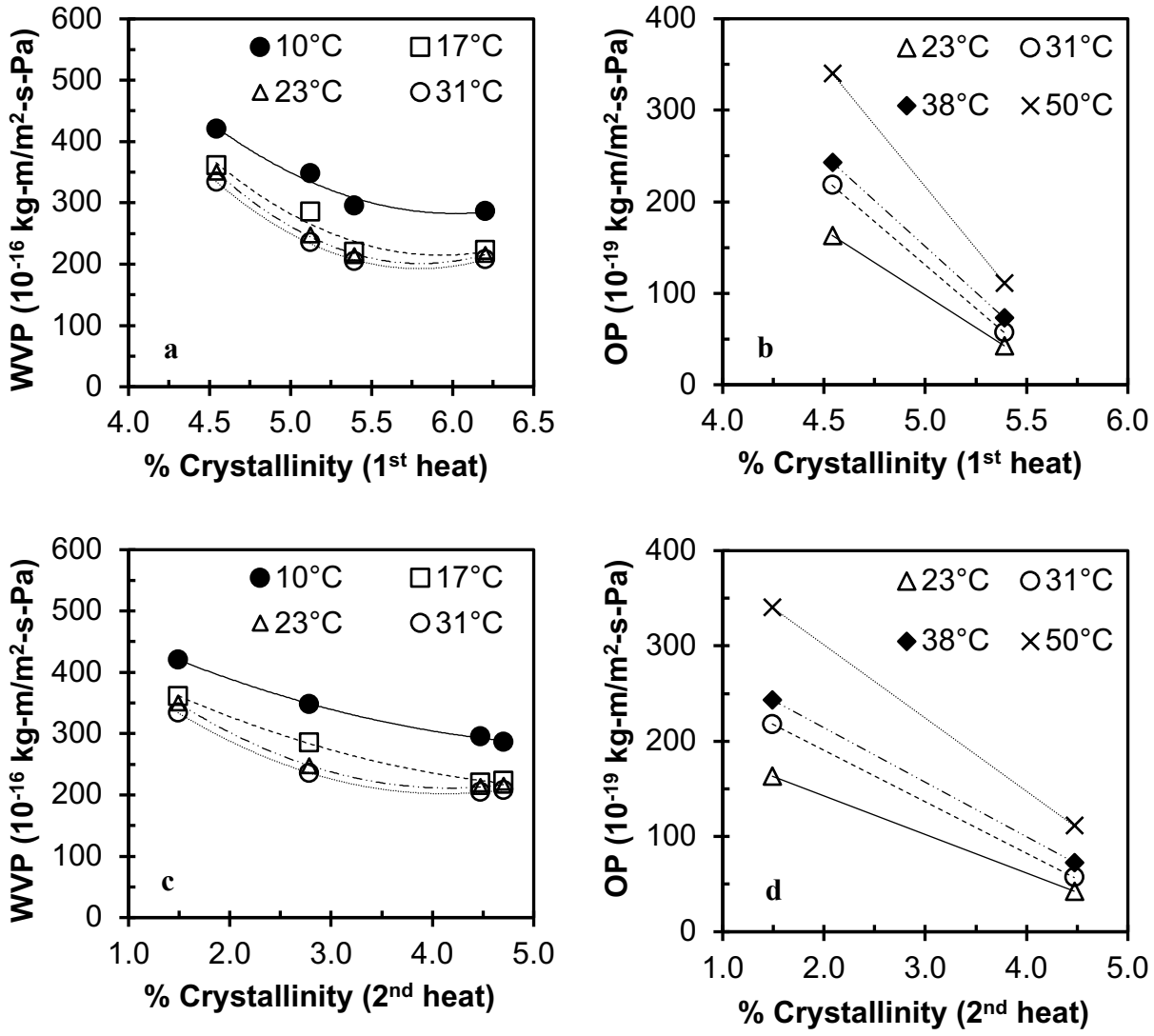

Figure 4.24 WVP and OP of PLA and nanocomposite films at various temperatures as a function of percent crystallinity obtained from 1st heat [(a) and (b)] and 2nd heat [(c) and (d)].

The exponential relationships between the permeability (water and oxygen) and temperature shown in Figure 4.23 can be described by the following Arrhenius relationship:

$$Y = A_0 \cdot \exp^{-E_p/RT} \quad \text{(Equation 4.7)}$$

where Y is the WVP or OP of the films; A_0 is the pre-exponential factor or Arrhenius constant, i.e., the WVP or OP of the film at very high temperature (approaching infinity) which has no physical meaning but represents permeability in the absence of polymer-polymer interaction [65]; E_p is the activation energy, i.e., the minimum energy barrier to be overcome by water vapor or oxygen to start permeating through the film; R is the universal gas constant (0.008314 kJ mol^{-1} K^{-1}); and T is the temperature (^oK).

Table 4.10 summarizes the regression analysis results for the activation energy (E_p) and pre-exponential factor (A_0) of PLA and PLA/CNC nanocomposite films from the Arrhenius plots shown in Figure 4.23. The activation energy for water vapor permeability is negative for the PLA and nanocomposite films. Negative activation energy values of -0.1 kJ/mol for semi-crystalline PLA [58], -3.93 kJ/mol for commercial PLA cast films [65], -9.8 kJ/mol for PLA 4030D with 98% L-Lactide [66] and -10.1 kJ/mol for PLA 4040D with 94% L-Lactide [66] have also been reported and attributed to the polarity of PLA [58,65], which affects the activation energies for diffusion (E_d) and sorption (or heat of solution, ΔH_s), two major components contributing to the overall activation energy for permeation given by:

$$E_p = E_d + \Delta H_s \quad \text{(Equation 4.8)}$$

Table 4.10 Effect of CNC content on the water vapor and oxygen activation energy (E_p) and pre-exponential factor (A_0) of PLA films.

CNC content in PLA films (%)	**WVP**			**OP**		
	A_0 (10^{-16} kg-m/m^2-s-Pa)	E_p (kJ/mol)	R^2	A_0 (10^{-14} kg-m/m^2-s-Pa)	E_p (kJ/mol)	R^2
0	16.7	-7.5	0.88	8.5	21.0	0.99
0.5	1.1	-13.5	0.93	-	-	-
1	1.9	-11.7	0.76	26.5	27.1	0.99
2	3.3	-10.3	0.79	-	-	-

Investigators have reported lower values of E_d for hydrophilic polymers due to their lower activation energy for water diffusion. Whereas, ΔH_s, which is controlled by two separate thermodynamic processes, is equal to the sum of the heats of condensation (ΔH_c) and mixing (ΔH_m). Polar polymers such as PLA, cellulose acetate (CA), cellulose acetate propionate (CAP) and ethyl cellulose (a hydrophilic polymer) have near-zero or negative values for ΔH_m [58,65]. Since ΔH_c is negative and equal to -42 kJ/mol for water vapor, ΔH_s becomes negative, resulting in negative values of E_p (equation 4.8) [58,65].

The activation energy for water permeability (absolute E_p values in Table 4.10) slightly increased by adding CNCs into the matrix, regardless of CNC content, suggesting that more energy is required to initiate water vapor permeation through the nanocomposite films. Similar trend is observed for OP where the E_p slightly increased by adding 1% CNC into PLA matrix, owing to the excellent oxygen barrier of cellulose nanomaterials [55]. The activation energy for oxygen

permeability of 21.0 kJ/mol obtained in this study for neat PLA films is consistent with the E_p values of 28.43 kJ/mol [66], 23.869 kJ/mol [67] and 24.9 kJ/mol [68] in the literature. It is worth mentioning that the Arrhenius equation parameters (A_0 and E_p) listed in Table 4.10 can be used in equation 4.7 to predict WVP and OP values of the PLA and PLA/CNC nanocomposite films at any absolute temperature (Kelvin).

Consider next the effects of CNC content and relative humidity (RH) on the WVTR and WVP of PLA films (Figure 4.25). It is generally accepted that the WVTR through a polymeric film depends on the concentration gradient of the permeant and is described by the Fick's law [69,70]:

$$J = -D\nabla c \qquad \text{(Equation 4.9)}$$

where J is the diffusion flux; D the diffusion coefficient; and ∇c the concentration gradient of the permeant in the film.

Since the diffusion coefficient (D) is independent of the permeant concentration at steady state, equation 4.9 can be combined with Henry's law ($c = S \cdot p$) and integrated to give [69,70]:

$$J_s = D \cdot \frac{c_1 - c_2}{l} = D \cdot S \cdot \frac{p_1 - p_2}{l} = P \cdot \frac{p_1 - p_2}{l} \qquad \text{(Equation 4.10)}$$

where J_s is the diffusion flux at steady state (WVTR); l is the film thickness; c_1 and c_2 are the concentrations of the permeant (water vapor) on the external and internal sides of the test film; S is the solubility coefficient; and P is the permeability coefficient, i.e., product of D and S.

Using $p_1 - p_2 = P_{sat} \cdot (RH_{out} - RH_{in})$, equation 4.10 can be rearranged as follows:

$$J_s = WVTR = \frac{P \cdot P_{sat}}{l} \cdot (RH_{out} - RH_{in}) \qquad \text{(Equation 4.11)}$$

It is clearly seen in Figure 4.25 (a) that WVTR increased linearly with increasing testing RH, irrespective of CNC content as expected from Fick's Law (equation 4.11), in agreement with results reported for PLA [53] and other plastics [71].

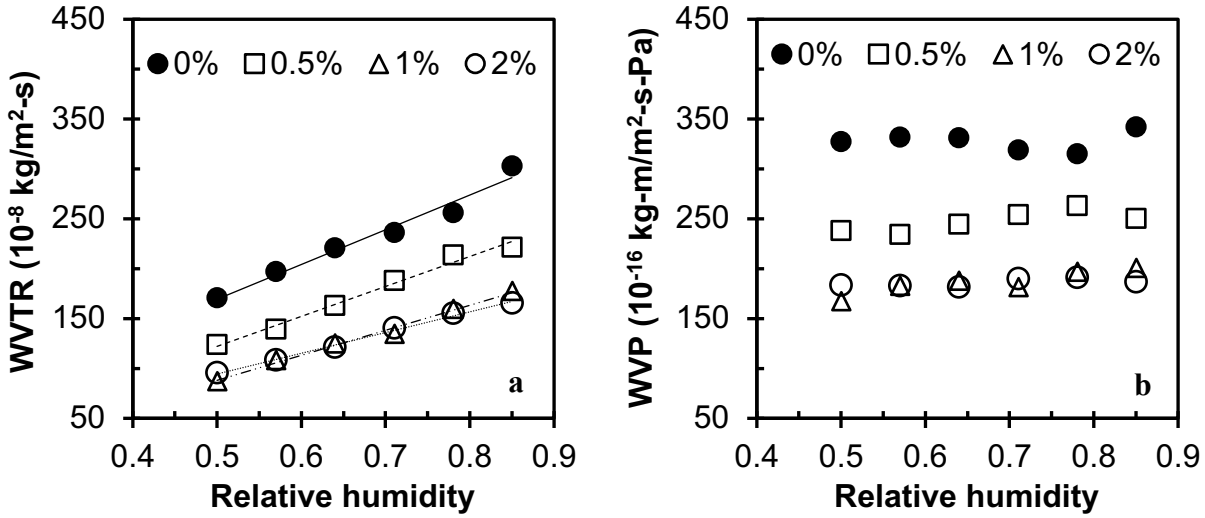

Figure 4.25 Effects of CNC content and RH on the (a) WVTR and (b) WVP of PLA films at 23°C.

The WVTR values of PLA and nanocomposite films were normalized by the film thickness and the difference in partial vapor pressures to obtain the permeability (equation 3.6). A plot of the obtained WVP as a function of RH for PLA and nanocomposite films is shown in Figure 4.25 (b). Since the difference in partial vapor pressure in equation 3.6 [$\Delta p = P_{sat} (RH_{out} - RH_{in})$] increases linearly with increasing testing RH (i.e., increase in RH_{out} only since $RH_{in} \approx 0\%$), the normalized WVP of PLA and nanocomposite films did not vary with changes in testing RH, in agreement with the findings reported in the literature for PLA 4030D with 98% L-Lactide and PLA 4040D with 94% L-Lactide [66]. Nevertheless, all nanocomposite films were better barriers to water vapor than neat PLA films attributable to the increased crystallinity (Figure 4.26), again validating the negative correlation between the WVP and crystallinity, insensitive to RH.

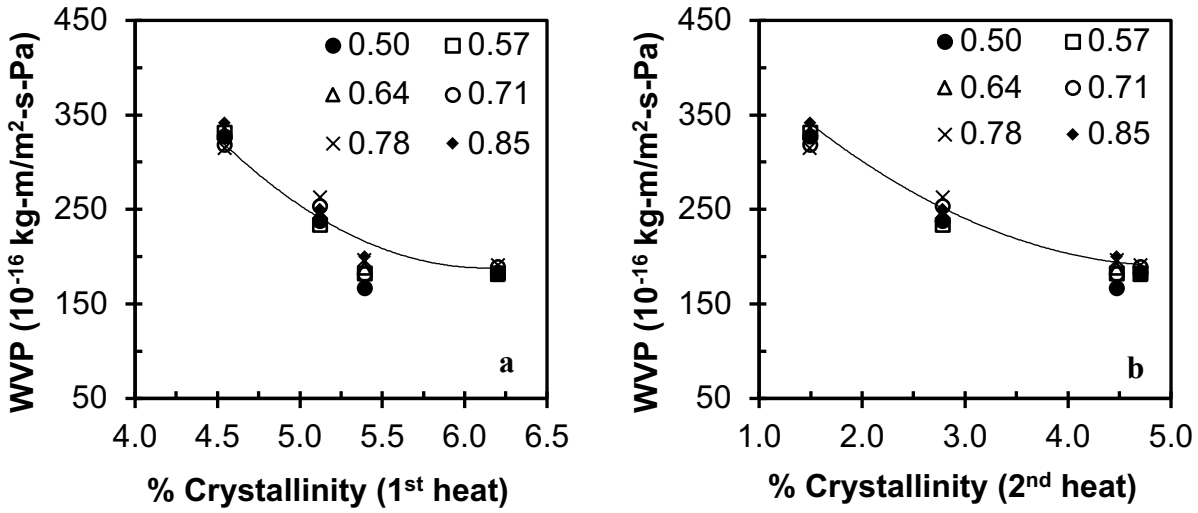

Figure 4.26 WVP of PLA and PLA/CNC nanocomposite films tested at various relative humidity conditions as a function of films' crystallinity obtained from (a) 1st heat and (b) 2nd heat.

4.4 Potential of extrusion-blown poly(lactic acid)/cellulose nanocrystals nanocomposite films for improving the shelf-life of a dry food product

The title and content of section 4.4 are part of the manuscript under preparation for submission to Food Packaging and Shelf-Life journal.

From the studies performed in the previous sections, it was evident that the direct dry-blending technique appeared to be the better approach for incorporating CNCs into the PLA matrix. Moreover, optimum improvements in barrier properties of PLA films occurred at 1% CNCs. Therefore, the main objective of this section was to assess the potential of the developed PLA/1% CNC nanocomposite films manufactured using the direct dry-blending approach in extending the shelf-life of moisture-sensitive food product (crackers) *(specific objective #4*).

4.4.1 Moisture sorption of food

The initial moisture content (IMC) of the crackers was 4.1% (dry basis), in corroboration with other researchers [72]. Since the IMC is low, the product has a tendency to absorb moisture from its surrounding atmosphere, making it a moisture-sensitive product. On absorbing moisture, the product becomes soggy and unappetizing. It is important to establish the sorption behavior of food products to estimate product stability at various storage conditions and to evaluates the requirements of packaging materials in order to ensure adequate product shelf-life. Therefore, the moisture content of unpackaged crackers was monitored under various conditions of relative humidity (RH) as a function of time (Figure 4.27). Two distinct trends were seen from Figure 4.27. Firstly, the moisture content of crackers increased as the RH increased, irrespective of the storage time. As expected, the moisture sorption of food increased with RH since more water molecules were available in the atmosphere to be absorbed at a higher RH, leading to a higher concentration

gradient, as per Fick's law. Secondly, the moisture content of food increased gradually with increasing time and then reached a constant value or an equilibrium for each RH condition, indicating that the product is susceptible to moisture gain due to its low IMC. The moisture content at the equilibrium condition, known as the equilibrium moisture content (EMC), was plotted against RH to generate the moisture sorption isotherm.

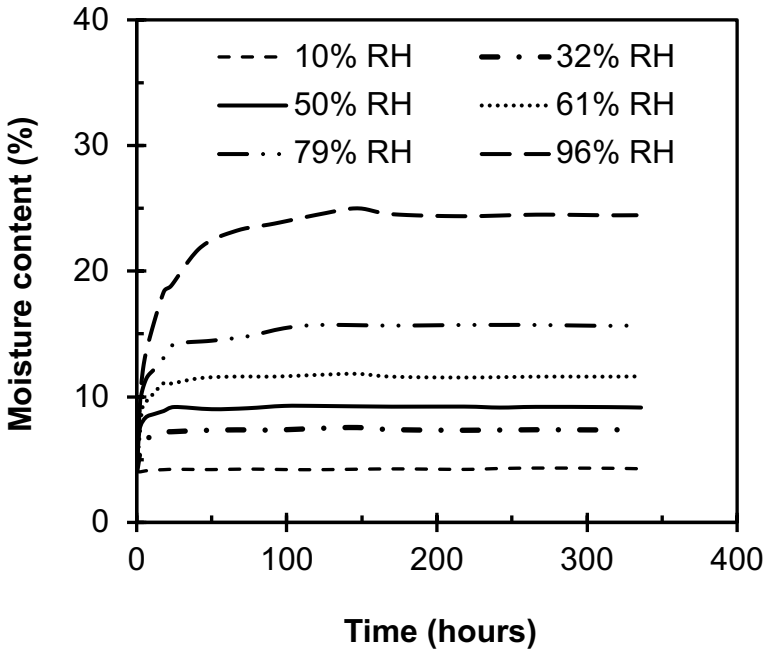

Figure 4.27 Moisture contents of crackers as a function of time recorded at 25°C and various storage relative humidity conditions.

Figure 4.28 shows a plot of the experimental EMC of the food (obtained from Figure 4.27) as a function of the storage RH at 25°C. The obtained experimental moisture isotherm (Figure 4.28) exhibited the sigmoidal (Type-II) or S-shape curve typically observed by other researchers in moisture-sensitive foods such as salted crackers [73], rice crackers [72] and cornflakes [74]. The EMC increased gradually at lower RH but rapidly at higher RH.

The experimental moisture sorption data was fitted using non-linear regression analysis to the Guggenheim Anderson de Boer (GAB) equation as follows [72-74]:

$$\mathrm{EMC_{pred}} = \frac{\mathrm{CKa_w W_m}}{(1 - \mathrm{Ka_w}) \cdot (1 - \mathrm{Ka_w} + \mathrm{CKa_w})} \qquad \text{(Equation 4.12)}$$

where EMC_{pred} is the predicted equilibrium moisture content of the product, C is the Guggenheim constant, K is the correction factor, W_m is the monolayer saturated water content, and a_w is the water activity (given as %RH/100).

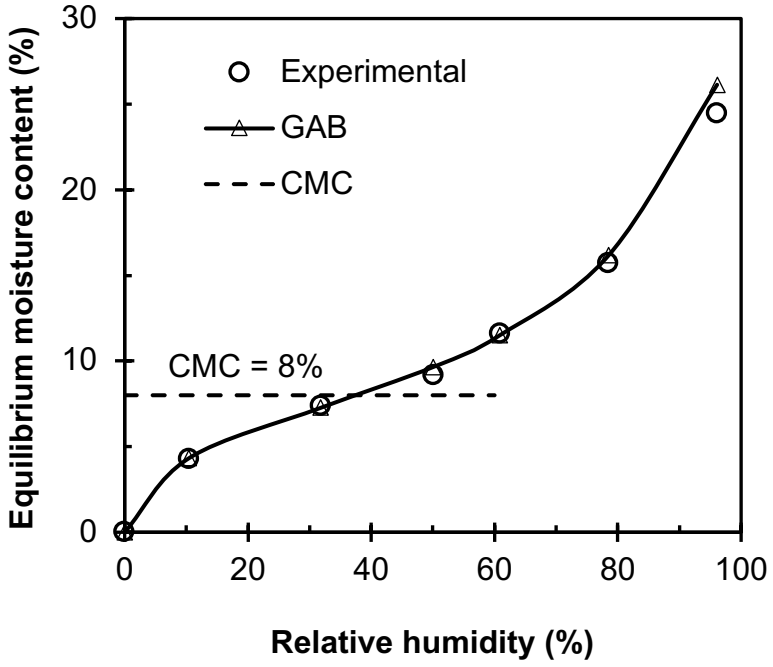

Figure 4.28 Moisture sorption isotherm of crackers at 25°C.

The precision of fit of the GAB model to the experimental data was calculated using the root mean square (RMS) value as follows [72-74]:

$$\mathrm{RMS} = \left[\sqrt{\frac{\sum_{i=1}^{N} \left(\frac{\mathrm{EMC_{exp}} - \mathrm{EMC_{pred}}}{\mathrm{EMC_{pred}}} \right)^2}{N}} \right] \times 100 \qquad \text{(Equation 4.13)}$$

where EMC_{exp} is the experimental equilibrium moisture content, EMC_{pred} is the equilibrium moisture content predicted by the GAB model, and N is the number of experimental points.

Generally, a low RMS value (below 10%) signifies a good fit of the model to the experimental data [72-74]. In this case, the RMS value obtained was 3.8% indicating that the GAB model was a good fit to the experimental data obtained for crackers. Our results corroborate other studies for moisture-sensitive foods such as salted crackers [73] and rice crackers [72] as well as cornflakes [74]. While several investigators have reported the usefulness of the GAB equation to fit sorption isotherms, it should be noted that this model works best below 90% RH [74].

As mentioned previously, the literature review showed an average CMC value of 8% for crackers. By drawing a horizontal line parallel to the X-axis (% RH) at the average CMC value (8%), the data produced an intersection with the moisture sorption isotherm at 37% RH (Figure 4.28). This result implies that the food product is shelf-stable when stored at a RH below 37% since the EMC values obtained below 37% RH are below the CMC. In other terms, when the food product is stored below 37% RH, it will reach its equilibrium moisture content before it can reach

the critical moisture content, making it shelf- stable below this storage relative humidity. On the other hand, when the food product is stored above 37% RH, it will absorb moisture and will eventually reach the CMC, beyond which it will be unacceptable to the consumer. Packaging materials such as PLA and PLA/CNC films can be used to delay this moisture absorption and shelf-stability, thereby extending the shelf-life of food.

4.4.2 Experimental shelf-life of crackers packaged in PLA and PLA/CNC composite films

Our previous studies demonstrated that the incorporation of 1% CNCs into a PLA matrix by a direct dry-blending approach improved the water and oxygen barrier performance of PLA by 40% and 60%, respectively [10,21,53]. In this section of the thesis, the effectiveness of the manufactured PLA/CNC nanocomposite films in extending the shelf-life of moisture-sensitive food products were assessed.

Table 4.11 summarizes the shelf-life of crackers packaged in PLA and PLA/CNC films stored at 25^{o}C and various RH conditions. The crackers packaged in both PLA and PLA/CNC films did not reach the critical moisture content value of 8% when stored below 50% RH, demonstrating shelf-stability at these storage conditions. It should be noted that the unpackaged crackers were shelf-stable up to 37% RH only, indicating that the packaging materials delayed moisture absorption and therefore increased the value of storage relative humidity until which the crackers were shelf-stable to 50% RH. The crackers packaged in both PLA and PLA/CNC films reached 8% CMC when stored above 50% RH. However, the time required to reach the CMC (known as shelf-life) varied with the storage environmental condition (percent RH) and the packaging film composition. Firstly, the shelf-life of packaged crackers decreased with increasing RH, irrespective of the film composition. This trend can be attributed to the low moisture gradient

between the inside of the package and the storage environment at lower RH. With increasing RH, the moisture gradient increases, leading to higher water vapor transmission rates and reduced shelf-life, irrespective of the packaging material composition. Secondly, above 50% RH the shelf-life of crackers packaged in PLA/CNC films was longer than those packaged in unfilled PLA films, irrespective of the storage RH, attributable to the superior water barrier performance of the PLA/CNC films compared to the neat PLA counterpart films (Table 4.12). Remarkably, the shelf-life of crackers packaged in the PLA/CNC films was approximately 40% longer than the crackers packaged in neat PLA films, irrespective of the storage RH, in corroboration with the improved water barrier performance of the nanocomposite films (~40%).

Table 4.11 Time for crackers packaged in PLA and PLA/CNC films to reach critical moisture. content of 8% at different relative humidity conditions and a constant temperature of 25°C.

% RH	**Shelf-life (hours)**		
	PLA	**PLA/1% CNC**	**Delay time to reach CMC**
10	Shelf-stable	Shelf-stable	
33	Shelf-stable	Shelf-stable	
50	Shelf-stable	Shelf-stable	
61	63.4 ± 0.6	86.1 ± 1.6	22.7
79	42.9 ± 0.7	59.9 ± 5.1	17.0
96	14.2 ± 0.2	20.1 ± 0.4	5.9

Table 4.12 Water vapor permeability values of PLA and PLA/CNC films at different relative humidity conditions and a constant temperature of 23°C.

% RH	Water vapor permeability (10^{-16} kg-m/m^2-s-Pa)		
	PLA	PLA/1% CNC	% Decrease
50	327.2 ± 16.1	166.9 ± 4.1	49
57	331.7 ± 20.6	182.7 ± 5.0	45
64	330.7 ± 27.3	187.7 ± 2.9	43
71	318.9 ± 21.3	181.6 ± 3.6	43
78	314.8 ± 43.9	196.5 ± 6.1	38
85	341.8 ± 50.0	200.3 ± 10.0	41

4.4.3 Shelf-life modelling of crackers packaged in PLA and PLA/CNC in films

Several mathematical models for predicting the shelf-life of a moisture sensitive product packaged in a film, described in section 2.8.2.2 of the literature review were used in this section of the thesis to predict the shelf-life of crackers packaged in PLA and PLA/CNC films.

The experimental shelf-life and the predicted shelf-life of crackers packaged in PLA and PLA/CNC films at several storage relative humidity conditions are listed in Table 4.13. Interestingly, shelf-life predictions support the experimental data that the crackers packaged in the PLA/CNC composite films have a higher shelf-life compared to those packaged in PLA films, irrespective of the storage relative humidity and mathematical models employed (Table 4.13). These results clearly demonstrate the effectiveness of PLA/CNC films to extend dry-foods' shelf-life compared to neat PLA films. Nevertheless, the shelf-life values predicted by the mathematical

models did not match those obtained experimentally (Table 4.13). These differences between the experimental and predicted shelf-life could be attributed to the limitations of the mathematical models, which predict shelf-life based solely on the relationship between moisture content of the food product and barrier property of the packaging material, may not be accurate. Besides the moisture content of food product and the package permeability, other factors such as food structure and composition may also significantly affect the shelf-life characteristics of the packaged foods. For instance, the salt and/or fat present in the crackers can affect the moisture absorption and hence shelf-life prediction through the modelling techniques used. Other researchers have also reported large deviations in the predicted and experimental shelf-life values of salted crackers [73] and rice crackers [72] attributable to the presence of additional food constituents such as salt [73] and fat [72]. Additional factors such as a non-uniformity of packaging film thickness as well as fluctuations in storage temperature, and relative humidity during testing, amongst others could also affect the accuracy of shelf-life predicted by mathematical models. Since the films used in this study were made in a laboratory using the blown film extrusion process, they were prone to thickness variations due to surface roughness [75] which could have also contributed to experimental errors and inaccurate shelf-life predictions. Based on these results, there is a need to develop other models that can predict the shelf-life of packaged crackers more accurately.

Table 4.13 Predicted and experimental shelf-life of crackers packaged in PLA and PLA/CNC films stored at various relative humidity conditions.

Models	**Shelf-life (hours)**					
	61% RH		**79% RH**		**96% RH**	
	PLA	**PLA/CNC**	**PLA**	**PLA/CNC**	**PLA**	**PLA/CNC**
Linear	24.9	43.9	19.2	33.8	13.4	23.6
Middle-point	13.2	23.3	11.3	19.9	8.9	15.7
Logarithmic	21.4	37.7	16.4	29.0	11.5	20.2
GAB	21.7	38.2	16.5	29.1	11.4	20.1
Experimental	63.4	86.1	42.9	59.9	14.2	20.1

APPENDICES

APPENDIX A: Extrusion blown films of poly(lactic acid) chain-extended with food grade multifunctional epoxies

Table A.1 Stock temperature and mixing torque of PLA and its blends with CE 4400 as a function of time generated by a torque rheometer.

Time (s)	%CE 4400 in PLA									
	0%		0.25%		0.5%		0.75%		1%	
	Temp (°C)	Torque (Nm)	Temp (°C)	Torque (Nm)	Temp (°C)	Torque (Nm)	Temp (°C)	Torque (Nm)	Temp (°C)	Torque (Nm)
0	203.1	0.0	202.3	0.0	202.6	0.0	203.3	0.0	205.2	0.0
2	186.0	2.3	187.1	2.2	190.7	2.1	189.1	2.1	187.7	2.0
4	180.2	7.0	181.2	6.2	190.7	5.2	185.5	5.1	183.5	5.9
6	175.7	11.4	169.4	9.3	177.7	9.0	176.8	8.0	172.5	8.7
8	166.6	16.7	165.0	14.2	172.9	12.6	167.6	10.8	170.2	14.4
10	163.0	23.4	162.1	18.0	164.2	17.3	162.8	16.2	162.7	20.7
12	160.0	29.2	158.0	26.4	160.6	24.9	160.2	24.3	160.6	27.4
14	158.8	33.9	155.2	33.7	159.3	31.8	158.5	30.8	157.9	30.3
16	158.8	36.0	157.9	37.0	157.9	35.2	158.7	31.4	158.1	31.3
18	158.0	33.2	156.3	36.5	159.8	34.6	158.5	31.8	157.5	29.2
20	160.1	31.2	156.8	33.6	159.3	31.8	158.9	31.0	159.8	29.0
22	159.9	28.8	159.4	29.6	161.8	27.4	159.8	28.3	160.7	27.8
24	160.8	23.4	158.4	26.1	162.2	25.6	157.4	25.4	160.7	24.4
26	162.3	20.6	160.6	23.4	164.2	23.4	157.6	22.5	160.3	21.6
28	163.8	18.1	163.6	21.5	164.4	21.8	161.3	19.9	161.1	19.1
30	163.0	15.8	162.9	19.5	160.6	20.0	162.5	18.0	164.9	16.5
32	166.1	14.0	162.9	16.6	165.9	17.3	164.0	15.5	164.6	14.3
34	166.2	12.2	165.4	14.0	167.6	15.3	166.4	13.8	166.2	12.8
36	169.0	10.8	168.4	12.8	167.8	13.5	169.2	12.2	170.7	11.6
38	172.0	9.8	169.5	11.9	170.3	12.5	170.4	11.6	171.8	11.0
40	173.6	9.3	171.2	11.3	171.7	11.7	172.6	11.2	173.5	10.5
42	174.7	8.8	172.8	10.6	173.9	11.3	173.2	10.5	175.0	10.3
44	176.5	8.3	174.9	10.1	175.5	10.8	175.4	10.2	176.6	9.9
46	177.6	7.9	175.9	9.6	175.9	10.1	176.9	9.9	177.4	9.6
48	178.8	7.6	176.8	9.1	177.2	9.8	178.4	9.3	178.8	9.3
50	179.9	7.4	178.4	8.9	178.6	9.5	179.0	9.0	180.3	9.0
52	180.9	7.2	179.5	8.5	179.7	9.2	180.3	8.8	181.6	8.7
54	181.8	7.0	180.6	8.3	180.5	8.9	181.3	8.6	182.5	8.5
56	182.6	6.8	181.3	8.1	181.4	8.7	182.3	8.4	183.5	8.3
58	183.2	6.6	182.3	7.9	182.3	8.4	183.2	8.2	184.3	8.1
60	184.1	6.5	183.0	7.7	183.4	8.3	184.0	7.9	185.4	7.9
62	184.6	6.4	183.6	7.5	184.1	8.1	184.7	7.8	186.1	7.8
64	185.3	6.3	184.6	7.4	184.6	7.9	185.4	7.6	186.9	7.7

Table A.1 (cont'd)

66	186.0	6.2	185.0	7.2	185.3	7.8	186.2	7.5	187.7	7.5
68	186.4	6.1	185.7	7.1	186.0	7.6	186.8	7.4	188.3	7.4
70	187.3	6.0	186.4	7.0	186.7	7.4	187.1	7.3	188.9	7.3
72	187.8	5.9	186.9	6.8	187.2	7.4	188.1	7.1	189.6	7.3
74	188.3	5.8	187.6	6.8	187.9	7.2	188.3	7.1	190.1	7.2
76	188.7	5.8	188.0	6.7	188.3	7.2	188.9	6.9	190.7	7.1
78	189.3	5.7	188.5	6.6	188.8	7.1	189.6	6.8	191.3	7.0
80	189.7	5.6	189.0	6.5	189.5	7.0	189.9	6.8	191.7	7.0
82	190.1	5.6	189.4	6.4	189.8	6.9	190.7	6.8	192.2	6.9
84	190.5	5.5	189.9	6.3	190.3	6.8	190.8	6.7	192.7	6.8
86	190.9	5.4	190.3	6.3	190.7	6.8	191.5	6.6	193.1	6.8
88	191.2	5.4	190.7	6.2	191.1	6.7	191.9	6.5	193.6	6.7
90	191.7	5.3	191.1	6.2	191.6	6.7	192.1	6.5	193.9	6.7
92	191.9	5.3	191.4	6.2	191.8	6.6	192.4	6.4	194.2	6.6
94	192.3	5.2	191.9	6.1	192.2	6.5	193.0	6.4	194.6	6.6
96	192.5	5.2	192.1	6.0	192.6	6.5	193.3	6.3	194.9	6.6
98	193.0	5.2	192.4	6.0	192.9	6.4	193.5	6.3	195.3	6.6
100	193.3	5.1	192.9	5.9	193.3	6.3	194.0	6.3	195.6	6.5
102	193.4	5.1	193.0	5.9	193.5	6.3	194.2	6.2	195.8	6.4
104	193.8	5.0	193.4	5.8	193.8	6.3	194.4	6.2	196.1	6.4
106	194.0	5.0	193.6	5.8	194.1	6.2	194.9	6.2	196.4	6.4
108	194.2	5.0	193.8	5.7	194.4	6.2	195.0	6.1	196.7	6.4
110	194.4	4.9	194.0	5.7	194.7	6.1	195.0	6.1	196.9	6.4
112	194.8	4.9	194.2	5.7	194.9	6.2	195.4	6.1	197.2	6.3
114	195.0	4.9	194.6	5.7	195.2	6.1	195.7	6.1	197.4	6.4
116	195.2	4.8	194.9	5.6	195.4	6.1	196.1	6.0	197.6	6.4
118	195.5	4.8	194.9	5.6	195.4	6.1	196.3	6.0	197.9	6.3
120	195.6	4.8	195.2	5.6	195.9	6.0	196.3	6.0	198.0	6.3
122	195.7	4.8	195.4	5.6	196.2	6.0	196.7	6.0	198.3	6.3
124	195.9	4.7	195.8	5.5	196.3	6.0	196.9	5.9	198.6	6.3
126	196.3	4.7	195.9	5.5	196.6	5.9	197.0	5.9	198.8	6.3
128	196.4	4.7	196.1	5.5	196.7	6.0	197.3	5.9	198.9	6.3
130	196.6	4.6	196.3	5.5	196.9	5.9	197.5	5.9	199.2	6.3
132	196.8	4.6	196.4	5.4	197.2	5.9	197.8	5.9	199.3	6.2
134	197.0	4.6	196.6	5.4	197.3	5.9	197.9	5.8	199.6	6.2
136	197.1	4.6	197.0	5.4	197.6	5.9	198.0	5.9	199.6	6.2
138	197.3	4.6	197.1	5.4	197.7	5.8	198.3	5.8	199.9	6.2
140	197.5	4.5	197.2	5.3	197.9	5.8	198.4	5.8	200.1	6.2
142	197.7	4.5	197.4	5.3	198.1	5.8	198.6	5.8	200.2	6.2
144	197.8	4.5	197.5	5.3	198.2	5.8	198.7	5.8	200.5	6.3
146	197.9	4.5	197.9	5.3	198.4	5.8	198.8	5.8	200.6	6.3
148	198.1	4.5	197.9	5.3	198.6	5.8	199.1	5.8	200.8	6.3
150	198.3	4.4	198.0	5.2	198.8	5.8	199.3	5.8	201.0	6.3

Table A.1 (cont'd)

152	198.4	4.4	198.3	5.2	198.9	5.8	199.4	5.8	201.1	6.3
154	198.5	4.4	198.3	5.2	199.0	5.8	199.7	5.8	201.4	6.3
156	198.5	4.4	198.6	5.2	199.2	5.8	199.7	5.8	201.5	6.3
158	198.8	4.4	198.7	5.2	199.4	5.8	200.0	5.8	201.7	6.3
160	198.9	4.3	198.8	5.1	199.5	5.8	200.1	5.8	201.9	6.3
162	199.1	4.3	199.1	5.1	199.8	5.8	200.2	5.8	201.9	6.3
164	199.2	4.3	199.2	5.1	199.8	5.8	200.4	5.8	202.1	6.3
166	199.3	4.3	199.3	5.1	200.0	5.7	200.6	5.8	202.2	6.3
168	199.4	4.3	199.4	5.1	200.1	5.7	200.7	5.8	202.4	6.3
170	199.6	4.3	199.7	5.1	200.2	5.7	200.9	5.8	202.6	6.3
172	199.7	4.2	199.9	5.1	200.4	5.7	201.0	5.8	202.7	6.3
174	199.8	4.3	200.0	5.1	200.5	5.7	201.1	5.8	202.8	6.4
176	199.9	4.2	200.1	5.1	200.7	5.7	201.3	5.8	203.0	6.4
178	200.0	4.2	200.2	5.0	200.7	5.7	201.4	5.8	203.0	6.4
180	200.0	4.2	200.3	5.0	200.8	5.7	201.4	5.8	203.2	6.4
182	200.2	4.2	200.5	5.0	201.0	5.7	201.5	5.8	203.3	6.5
184	200.3	4.2	200.6	5.0	201.2	5.7	201.7	5.8	203.5	6.4
186	200.4	4.1	200.6	5.0	201.3	5.7	201.9	5.8	203.6	6.5
188	200.5	4.1	200.9	5.0	201.3	5.7	202.0	5.8	203.7	6.5
190	200.6	4.1	200.9	5.0	201.5	5.7	202.1	5.8	203.9	6.5
192	200.7	4.1	201.1	4.9	201.7	5.7	202.2	5.9	203.9	6.5
194	200.8	4.1	201.1	5.0	201.8	5.7	202.3	5.8	204.0	6.6
196	201.0	4.1	201.2	4.9	201.9	5.7	202.5	5.9	204.2	6.6
198	201.0	4.1	201.5	4.9	202.0	5.7	202.5	5.9	204.2	6.6
200	201.1	4.0	201.5	4.9	202.0	5.7	202.8	5.9	204.4	6.6
202	201.2	4.0	201.6	4.9	202.2	5.6	202.7	5.9	204.4	6.7
204	201.3	4.0	201.7	4.9	202.4	5.6	202.9	5.9	204.5	6.7
206	201.4	4.0	201.8	4.8	202.5	5.7	203.0	5.9	204.6	6.7
208	201.6	4.0	202.0	4.8	202.7	5.6	203.1	5.9	204.7	6.7
210	201.6	4.0	202.1	4.9	202.7	5.7	203.2	5.9	204.9	6.7
212	201.7	4.0	202.2	4.8	202.8	5.7	203.4	5.9	205.0	6.7
214	201.8	4.0	202.2	4.8	202.9	5.7	203.5	5.9	205.0	6.8
216	201.9	3.9	202.3	4.8	202.9	5.7	203.5	5.9	205.2	6.8
218	202.0	3.9	202.5	4.8	203.1	5.6	203.7	6.0	205.3	6.8
220	202.1	3.9	202.6	4.8	203.2	5.7	203.8	5.9	205.4	6.8
222	202.3	3.9	202.7	4.8	203.3	5.7	203.9	5.9	205.5	6.8
224	202.3	3.9	202.8	4.8	203.4	5.7	204.1	6.0	205.5	6.8
226	202.3	3.9	202.8	4.8	203.5	5.7	204.1	6.0	205.7	6.9
228	202.5	3.9	203.0	4.8	203.6	5.6	204.2	6.0	205.8	6.9
230	202.6	3.9	203.1	4.8	203.8	5.7	204.4	6.0	206.0	6.9
232	202.7	3.8	203.1	4.8	203.9	5.7	204.4	6.0	206.0	6.9
234	202.7	3.8	203.4	4.8	203.9	5.7	204.6	6.0	206.1	7.0
236	202.9	3.8	203.4	4.8	204.0	5.7	204.7	6.0	206.4	7.0

Table A.1 (cont'd)

238	202.9	3.8	203.5	4.7	204.1	5.7	204.7	6.0	206.3	7.0
240	203.0	3.8	203.5	4.7	204.2	5.7	204.9	6.0	206.5	7.0
242	203.1	3.8	203.6	4.7	204.2	5.7	205.0	6.1	206.6	7.0
244	203.1	3.8	203.7	4.7	204.3	5.7	205.0	6.1	206.6	7.1
246	203.2	3.8	203.8	4.8	204.4	5.7	205.3	6.0	206.8	7.1
248	203.2	3.8	203.9	4.7	204.4	5.7	205.3	6.1	206.8	7.1
250	203.4	3.8	203.9	4.7	204.6	5.8	205.4	6.1	206.9	7.1
252	203.5	3.8	204.0	4.7	204.7	5.8	205.4	6.1	207.1	7.2
254	203.5	3.8	204.2	4.7	204.8	5.7	205.5	6.1	207.1	7.2
256	203.5	3.7	204.2	4.7	204.9	5.8	205.7	6.1	207.2	7.2
258	203.6	3.7	204.3	4.7	204.9	5.8	205.7	6.1	207.3	7.2
260	203.7	3.7	204.4	4.7	205.0	5.8	205.8	6.2	207.4	7.3
262	203.8	3.7	204.3	4.7	205.1	5.8	205.9	6.2	207.5	7.3
264	203.9	3.7	204.5	4.7	205.2	5.7	205.9	6.2	207.5	7.4
266	203.9	3.7	204.6	4.7	205.3	5.8	206.1	6.2	207.6	7.3
268	204.0	3.7	204.6	4.7	205.3	5.8	206.1	6.2	207.8	7.4
270	204.0	3.7	204.7	4.7	205.4	5.7	206.2	6.2	207.8	7.4
272	204.1	3.7	204.7	4.7	205.5	5.8	206.3	6.2	208.0	7.4
274	204.2	3.7	204.8	4.7	205.5	5.8	206.3	6.3	207.9	7.4
276	204.2	3.6	204.8	4.7	205.5	5.8	206.4	6.3	208.1	7.5
278	204.2	3.6	204.9	4.7	205.6	5.8	206.5	6.3	208.3	7.5
280	204.2	3.6	205.1	4.7	205.7	5.8	206.5	6.3	208.2	7.6
282	204.4	3.6	205.0	4.7	205.8	5.8	206.7	6.3	208.4	7.5
284	204.4	3.6	205.2	4.6	205.8	5.9	206.7	6.3	208.4	7.5
286	204.4	3.6	205.2	4.6	206.0	5.9	206.8	6.3	208.5	7.6
288	204.5	3.6	205.2	4.7	205.9	5.9	206.9	6.3	208.6	7.6
290	204.6	3.6	205.4	4.6	206.1	5.8	206.9	6.4	208.6	7.7
292	204.6	3.6	205.5	4.7	206.1	5.9	207.1	6.4	208.7	7.7
294	204.7	3.6	205.5	4.6	206.2	5.9	207.1	6.4	208.8	7.7
296	204.7	3.6	205.5	4.7	206.4	5.9	207.1	6.4	208.8	7.7
298	204.8	3.6	205.6	4.6	206.3	5.9	207.2	6.4	208.9	7.7
300	204.9	3.5	205.7	4.7	206.4	5.9	207.2	6.4	208.9	7.8

Table A.2 Stock temperature and mixing torque of PLA and its blends with CE 4468 as a function of time generated by a torque rheometer.

Time (s)	%CE 4468 in PLA							
	0.25%		0.5%		0.75%		1%	
	Temp (°C)	Torque (Nm)	Temp (°C)	Torque (Nm)	Temp (°C)	Torque (Nm)	Temp (°C)	Torque (Nm)
0	202.1	0.0	203.1	0.0	202.4	0.0	203.5	0.0
2	189.5	2.2	192.7	1.6	189.0	1.9	189.9	2.2
4	178.7	6.6	187.6	4.1	184.6	5.4	185.4	5.4
6	169.7	11.5	175.6	7.2	178.5	8.0	177.1	8.5
8	170.1	15.0	175.6	9.0	173.8	11.6	169.4	11.7
10	163.6	21.1	165.8	15.1	169.1	17.6	165.9	18.9
12	162.0	30.0	162.5	23.5	163.0	24.4	162.9	26.8
14	158.1	35.1	160.1	30.3	159.2	29.2	159.3	31.1
16	158.6	39.3	157.2	33.5	158.0	33.4	157.0	32.2
18	158.4	39.2	157.6	37.2	158.2	35.8	157.4	34.0
20	157.4	35.4	158.2	37.8	157.6	35.9	158.3	31.5
22	160.7	30.9	157.3	33.3	160.4	33.0	160.8	30.2
24	162.4	28.4	158.6	31.0	160.8	31.7	163.2	27.3
26	165.8	25.0	162.9	28.2	160.9	25.7	166.0	22.8
28	165.9	22.5	161.9	24.4	165.6	23.5	164.2	21.6
30	164.9	19.7	164.0	21.7	165.2	22.0	163.7	20.8
32	164.3	17.7	164.3	19.3	164.7	19.2	166.6	18.5
34	166.9	15.9	166.2	16.8	164.1	17.2	168.0	16.9
36	166.9	14.2	164.0	14.7	167.5	15.8	167.2	15.4
38	168.9	13.0	168.0	13.5	169.6	14.2	167.6	14.9
40	170.8	12.5	170.1	12.6	171.9	12.9	168.8	13.5
42	173.6	11.7	171.9	11.9	172.0	12.4	171.8	12.8
44	175.2	10.8	173.4	11.3	173.9	11.9	173.7	12.1
46	176.6	10.3	174.8	10.7	175.6	11.5	175.6	11.5
48	177.0	9.9	176.5	10.4	176.9	11.0	176.9	11.2
50	178.3	9.5	177.7	10.1	178.6	10.7	178.0	10.8
52	179.5	9.2	178.6	9.7	178.5	10.3	178.9	10.5
54	179.9	9.0	179.7	9.6	179.8	10.1	179.7	10.2
56	181.0	8.6	180.4	9.3	180.8	9.8	181.3	10.0
58	181.7	8.4	181.5	9.1	181.5	9.7	182.1	9.8
60	182.4	8.3	182.5	8.8	182.4	9.5	183.0	9.7
62	183.2	8.1	182.7	8.7	183.3	9.2	183.1	9.6
64	184.4	8.0	184.0	8.6	184.2	9.1	184.6	9.4

Table A.2 (cont'd)

66	184.6	7.9	184.8	8.4	184.8	9.0	185.2	9.3
68	185.2	7.6	185.5	8.3	185.5	8.8	186.2	9.2
70	186.1	7.6	186.1	8.2	186.0	8.7	186.7	9.1
72	186.5	7.5	186.8	8.0	186.8	8.6	186.9	9.0
74	187.0	7.4	187.4	8.0	187.5	8.4	187.7	9.0
76	187.7	7.3	188.0	7.9	187.5	8.5	188.6	8.9
78	188.1	7.2	188.6	7.8	188.5	8.4	189.1	8.9
80	188.7	7.1	189.0	7.7	188.7	8.3	189.5	8.9
82	188.9	7.0	189.6	7.7	189.4	8.3	190.1	8.8
84	189.5	6.9	190.0	7.6	190.0	8.1	190.3	8.8
86	189.9	6.9	190.5	7.5	190.3	8.1	191.2	8.8
88	190.2	6.8	190.9	7.5	190.9	8.0	191.4	8.8
90	190.8	6.7	191.2	7.5	191.2	8.1	191.8	8.8
92	190.9	6.7	191.8	7.4	191.4	8.1	192.3	8.8
94	191.3	6.7	192.1	7.4	192.1	8.0	192.6	8.9
96	191.7	6.6	192.4	7.3	192.2	8.0	192.9	8.9
98	192.0	6.6	192.9	7.3	192.7	7.9	193.6	9.0
100	192.3	6.5	193.0	7.3	193.1	7.9	193.8	8.9
102	192.7	6.5	193.5	7.3	193.2	7.9	194.1	8.9
104	192.9	6.4	193.7	7.2	193.7	7.9	194.6	8.9
106	192.9	6.4	194.0	7.2	193.8	7.9	194.8	8.9
108	193.3	6.4	194.5	7.1	194.2	7.9	194.9	9.0
110	193.6	6.3	194.6	7.2	194.6	7.8	195.3	8.9
112	193.9	6.3	194.9	7.1	194.7	7.8	195.7	9.0
114	194.2	6.3	195.2	7.1	195.0	7.8	195.9	9.0
116	194.3	6.3	195.4	7.1	195.2	7.8	196.3	9.0
118	194.5	6.3	195.7	7.1	195.5	7.8	196.4	9.0
120	194.8	6.2	195.9	7.1	195.9	7.8	196.6	9.1
122	195.0	6.2	196.2	7.0	196.0	7.9	197.1	9.1
124	195.3	6.2	196.4	7.0	196.3	7.8	197.2	9.1
126	195.5	6.1	196.5	7.1	196.3	7.8	197.5	9.1
128	195.6	6.1	196.9	7.0	196.6	7.8	197.8	9.2
130	195.9	6.1	197.1	7.0	197.0	7.8	197.9	9.2
132	196.1	6.1	197.3	7.0	196.9	7.8	198.1	9.2
134	196.1	6.1	197.5	7.0	197.3	7.8	198.4	9.3
136	196.4	6.1	197.6	7.0	197.5	7.8	198.7	9.2
138	196.5	6.1	197.9	7.0	197.5	7.9	199.0	9.3
140	196.7	6.1	198.1	7.0	198.0	7.8	199.1	9.3
142	196.9	6.0	198.2	7.0	198.0	7.8	199.3	9.3
144	197.1	6.1	198.5	7.0	198.3	7.9	199.4	9.4
146	197.3	6.0	198.6	7.0	198.6	7.9	199.9	9.3
148	197.5	6.0	198.8	7.0	198.5	7.9	200.1	9.4
150	197.7	6.0	199.0	7.0	198.8	7.9	200.1	9.5

Table A.2 (cont'd)

152	197.9	6.0	199.1	7.1	198.9	7.9	200.6	9.4
154	198.0	6.0	199.5	7.0	199.2	7.9	200.6	9.5
156	198.2	6.0	199.6	7.0	199.3	7.9	200.8	9.5
158	198.3	6.0	199.8	7.0	199.4	8.0	201.1	9.5
160	198.5	6.0	199.9	7.0	199.7	8.0	201.1	9.6
162	198.7	6.0	200.1	7.0	199.7	8.0	201.6	9.6
164	198.7	5.9	200.2	7.0	200.0	8.0	201.7	9.6
166	198.9	5.9	200.5	7.0	200.2	8.0	201.7	9.6
168	199.1	5.9	200.6	7.0	200.2	8.0	202.1	9.7
170	199.1	5.9	200.7	7.0	200.3	8.0	202.1	9.8
172	199.4	5.9	200.8	7.1	200.6	8.0	202.5	9.7
174	199.4	5.9	201.1	7.1	200.7	8.2	202.7	9.8
176	199.6	5.8	201.2	7.1	201.0	8.1	202.7	9.8
178	199.8	5.9	201.4	7.1	201.0	8.2	202.9	9.8
180	199.8	5.9	201.6	7.1	201.2	8.2	203.0	9.8
182	200.1	5.9	201.5	7.2	201.4	8.2	203.4	9.9
184	200.2	5.9	201.9	7.1	201.4	8.2	203.5	10.0
186	200.3	5.9	201.9	7.2	201.6	8.2	203.6	10.0
188	200.3	5.9	202.1	7.2	201.8	8.2	203.8	10.0
190	200.5	5.8	202.3	7.2	202.0	8.2	204.0	10.0
192	200.6	5.8	202.3	7.2	202.0	8.2	204.2	10.0
194	200.8	5.8	202.4	7.2	202.2	8.3	204.4	10.1
196	200.9	5.8	202.6	7.2	202.4	8.3	204.3	10.1
198	201.1	5.8	202.7	7.3	202.6	8.3	204.7	10.1
200	201.1	5.8	202.9	7.3	202.7	8.4	204.7	10.1
202	201.3	5.7	203.1	7.3	202.8	8.3	204.8	10.2
204	201.4	5.7	203.0	7.2	202.9	8.4	205.1	10.1
206	201.5	5.7	203.1	7.3	203.2	8.4	205.1	10.3
208	201.7	5.7	203.3	7.3	203.3	8.4	205.4	10.2
210	201.6	5.7	203.5	7.3	203.3	8.5	205.6	10.3
212	201.9	5.7	203.6	7.4	203.6	8.5	205.5	10.3
214	202.0	5.7	203.6	7.3	203.6	8.5	205.7	10.3
216	202.0	5.7	203.8	7.3	203.6	8.6	205.9	10.4
218	202.3	5.7	203.9	7.4	203.9	8.6	206.1	10.3
220	202.3	5.7	204.1	7.4	203.9	8.6	206.2	10.4
222	202.5	5.7	204.2	7.4	204.2	8.6	206.3	10.5
224	202.5	5.7	204.2	7.4	204.3	8.6	206.5	10.5
226	202.2	5.7	204.5	7.5	204.5	8.6	206.6	10.5
228	202.3	5.7	204.5	7.4	204.5	8.7	206.8	10.5
230	202.4	5.7	204.6	7.4	204.6	8.8	206.9	10.6
232	202.5	5.7	204.8	7.5	204.8	8.7	206.9	10.5
234	202.5	5.6	204.9	7.5	204.9	8.7	207.2	10.5
236	202.6	5.7	205.0	7.5	204.9	8.8	207.2	10.6

Table A.2 (cont'd)

238	202.8	5.7	205.1	7.5	205.1	8.7	207.4	10.6
240	202.9	5.7	205.3	7.5	205.2	8.9	207.5	10.6
242	203.0	5.7	205.3	7.5	205.3	8.9	207.5	10.7
244	203.1	5.7	205.5	7.6	205.4	8.9	207.9	10.7
246	203.1	5.8	205.6	7.5	205.5	9.0	208.0	10.7
248	203.3	5.7	205.6	7.5	205.7	8.9	207.9	10.8
250	203.3	5.7	205.8	7.6	205.7	8.9	208.2	10.7
252	203.4	5.7	205.9	7.6	205.8	8.9	208.3	10.9
254	203.5	5.7	206.0	7.6	206.0	9.0	208.5	10.9
256	203.5	5.7	206.2	7.6	206.0	9.0	208.7	10.9
258	203.7	5.7	206.2	7.6	206.3	9.0	208.6	10.9
260	203.8	5.7	206.3	7.7	206.4	9.1	208.8	10.9
262	203.7	5.7	206.5	7.7	206.3	9.1	209.0	11.0
264	203.8	5.7	206.6	7.7	206.7	9.1	209.2	11.0
266	203.9	5.7	206.7	7.7	206.7	9.2	209.2	11.0
268	203.9	5.7	206.8	7.7	206.9	9.1	209.3	11.1
270	204.1	5.7	206.7	7.8	207.1	9.2	209.5	11.0
272	204.1	5.7	207.0	7.8	207.1	9.2	209.4	11.1
274	204.2	5.7	207.0	7.8	207.2	9.2	209.7	11.2
276	204.4	5.7	207.0	7.8	207.3	9.3	209.8	11.1
278	204.4	5.7	207.2	7.8	207.4	9.2	209.8	11.2
280	204.5	5.7	207.3	7.9	207.5	9.3	210.1	11.2
282	204.6	5.7	207.3	7.9	207.6	9.3	210.0	11.3
284	204.7	5.7	207.3	7.9	207.7	9.3	210.1	11.3
286	204.7	5.7	207.5	8.0	207.8	9.3	210.4	11.3
288	204.7	5.7	207.5	7.9	207.8	9.4	210.3	11.4
290	204.9	5.7	207.7	8.0	208.0	9.4	210.6	11.3
292	205.0	5.7	207.8	7.9	208.0	9.5	210.7	11.4
294	205.0	5.7	207.8	8.0	208.3	9.4	210.5	11.5
296	205.1	5.7	207.8	8.0	208.3	9.5	210.9	11.5
298	205.0	5.7	208.0	7.9	208.3	9.6	210.9	11.5
300	205.2	5.7	208.0	8.0	208.6	9.6	210.9	11.5

Table A.3 Molecular weights, zero-shear viscosity and crystallinity values of PLA chain-extended with CE 4468 in an internal mixer.

% CE 4468 in PLA	Average molecular weights (g/mol)			Zero-shear viscosity (Pa-s)	Crystallinity (%)	
	M_n	M_w	M_v		1st heat	2nd heat
0	123,164	212,139	197,529	1,086	3.8	2.8
0.25	139,244	339,817	295,637	1,838	2.9	1.9
0.5	157,040	474,904	406,631	7,270	2.5	1.8
0.75	180,606	503,107	433,068	53,441	2.1	1.6
1	220,830	582,952	468,564	240,727	1.5	1.6

Table A.4 Effect of CE content on the crystallinity and failure mass of PLA films.

% CE 4468 in PLA films	Crystallinity (%)		Failure mass (g)
	1st heat	2nd heat	
0	4.3	2.5	19.0
0.25	2.8	1.2	22.7
0.5	0.9	1	29.7
0.75	NOT PROCESSABLE		
1			

APPENDIX B: Performance of poly(lactic acid)/cellulose nanocrystal composite blown films processed by two different compounding approaches.

Table B.1 Effects of CNC addition and blending process on the transparency of PLA and PLA/CNC composite films.

Wavelength (nm)	Transmission (%)		
	PLA	PLA/CNC (DB)	PLA/CNC (MB)
900	92.190	79.488	76.260
890	92.381	79.553	76.216
880	92.047	79.650	76.188
870	92.504	79.626	76.166
860	91.913	79.554	76.107
850	92.529	79.511	76.098
840	91.948	79.477	76.094
830	92.399	79.455	76.068
820	92.167	79.424	75.901
810	92.019	79.410	75.903
800	92.619	79.410	75.963
790	91.681	79.409	75.850
780	92.521	79.369	75.821
770	92.195	79.319	75.793
760	91.690	79.291	75.736
750	92.605	79.264	75.709
740	92.191	79.234	75.676
730	91.531	79.184	75.636
720	92.239	79.135	75.584
710	92.566	79.132	75.671
700	91.937	79.084	75.892
690	91.597	79.061	76.679
680	91.904	78.996	75.333
670	92.192	78.967	75.271
660	92.254	78.915	75.197
650	92.122	78.911	75.103
640	92.022	78.844	75.050
630	91.964	78.814	75.137
620	91.922	78.743	75.121
610	91.911	78.696	75.060
600	91.896	78.603	74.973
590	91.887	78.568	74.910
580	91.846	78.655	74.841
570	91.767	78.661	74.704
560	91.643	78.648	74.746

Table B.1 (cont'd)

550	91.807	78.627	74.634
540	91.714	78.564	74.544
530	91.437	78.491	74.489
520	91.829	78.434	74.422
510	91.325	78.357	74.395
500	91.724	78.341	74.357
490	91.258	78.302	74.280
480	91.349	78.266	74.132
470	91.439	78.262	74.082
460	91.250	78.257	74.011
450	91.225	78.201	73.896
440	91.202	78.101	73.791
430	90.887	78.113	73.639
420	90.574	78.063	73.484
410	91.209	77.988	73.309
400	90.645	77.870	73.101
390	90.982	77.735	72.863
380	90.216	77.341	72.623
370	90.266	77.400	72.280
360	90.303	77.244	71.835
350	90.124	77.092	71.425
340	89.676	76.955	70.917
330	89.232	76.625	69.650
320	88.908	76.557	69.142
310	88.657	76.237	68.566
300	88.427	75.774	67.617
290	87.967	75.172	66.588
280	87.031	74.451	65.695
270	86.244	73.655	64.516
260	85.198	72.769	60.671
250	81.910	69.839	58.198
240	61.044	51.854	48.849
230	18.123	17.171	20.337
220	2.178	3.678	0.079
210	0.692	1.791	0.187
200	1.700	3.138	2.518

Table B.2 Carboxyl indices using the intensities of reference peaks at 2994 cm^{-1} and 2945 cm^{-1} of PLA, PLA/1% CNC (DB) and PLA/1% CNC (MB) films.

Materials	**Carboxyl Index**	
	Reference peak at 2994 cm^{-1}	**Reference peak at 2945 cm^{-1}**
PLA	0.302 ± 0.007	0.393 ± 0.006
PLA/CNC (DB)	0.359 ± 0.007	0.456 ± 0.006
PLA/CNC (MB)	0.390 ± 0.008	0.487 ± 0.008

APPENDIX C: Water vapor and oxygen barrier properties of extrusion-blown poly(lactic acid)/cellulose nanocrystals nanocomposite films.

Table C.1 Water vapor permeability (23ºC and 85% RH), oxygen permeability (23ºC and 0% RH) as well as crystallinity of PLA/CNC films.

% CNC	WVP (10^{-16} kg-m/m^2-s-Pa)	OP (10^{-19} kg-m/m^2-s-Pa)	Crystallinity	
			1st heat	2nd heat
0	349.8 ± 51.9	163.2 ± 14.3	4.54	1.49
0.5	248.1 ± 19.1	59.8 ± 9.3	5.12	2.78
1	213.9 ± 10.3	42.6 ± 3.0	5.39	4.47
2	216.1 ± 8.0	41.0 ± 9.5	6.20	4.70

Table C.2 Effects of CNC content and testing temperature on the WVP of PLA films at 85% RH.

Temperature (ºC)	Water vapor permeability (10^{-16} kg-m/m^2-s-Pa)			
	PLA	PLA/0.5% CNC	PLA/1% CNC	PLA/2% CNC
10	420.5 ± 87.8	348.4 ± 71.2	295.6 ± 31.9	286.3 ± 19.8
17	361.4 ± 25.4	285.2 ± 64.8	219.4 ± 4.8	222.6 ± 6.9
23	349.8 ± 51.9	248.1 ± 19.1	213.9 ± 10.3	216.1 ± 8.0
31	334.1 ± 45.7	236.1± 31.8	205.2 ± 5.6	207.7 ± 9.2

Table C.3 Effects of CNC content and relative humidity (RH) on the WVP of PLA films at 23°C.

RH	Water vapor permeability (10^{-16} kg-m/m^2-s-Pa)			
	PLA	PLA/0.5% CNC	PLA/1% CNC	PLA/2% CNC
0.50	327.2 ± 16.1	238.0 ± 21.4	166.9 ± 4.1	183.3 ± 4.5
0.57	331.7 ± 20.6	234.1 ± 44.4	182.7 ± 5.0	182.3 ± 10.1
0.64	330.7 ± 27.3	244.0 ± 66.8	187.7 ± 2.9	181.1 ± 9.3
0.71	318.9 ± 21.3	253.7 ± 22.8	181.6 ± 3.6	189.4 ± 9.8
0.78	314.8 ± 43.9	263.0 ± 19.7	196.5 ± 6.1	190.9 ± 12
0.85	341.8 ± 50.0	250.0 ± 23.2	200.3 ± 10.0	186.6 ± 10.8

Table C.4 Effects of CNC addition and testing temperature on the OP of PLA films at 0% RH.

Temperature (°C)	Oxygen permeability (10^{-19} kg-m/m^2-s-Pa)	
	PLA	PLA/1% CNC
17	-	35.6 ± 2.7
23	163.2 ± 14.3	42.6 ± 3.0
31	218.0 ± 26.3	56.9 ± 5.0
38	243.3 ± 36.7	72.8 ± 4.2
50	340.3 ± 17.8	111.3 ± 9.3

APPENDIX D: Potential of extrusion-blown poly(lactic acid)/cellulose nanocrystals nanocomposite films for improving the shelf-life of a dry food product.

Table D.1 Moisture contents of crackers as a function of time recorded at 25°C and various storage relative humidity conditions.

Time (hours)	Moisture content (%)			Time (hours)	Moisture content (%)		
	10% RH	50% RH	79% RH		32% RH	61% RH	96% RH
0	4.10	4.10	4.10	0	4.10	4.10	4.10
2	4.02	7.43	9.27	2	5.49	7.01	9.01
6	4.11	8.35	11.34	4	6.38	9.22	12.00
12	4.17	8.64	12.23	8	6.75	9.82	14.39
18	4.20	8.87	13.10	18	7.21	11.09	18.34
25	4.23	9.19	14.17	23	7.22	11.05	18.84
50	4.21	9.01	14.46	43	7.32	11.49	21.88
74	4.25	9.09	14.81	67	7.37	11.61	23.22
98	4.21	9.27	15.45	92	7.35	11.61	23.78
122	4.20	9.27	15.72	123	7.49	11.75	24.55
170	4.26	9.21	15.67	147	7.55	11.83	25.00
218	4.22	9.22	15.72	170	7.39	11.60	24.53
242	4.29	9.14	15.72	218	7.34	11.53	24.37
266	4.33	9.20	15.72	266	7.38	11.60	24.50
314	4.31	9.18	15.65	314	7.36	11.60	24.45
336	4.27	9.14	15.69	333	7.42	11.62	24.45

Table D.2 Equilibrium moisture content values of crackers obtained experimentally and predicted by GAB equation at 25°C.

Relative humidity (%)	**Equilibrium moisture content (%)**	
	Experimental	**Predicted by GAB**
0.0	0.0000	0.0000
10.4	4.2840	4.3176
31.8	7.3779	7.2658
50.1	9.1765	9.6574
60.9	11.5916	11.5139
78.5	15.6974	16.1692
96.1	24.4601	26.1347

REFERENCES

REFERENCES

1. Karkhanis, S.S. and Matuana, L.M., Extrusion blown films of poly(lactic acid) chain-extended with food grade multifunctional epoxies, Polymer Engineering and Science, 59(11): 2211-2219 (2019).

2. Liu, J., Lou, L., Yu, W., Liao, R., Li, R., and Zhou, C., Long chain branching polylactide: structures and properties, Polymer, 51(22): 5186-5197 (2010).

3. Cavalcanti, F.N., Teofilo, E.T., Rabello, M.S., and Silva, S.M.L., Chain extension and degradation during reactive processing of PET in the presence of triphenyl phosphite, Polymer Engineering and Science, 47(12): 2155-2163 (2007).

4. Arruda, L.C., Magaton, M., Bretas, R.E.S., and Ueki, M.M., Influence of chain extender on mechanical, thermal and morphological properties of blown films of PLA/PBAT blends, Polymer Testing, 43: 27-37 (2015).

5. Tee, Y.B., Talib, R.A., Abdan, K., Chin, N.L., Basha, R.K., and Yunos, K.F.M., Toughening poly(lactic acid) and aiding the melt-compounding with bio-sourced plasticizers, Agriculture and Agricultural Science Procedia, 2: 289-295 (2014).

6. Ojijo V. and Ray, S.S., Super toughened biodegradable polylactide blends with non-linear copolymer interfacial architecture obtained via facile in-situ reactive compatibilization, Polymer, 80: 1-17 (2015).

7. Wang, Y., Fu, C., Luo, Y., Ruan, C., Zhang, Y., and Fu, Y., Melt synthesis and characterization of poly(L-lactic acid) chain linked by multifunctional epoxy compound, Journal Wuhan University of Technology, Materials Science Edition, 25(5): 774-779 (2010).

8. Tanaka, Y. and Kakiuchi, H., J., Study of epoxy compounds . part vi . curing reactions of epoxy resin and acid anhydride with amine , acid , alcohol , and phenol as catalysts, Journal of Polymer Science: Part A, 2: 3405-3430 (1964).

9. Wang, X., Mi, J., and Zhou, H., J., Transition from microcellular to nanocellular chain extended poly (lactic acid)/ hydroxyl-functionalized graphene foams by supercritical CO_2, Journal of Materials Science, 54(5): 3863-3877 (2019).

10. Karkhanis, S.S., Stark, N.M., Sabo, R.C., and Matuana, L.M., Performance of poly(lactic acid)/cellulose nanocrystal composite blown films processed by two different compounding approaches, Polymer Engineering and Science, 58(11): 1965-1974 (2017).

11. Dong, W., Zou, B., Yan, Y., Ma, P., and Chen, M., Effect of chain-extenders on the properties and hydrolytic degradation behavior of the poly(lactide)/ poly(butylene adipate-co-terephthalate) blends, International Journal of Molecular Sciences, 14(10): 20189-20203 (2013).

12. Jaszkiewicz, A., Bledzki, A. K., & Meljon, A., Online observations and process analysis of chain extended polylactides during injection moulding, Polymer Degradation and Stability, 101(1): 65-70 (2014).

13. Afrifah, K.A. and Matuana, L.M., Impact modification of polylactide with a biodegradable ethylene/acrylate copolymer, Macromolecular Materials and Engineering, 295(9): 802-811 (2010).

14. Mallet, B., Lamnawar, K., and Maazouz, A., Improvement of blown film extrusion of poly(lactic acid): structure-processing-properties relationships, Polymer Engineering and Science, 54(4): 840-857 (2014).

15. Raffa, P., Coltelli, M.B., Savi, S., Bianchi, S., and Castelvetro, V., Chain extension and branching of poly(ethylene terephthalate) (PET) with di- and multifunctional epoxy or isocyanate additives: an experimental and modelling study, Reactive and Functional Polymers, 72: 50-60 (2012).

16. Dalsin, S.J., Hillmyer, M.A., and Bates, F.S., Molecular weight dependence of zero-shear viscosity in atactic polypropylene bottlebrush polymers, Macro Letters, 3(5): 423-427 (2014).

17. Ludwiczak, J. and Kozlowski, M., Foaming of polylactide in the presence of chain extender, Journal of Polymers and the Environment, 23, 137-142 (2015).

18. Wang, J., Thurber, C., Bishop, M., Monaenkova, D., Marchbanks, E., Kim, H., Keene, E., and Chen, X., Study of residence time distribution for a blown film line using inline uv-vis spectroscopy and optical imaging on a film bubble, SPE Antec 2017-Anaheim, California, 1168-1174 (2017).

19. Wesholowski, J., Berghaus, A., and Thommes, M., Inline determination of residence time distribution in hot-melt-extrusion, Pharmaceutics, 10(2): 49 (2018).

20. Karkhanis, S.S., Stark, N.M., Sabo, R.C., and Matuana, L.M., Blown film extrusion of poly(lactic acid) without melt strength enhancers, Journal of Applied Polymer Science, 134(34): 45212 (2017).

21. Karkhanis, S.S., Stark, N.M., Sabo, R.C., and Matuana, L.M., Water vapor and oxygen barrier properties of extrusion-blown poly(lactic acid)/cellulose nanocrystals nanocomposite films, Composites Part A: Applied Science and Manufacturing, 114: 204-211 (2018).

22. Selke, S.E.M. and Cutler, J.D., Plastics Packaging: Properties, Processing, Applications and Regulations, Hanser Publications, Cincinnati, pp. 159-184 (2016).

23. Herrera, N., Mathew, A.P., and Oksman, K., Plasticized polylactic acid/cellulose nanocomposites prepared using melt-extrusion and liquid feeding: mechanical, thermal and optical properties, Composites Science and Technology, 106: 149-155 (2015).

24. Zhou, Y., Fuentes-Hernandez, C., Khan, T.M., Liu, J.C., Hsu, J., Shim, J.W., Dindar, A., Youngblood, J.P., Moon, R.J., and Kippelen, B., Recyclable organic solar cells on cellulose nanocrystal surface, Scientific Reports, 3: 1536 (2013).

25. Lizundia, E., Fortunati, E., Dominici, F., Vilas, J.L., León, L.M., Armentano, I., Torre, L., and Kenny, J.M., PLLA-grafted cellulose nanocrystals: role of the CNC content and grafting on the PLA bionanocomposite film properties, Carbohydrate Polymers, 142: 105-113 (2016).

26. Tripathi, N., Monika, and Katiyar, V., Poly(lactic acid)/modified gum arabic based bionanocomposite films: thermal degradation kinetics, Polymer Engineering and Science, 57(11): 1193-1206.

27. Wang, Y., Steinhoff, B., Brinkmann, C., and Alig, I., In-line monitoring of the thermal degradation of poly(L-lactic acid) during melt extrusion by UV-Vis spectroscopy, Polymer, 49(5): 1257-1265 (2008).

28. Al-Itry, R., Lamnawar, K., and Maazouz, A., Improvement of thermal stability, rheological and mechanical properties of PLA, PBAT and their blends by reactive extrusion with functionalized epoxy, Polymer Degradation and Stability, 97(10): 1898-1914 (2012).

29. Jamshidi, K., Hyon, S.H., and Ikada, Y., Thermal characterization of polylactides, Polymer, 29(12): 2229-2234 (1988).

30. Sperling, L.H., Introduction to Physical Polymer Science, John Wiley & Sons Publication, New Jersey, pp. 349-426 (2006).

31. Piorkowska, E. and Rutledge, G.C., Handbook of polymer crystallization, John Wiley & Sons Publication, New Jersey, pp. 125-163 (2013).

32. Shi, Q., Zhou, C., Yue, Y., Guo, W., Wu, Y., and Wu, Q., Mechanical properties and in vitro degradation of electrospun bio-nanocomposite mats from PLA and cellulose nanocrystals, Carbohydrate Polymers, 90(1): 301-308 (2012).

33. Cacciotti, I., Fortunati, E., Puglia, D., and Kenny, J.M., Effect of silver nanoparticles and cellulose nanocrystals on electrospun poly(lactic) acid mats: morphology, thermal properties and mechanical behavior, Carbohydrate Polymers, 103(1) 22-31 (2014).

34. Sullivan, E.M., Moon, R.J., and Kalaitzidou, K., Processing and characterization of cellulose nanocrystals/polylactic acid nanocomposite films, Materials, 8(12): 8106-8116 (2015).

35. Gupta, A., Simmons, W., Schueneman, G.T., Hylton, D., and Mintz, E.A., Rheological and thermo-mechanical properties of poly(lactic acid)/lignin-coated cellulose nanocrystal composites, ACS Sustainable Chemistry and Engineering, 5(2): 1711-1720 (2017).

36. Mathew, A. P., Oksman, K., and Sain, M., The effect of morphology and chemical characteristics of cellulose reinforcements on the crystallinity of polylactic acid, Journal of Applied Polymer Science, 101(1): 300-310 (2006).

37. Wang, X., Sun, H., Bai, H., & Zhang, L., Thermal, mechanical, and degradation properties of nanocomposites prepared using lignin-cellulose nanofibers and poly(lactic acid), BioResources, 9(2): 3211-3224 (2014).

38. Halasz, K. and Csóka, L., Plasticized biodegradable poly(lactic acid) based composites containing cellulose in micro- and nanosize, Journal of Engineering, 2013: 1 (2013).

39. Kopinke, F. D., Remmler, M., Mackenzie, K., Moder, M., and Wachsen, O., Thermal decomposition of biodegradable polyesters - II. poly(lactic acid), Polymer Degradation and Stability, 53(3): 329-342 (1996).

40. Rasselet, D., Ruellan, A., Guinault, A., Miquelard-Garnier, G., Sollogoub, C., and Fayolle, B., Oxidative degradation of polylactide (PLA) and its effects on physical and mechanical properties, European Polymer Journal, 50(1): 109-116 (2014).

41. Saito, O., Effects of high energy radiation on polymers II. end-linking and gel fraction, Journal of the Physical Society of Japan, 13(12): 1451-1464 (1958).

42. Holland, B. J. and Hay, J. N., The thermal degradation of poly(vinyl acetate) measured by thermal analysis-Fourier transform infrared spectroscopy, Polymer, 43(8): 2207-2211 (2002).

43. Aoyagi, Y., Yamashita, K., and Doi, Y., Thermal degradation of poly[(R)-3-hydroxybutyrate], poly[ε-caprolactone], and poly[(S)-lactide], Polymer Degradation and Stability, 76(1): 53-59 (2002).

44. Stark, N.M and Matuana, L.M., Surface chemistry changes of weathered HDPE/wood-flour composites studied by XPS and FTIR spectroscopy, Polymer Degradation and Stability, 86(1): 1-9 (2004).

45. Fechine, G.J.M., Rabello, M.S., Souto Maior, R.M., and Catalani, L.H., Surface characterization of photodegraded poly(ethylene terephthalate). The effect of ultraviolet absorbers, Polymer, 45(7): 2303-2308 (2004).

46. Xing, C. and Matuana, L.M., Epoxidized soybean oil-plasticized poly(lactic acid) films performance as impacted by storage, Journal of Applied Polymer Science, 133(12): 43201 (2016).

47. Liu, X., Zou, Y., Li, W., Cao, G., and Chen, W., Kinetics of thermo-oxidative and thermal degradation of poly(D,L-lactide) (PDLLA) at processing temperature, Polymer Degradation and Stability, 91(12): 3259-3265 (2006).

48. Carlborn, K. and Matuana, L.M., Composite materials manufactured from wood particles modified through a reactive extrusion process, Polymer Composites, 26(4): 534-541 (2005).

49. Carlborn, K. and Matuana, L.M., Modeling and optimization of formaldehyde-free wood-based composites using a box-behnken design, Polymer Composites, 27(6): 599-607 (2006).

50. Carlborn, K. and Matuana, L.M., Functionalization of wood particles through a reactive extrusion process, Journal of Applied Polymer Science, 101(5): 3131-3142 (2006).

51. Li, Q. and Matuana, L.M., Surface of cellulosic materials modified with functionalized polyethylene coupling agents, Journal of Applied Polymer Science, 88(2): 278-286 (2003).

52. Palacios, J., Albano, C., Gonzalez, G., Castillo, R.V., Karam, A., and Covis, M., Characterization and thermal degradation kinetics of poly(l-lactide) nanocomposites with carbon nanotubes, Polymer Engineering and Science, 55(3): 710-718 (2015).

53. Matuana, L.M., Karkhanis, S.S., Stark, N.M., and Sabo, R.C., Cellulose nanocrystals as barrier performance enhancer of extrusion-blown PLA films for food applications, Biotech, Biomaterials and Biomedical - TechConnect Briefs, 3: 1-4 (2016).

54. George, J. and Sabapathi, S.N., Cellulose nanocrystals: synthesis, functional properties, and applications, Nanotechnology, Science and Applications, 8: 45-54 (2015).

55. Stark, N.M., Opportunities for cellulose nanomaterials in packaging films: a review and future trends, Journal of Renewable Materials, 4(5): 313-326 (2016).

56. Fortunati, E., Peltzer, M., Armentano, I., Torre, L., Jimenez, A., and Kenny, J.M., Effects of modified cellulose nanocrystals on the barrier and migration properties of PLA nano-biocomposites, Carbohydrate Polymers, 90(2): 948-956 (2012).

57. Matuana-Malanda, L., Park, C.B., and Balatinecz, J.J., Characterization of microcellular foamed PVC/cellulosic-fibre composites, Journal of Cellular Plastics, 32(5):449-469 (1996).

58. Shogren, R., Water vapor permeability of biodegradable polymers, Journal of Environmental Polymer Degradation, 5(2): 91-95 (1997).

59. Sanchez-Garcia, M.D. and Lagaron, J.M., On the use of plant cellulose nanowhiskers to enhance the barrier properties of polylactic acid, Cellulose, 17(5): 987-1004 (2010).

60. Luzi, F., Fortunati, E., Jimenez, A., Puglia, D., Pezzolla, D., Gigliotti, G., Kenny, J.M., Chiralt, A., and Torre, L., Production and characterization of PLA_PBS biodegradable blends reinforced with cellulose nanocrystals extracted from hemp fibres, Industrial Crops and Products, 93: 276-289.

61. Petersson, L. and Oksman, K., Biopolymer based nanocomposites: comparing layered silicates and microcrystalline cellulose as nanoreinforcement, Composites Science and Technology, 66(13): 2187-2196 (2006).

62. Wei, L., Luo, S., McDonald, A.G., Agarwal, U.P., Hirth, K.C., Matuana, L.M., Sabo, R.C., and Stark, N.M., Preparation and characterization of the nanocomposites from chemically modified nanocellulose and poly(lactic acid), Journal of Renewable Materials, 5(5): 410-422 (2017).

63. Herrera, N., Salaberria, A.M., Mathew, A.P., and Oksman, K., Plasticized polylactic acid nanocomposite films with cellulose and chitin nanocrystals prepared using extrusion and compression molding with two cooling rates: effects on mechanical, thermal and optical properties, Composites Part A: Applied Science and Manufacturing, 83: 89-97 (2016).

64. Arrieta, M.P, Fortunati. E., Dominici, F., Rayon, E., Lopez, J., Kenny, J.M., PLA-PHB/cellulose based films: mechanical, barrier and disintegration properties, Polymer Degradation and Stability, 107: 139-149 (2014).

65. Flodberg, G., Helland, I., Thomsson, L., Fredriksen, S.B., Barrier properties of polypropylene carbonate and poly(lactic acid) cast films, European Polymer Journal, 63: 217-226 (2015).

66. Auras, R.A., Harte, B., Selke, S., and Hernandez, R., Mechanical, physical, and barrier properties of poly(lactide) films, Journal of Plastic Film and Sheeting, 19(2): 123-135 (2003).

67. Yuniarto, K., Welt, B.A., Purwanto, A., Purwadaria, H.K., and Abdellatief, A., Effect of plasticizer on oxygen permeability of cast polylactic acid (PLA) films determined using dynamic accumulation method, Journal of Applied Packaging Research, 6(2): 51-57 (2014).

68. Bao, L., Dorgan, J.R., Knauss, D., Hait, S., Oliveira, N.S., and Maruccho, I.M., Gas permeation properties of poly(lactic acid) revisited, Journal of Membrane Science, 285(1–2): 166-172 (2006).

69. Siracusa V., Food packaging permeability behaviour: a report, International Journal of Polymer Science, 2012: 1-11 (2012).

70. Hao, F., Lu, L., and Wang, J., Finite element simulation of shelf life prediction of moisture-sensitive crackers in permeable packaging under different storage conditions, Journal of Food Processing and Preservation, 40(1): 37-47 (2016).

71. Mo, C., Yuan, W., Lei, W., and Shijiu, Y., Effects of temperature and humidity on the barrier properties of biaxially-oriented polypropylene and polyvinyl alcohol films, Journal of Applied Packaging Research, 6(1): 40-46 (2014).

72. Sirpatrawan, U., Shelf-life simulation of packaged rice crackers, Journal of Food Quality, 32(2): 224-239 (2009).

73. Rachtanapun, P., Shelf life study of salted crackers in pouch by using computer simulation models, Chiang Mai Journal of Science, 34(2): 209-218 (2007).

74. Azanha, A.B. and Faria, J.A.F., Use of mathematical models for estimating the shelf-life of cornflakes in flexible packaging, Packaging Technology and Science, 18(4): 171-178 (2005).

75. Liu, Y. and Matuana, L.M., Surface texture and barrier performance of poly(lactic acid)-cellulose nanocrystal extruded-cast films, Journal of Applied Polymer Science, 136(22): 47594 (2019).

Chapter 5

CONCLUSIONS

5.1 Conclusions

The main goal of this research project was to gain fundamental understanding of nanoscale dispersion and distribution of CNCs into a PLA matrix in order to develop a nanocomposite film with improved barrier performance through solvent-free processing methods for food packaging applications. To achieve this goal, the following four specific objectives were studied, and conclusions were drawn from each specific objective:

1. Specific objective #1 consisted of two parts. In the first part of this objective, the effectiveness and efficiency of FDA-approved food grade polymeric chain extenders (CE) with low (CE 4468) and high (CE 4400) epoxy equivalent weights in chain extending PLA were studied using a torque rheometer. Based on the experimental results, the following conclusions were made:

    A. The residence time and melt stock temperature exceeded at least 120 s recommended by the manufacturer for the reaction between PLA and CE to be over 99% complete at 200°C, clearly indicating that the blends were processed at conditions favoring chain extension reaction. This chain extension proceeded via the ring opening reaction of epoxide groups in the CE with PLA's hydroxyl and/or carboxyl groups, as confirmed by Fourier transform infrared spectroscopy.

    B. Both CE grades were effective at chain extending PLA because they significantly increased PLA's torque during mixing. The torque increase was related to increased

melt viscosity caused by molecular weight increase. Additionally, the reduced crystallinity of the blends compared to neat PLA indicated chain branching of PLA. Nevertheless, the CE with lower epoxy equivalent weight (CE 4468) was more efficient in increasing the torque of PLA compared to its counterpart with high epoxy equivalent weight (CE 4400) due to its higher reactivity.

In the second part of this objective, the processabilities of PLA films chain-extended and branched with various amounts of the most efficient CE were assessed, leading to the following conclusions:

A. Film manufacture was only feasible with blends containing up to 0.5% CE but difficult above this content due to chain entanglement leading to significant increase in melt viscosity. Blends with 0.25 and 0.5% CE experienced residence times and melt temperatures of at least 132 s and 211^{o}C in the extruder, respectively. Exposure to these processing conditions favored 99% completion of the chain extension reaction, confirmed by the increased melt pressure in the extruder as well as the increased molecular weight and decreased crystallinity of PLA/CE blends compared to neat PLA.

B. Chain branching reduced crystallinity and improved the ductility of PLA films. The addition of only 0.5% CE into the PLA films increased its failure mass by ~56%.

2. Two different approaches of incorporating CNCs into a PLA matrix were examined in specific objective #2. The first method involved the melt-blending of PLA and CNCs in a three-piece internal mixer for homogenous dispersion of CNCs into the matrix. The second method, direct dry-blending, consisted of direct dry-mixing of PLA and CNCs in a high intensity mixer. The compounded materials were then blown into films and compared in terms of particle dispersion, optical, thermal, molecular weight and barrier properties. Our experimental results, led to the following conclusions:

    A. The distribution and dispersion of CNCs were not influenced by the blending method. Good distribution of CNCs was achieved in the PLA matrix but some agglomerations were still visible, indicative of not well-dispersed CNCs in the matrix, irrespective of the blending process. Poor dispersion negatively impacted the transparency of PLA/CNC composite films. Nevertheless, composite films with 75-78% transmission were obtained, demonstrating that reasonably good transparency remains despite limited dispersion.

    B. Overall, PLA/CNC composite films produced by both direct dry- and melt-blending approaches thermally degraded during the blending process, but at different extents. The degradation was demonstrated and quantified using various analytical methods such as GPC, FTIR, and DSC, which clearly indicated that the PLA/CNC melt-blended films degraded more than their direct dry-blended counterparts. The β-C-H transfer appeared to be the dominant mechanism of degradation for the composite films.

C. The incorporation of CNCs into the PLA matrix by the direct dry- and melt-blending processes improved the water vapor barrier properties of unfilled PLA films by 30% and 24%, respectively and oxygen barrier properties by 60% and 39%, respectively. The inferior barrier performance of the PLA/CNC melt-blended films compared to the direct dry-blended counterpart films could be attributed to the thermal degradation caused by the extra heat exposure of the compound during the melt-blending process in a three-piece mixer prior to blown film extrusion.

Therefore, the direct dry-blending technique appeared to be the better approach for incorporating CNCs into the PLA matrix because it exposes the samples to less heat and thus minimizes thermal degradation.

3. In the third specific objective, emphasis was placed on studying the effect of CNC content on the water vapor (WVP) and oxygen (OP) barrier properties of blown PLA films was evaluated at various temperatures and relative humidity conditions. The following conclusions were inferred from this study:

   A. Both WVP and OP of PLA and PLA/CNC nanocomposite films varied exponentially with temperature as expected from the Arrhenius equation, whereas the WVP remained constant with relative humidity as expected from Fick's law. However, two distinct trends were observed for the change in WVP and OP as function of testing temperature. WVP decreased with increasing temperature whereas an opposite trend was observed for OP, resulting in negative activation energy for water permeability attributed to PLA's polarity but positive activation energy for oxygen permeability, irrespective of CNC content. The activation energy

for both water vapor and oxygen permeabilities increased by adding CNC into PLA matrix.

B. The nanocomposite films were better barriers to both water and oxygen compared to PLA films irrespective of the testing temperature and relative humidity, attributable to the presence of highly crystalline CNCs, which increased the degree of crystallinity of the nanocomposites and acted as impermeable regions in the matrix, thus creating a tortuosity effect.

C. The values of WVP and OP negatively correlated with the degree of crystallinity, i.e., as the crystallinity increased the WVP and OP decreased. In fact, depending on testing temperature or humidity, optimum improvements in WVP (30-40%) and OP (65-75%) of PLA films occurred at 1% CNCs, a CNC content that correlated very well with the maximum increase in crystallinity.

D. The combined effects of increased crystallinity and CNC agglomerations negatively affected the light transmission of nanocomposite films by scattering light without affecting their visual clarity.

E. The transparent blown PLA/CNC nanocomposite films with better barrier performance developed in this study have tremendous potential for food packaging applications.

4. This specific objective was aimed at assessing the potential of CNC-based PLA films to extend the shelf-life of moisture-sensitive food products (such as crackers) compared to unfilled PLA films. The major findings from this research objective are as follows:

    A. The moisture sorption isotherm determined for the crackers exhibited a sigmoidal shape which could be described effectively by the GAB model.

    B. Crackers packaged within both PLA and PLA/CNC packages did not reach the critical moisture content (CMC) of 8% when stored below 50%RH at 25oC, indicating that the packaged crackers were shelf-stable at these conditions. Above a storage RH of 50%, the crackers inside both packages reached the CMC but at different times with CNC-based packages having approximately 40% longer shelf-life compared to the neat PLA package, irrespective of the RH.

    C. The linear, middle-point, logarithmic and GAB mathematical models were used to estimate the shelf-life of crackers packaged in PLA and PLA/CNC films. However, none of the models could accurately predict the shelf-life of the product-package system attributable to factors such as the food composition, thickness variations in packaging films and fluctuations in storage temperature and relative humidity. Nevertheless, all models predicted a longer shelf-life for crackers packaged in the PLA/CNC composite films compared to their neat PLA counterpart films, irrespective of the relative humidity.

In conclusion, the results of this dissertation indicate that the developed composite films have tremendous potential for food packaging applications because of their improved ductility and barrier performance.

5.2 Future work

This study was aimed at gain fundamental understanding of nanoscale dispersion and distribution of CNCs into a PLA matrix in order to develop a nanocomposite film with improved barrier performance through solvent-free processing methods for food packaging applications. In this study, PLA/CNC nanocomposite films with enhanced water and oxygen barrier performance were developed and their potential to enhance the shelf-life of a moisture sensitive product was assessed. However, a more in-depth shelf-life study with exploration of other shelf-life modeling techniques is proposed for future studies. Moreover, the potential of the nanocomposite films to extend the shelf-life of an oxygen-sensitive product must also be evaluated.